Selective Capture of Carbon Dioxide from Hydrocarbons Using a Metal-Organic Framework: Relevance to the Purification of Natural Gas and Acetylene

Omid T. Qazvini[1,2] and Shane G. Telfer*[,1]

[1]MacDiarmid Institute for Advanced Materials and Nanotechnology, School of Fundamental Sciences, Massey University, Palmerston North, New Zealand
[2]Department of Chemical Engineering and Analytical Science, The University of Manchester, Oxford Road, Manchester M13 9PL, UK.

Abstract: Efficient and sustainable methods for carbon dioxide (CO_2) capture are highly sought after. Mature technologies involve chemical reactions that absorb CO_2, but they have many drawbacks. Energy-efficient alternatives may be realized by porous physisorbents with void spaces that are complementary in size and electrostatic potential to molecular CO_2. Here, we present a robust, recyclable and inexpensive adsorbent termed MUF-16 (MUF = Massey University Framework). This metal-organic framework captures CO_2 with a high affinity in its one-dimensional channels. The position of the CO_2 molecules sequestered in the framework pores, as determined by X-ray crystallography, illustrate how complementary noncovalent interactions envelop the CO_2 while repelling other guest molecules. The low affinity of the MUF-16 pores for these competing gases underpins new benchmarks for the adsorption of CO_2 over methane, acetylene, ethylene, ethane, propylene and propane. IAST calculations show that for 50/50 mixtures at 293 K and 1 bar, the CO_2/CH_4 selectivity is 6690 and the CO_2/C_2H_2 selectivity is 510, for example. Breakthrough gas separations under dynamic conditions benefit from short time lags in the elution of the weakly-adsorbed component to deliver high-purity hydrocarbon products. Ultimately, MUF-16 may be applicable to the removal of CO_2 from sources such as natural gas and chemical feedstocks.

Introduction

Chemical separation processes consume vast quantities of energy.[1] Economical and practical pathways to alleviating this burden are required. This is especially relevant to the capture of CO_2, which is a common impurity in crude gas streams. CO_2 removal is integral to upgrading natural gas and biogas, for example, and to the purification of valuable hydrocarbons prior to polymerization or chemical derivatization.[2] These processes are separations that rely on discrimination between CO_2 and other gases. One established technology is to trap the CO_2 by a chemical reaction with an absorbent. This typically involves chemisorption to an amine in aqueous solution.[3, 4] Chemisorption incurs multiple drawbacks, however, including a high energy penalty during regeneration, amine losses due to degradation and evaporation, and the corrosion of hardware and pipelines.[5] Other conventional separation methods involve solvent extraction or cryogenic distillation, which are burdened with a high energy penalty and large amount of solvent waste.

The physisorption of CO_2 in nanoporous materials is an attractive alternative.[6, 7] Physisorption is governed by weak, noncovalent bonding interactions in pores that are structured on the molecular scale.[8] Ideally, they lower the energy requirements for regeneration since driving off the trapped CO_2 simply involves breaking interactions that are inherently weak. Effective physisorbents combine rapid guest diffusion, recyclability and long-term stability with selectivity for CO_2 over competing gases at relevant concentrations.[9] Thus, they may offer a sustainable solution to CO_2 capture. In this context, metal-organic frameworks (MOFs) have risen to prominence.[10-14] MOF materials are built up from metal ions and organic ligands, and their pore shape, size and chemical environment can be systematically designed. In turn, this allows interactions between framework hosts and molecular guests to be tailored. In the search of effective MOF physisorbents, it is clear that simply searching for materials with ever-higher levels of CO_2 uptake *per se* is unlikely to produce an adsorbent that is adept at gas separations. Instead, significant advances will emerge by suppressing the uptake of competing gases,[15, 16] developing scalable synthetic protocols, mitigating the impact of common impurities such as water vapour and oxygen, and developing low energy pathways to adsorbent recycling.

The removal of CO_2 from hydrocarbons is an important process.[2] While natural gas and biogas are primarily composed of methane (at high pressure and low pressure, respectively), contamination by CO_2 can prevent optimal heat release from gas combustion, and cause pipeline corrosion and dry ice formation.[17] MOFs, however, offer a means of reducing the CO_2 concentration in the presence of dominant quantities of methane.[10, 18, 19] Acetylene (C_2H_2) is an essential feedstock for the industrial production of commodity materials.[20, 21] When acetylene is generated, however, it typically coexists with CO_2 impurities.[22] The separation of C_2H_2 and CO_2 is challenging due to their similar physical properties (Table S4). MOF physisorbents offer a potential solution but most show an affinity toward C_2H_2 rather than CO_2.[11] The selective adsorption of the CO_2 component has seldom been reported despite its operational simplicity in process design and the promise of energy efficiency. Conversely, gas purification using hydrocarbon-selective MOFs requires additional stages if the eluent is contaminated by adsorbed CO_2 during the desorption step.[23] Despite recent advances in MOF chemistry, challenges remain in producing framework adsorbents that combine good separation capabilities with wider performance characteristics such as

scalability, recyclability and easy low-energy regeneration. MOF adsorbents that may be applied to methane purification and that preferentially adsorb CO_2 from C_2H_2 are in particular demand.

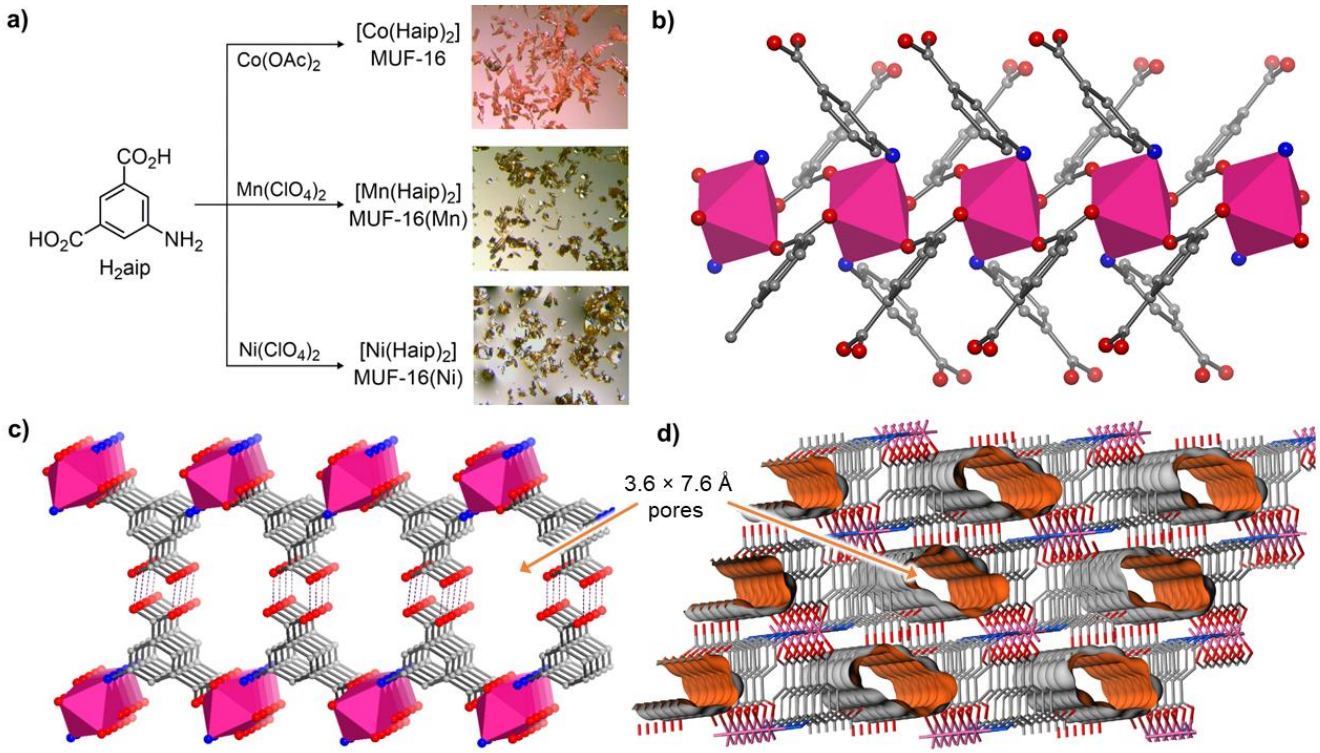

Figure 1. (a) Synthetic routes to the MUF-16 family and optical micrographs of the reaction products. (b) Infinite secondary building units (iSBUs) in MUF-16 comprise one-dimensional cobalt(II) chains connected by μ_2-bridging carboxylate groups of the Haip ligands (H_2aip = 5-aminoisophthalic acid). The cobalt(II) ions are depicted as filled octahedra. (c) The iSBUs are linked into planar two-dimensional sheets by the Haip ligands and further connected into a three-dimensional framework by hydrogen bonding (depicted as dashed lines) between adjacent sheets. (d) MUF-16 features one-dimensional channels with approximate dimensions of 3.6 × 7.6 Å that propagate through the framework. The Connolly surface of the framework is shown in orange and defined with a probe of diameter 1.0 Å. Colour code: Co = magenta; O = red; C = grey, N = blue.

Results and Discussion

Inspired by the superb properties of MOFs derived from straightforward and readily-available linkers,[24, 25] our interest was captured by the MUF-16 (MUF = Massey University Framework) series of materials. These frameworks are prepared by combining 5-aminoisophthalic acid (H_2aip), an inexpensive, commercially-available linker, with cobalt(II), nickel(II), or manganese(II) salts in methanol (Figure 1a). This delivers a family of compounds with the general formula $[M(Haip)_2]$,[26, 27] referred to as MUF-16 (M =Co), MUF-16(Ni) and MUF-16(Mn), respectively. These easily-handled crystalline materials are high yielding on gram scales and tolerant to oxygen and water vapour. Their crystal structures were determined by single crystal X-ray diffraction (Table S1). The three frameworks are isostructural, belonging to the *I*2/a space group. Individually, the metal ions adopt an octahedral geometry with four carboxylate and two amino donors arranged *trans* to one another. These ions are aligned into one-dimensional chains along a crystallographic axis supported on each side by μ_2-bridging carboxylate groups (Figure 1b). Adjacent chains are connected into two-dimensional sheets by Haip ligands that extend across the plane by coordinating to adjacent one-dimensional chains with both their amino and carboxylate donors (Figure 1b). Only one of the two carboxyl groups of each Haip ligand coordinates to the metal. The other remains protonated and engages in hydrogen-bonding with a partner from an adjacent layer (Figure 1c). These interactions link the layers into three-dimensional frameworks. The frameworks support one-dimensional channels of approximately 3.6 × 7.6 Å (accounting for the van der Waals surfaces of the atoms, Figure 1d). In their as-synthesized form the pores contain occluded water, which can be easily removed by heating at 130 °C *in vacuo*.

Thermogravimetric analysis demonstrated the thermal stability of the MUF-16 materials beyond 330 °C (Figure S2). Their purity was established by both elemental analysis and powder X-ray diffraction (Figure S5). The frameworks are chemically

robust, being unaffected by soaking in water or exposure to humid air for prolonged periods, as confirmed by powder X-ray diffraction and gas adsorption analysis (*vide infra* and Figures S6-S8 and S13).

As suggested by SCXRD, the MUF-16 frameworks are accessible to a range of incoming gases. Activation to give permanently porous materials is straightforward. Nitrogen adsorption isotherms measured at 77 K gave BET surface areas of 214, 205 and 204 m^2/g for MUF-16, MUF-16(Mn), and MUF-16(Ni), respectively (Figures S19-S21). Total pore volumes of 0.11 cm^3/g were established for all three frameworks (Table S3). These values are comparable with the geometric surface areas and pore volumes calculated from the crystallographic coordinates. The pore size distribution of MUF-16 also was calculated, which is consistent with the pore dimensions observed by SCXRD (Figure S12).

CO_2 isotherms were collected at 293 K and up to 1 bar (Figure 2a and see Figure S11 for other temperatures). Both MUF-16 and MUF-16(Ni) take up 2.13 mmol/g (48 cm^3/g) at 1 bar, and MUF-16(Mn) adsorbs 2.25 mmol/g (50.5 cm^3/g). This equates to approximately 0.9 molecules of CO_2 per metal site (Table S5). CO_2 saturation is only marginally higher at 273 K (Figure S11). The isosteric heat of adsorption (Q_{st}) at zero-coverage was calculated to be 32 kJ/mol for MUF-16 and 37 kJ/mol for its Ni and Mn analogues (Figure 2b). The Q_{st} increases at higher loadings, which can be attributed to intermolecular interactions between the adsorbates when the CO_2 loading levels are high. These interactions were experimentally verified by SCXRD (*vide infra*). The moderate Q_{st} values, even at high CO_2 loading, are well below values observed for MOFs with open metal sites[28]. It follows that the energy required to regenerate the frameworks by CO_2 desorption is likely to be low.

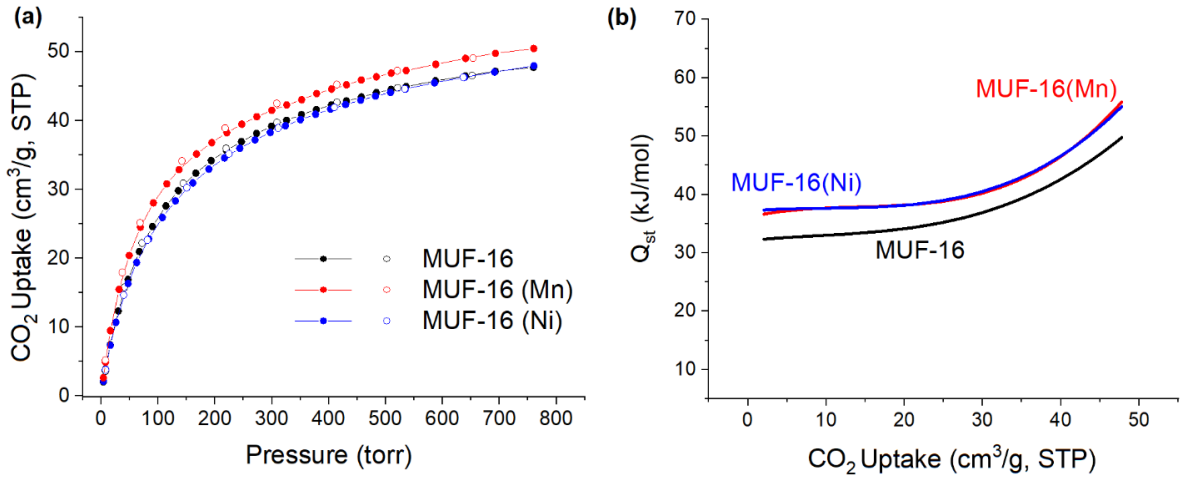

Figure 2. (a) Volumetric adsorption (filled circles) and desorption (open circles) isotherms of CO_2 at 293 K and for MUF-16 (black), MUF-16(Mn) (red), and MUF-16(Ni) (blue). (b) Heats of adsorption (Q_{st}) calculated for CO_2 binding to MUF-16 (black), MUF-16(Mn) (red), and MUF-16(Ni) (blue) as a function of CO_2 uptake. A high affinity for CO_2 coupled to a moderate heat of adsorption promise an adsorbent that takes up significant quantities of gas yet is easily recycled.

Single-crystal X-ray diffraction was used to identify the CO_2 binding sites in these frameworks. MUF-16(Mn) was selected for this study since its darker colour streamlined crystal handling (the pale colour of the Co(II) and Ni(II) analogues make them difficult to see when loaded in a glass capillary). The results obtained for MUF-16(Mn) are directly applicable to MUF-16 and MUF-16(Ni) due to their identical structure and CO_2 adsorption behavior (Figures 2a and S5). After transferring a MUF-16(Mn) single crystal into a capillary, it was activated *in vacuo* and the capillary flame-sealed. This allowed the guest-free structure of MUF-16(Mn) to be determined crystallographically (Table S2). We then filled CO_2 into the capillary to a pressure of 1.1 bar to determine the structure of the CO_2-loaded framework. We noted only minor changes to the framework itself upon evacuation and filling with CO_2. A clear picture of the affinity of MUF-16 for CO_2 arises from the CO_2-loaded SCXRD structure. First, the dimensions of the framework pores are well matched to the size of the CO_2 molecules. This allows the guests to be enveloped by multiple non-covalent contacts (Figure 3a). Second, these contacts are favourable since the electric quadrupole of the CO_2 is complementary to the polarization of the MUF-16 pore surface. For example, one of the electronegative oxygen atoms of each CO_2 molecule engages in N-H···O and C-H···O interactions with hydrogen atoms of amino and phenyl groups at distances of 2.55, 2.81, and 2.87 Å. The electropositive carbon atom of each CO_2 molecule engages in similar close-range contacts with the oxygen atoms of two non-coordinated carboxyl groups (2.87 and 3.04 Å). Two sites, which are related by crystallographic symmetry and share a common location for one of the oxygen atoms, are available to the CO_2 guests. They are occupied with a 50/50 ratio to give one CO_2 molecule per Mn centre overall, in accord with the adsorption isotherm. The CO_2 guest molecules are aligned along the channels and tilted with respect to the pore axis (Figure 3b). Attractive C···O intermolecular interactions

between adjacent molecules are evident at a distance of 3.78 Å. This array of CO_2 guests probably underlies the observed increase in Q_{st} as a function of gas loading observed in the adsorption isotherms.

The adsorption of nitrous oxide, N_2O, by MUF-16 corroborates this model of CO_2 affinity. The molecular size and electrostatic distribution of N_2O closely matches that of CO_2 (Figure S9). In parallel with CO_2, N_2O possesses atoms with partial negative charges at its termini that can bind to positively-charged regions of the pore surface, and vice-versa for its central nitrogen atom. MUF-16 adsorbs 1.91 mmol/g (43 cm^3/g) of N_2O at 1 bar and 293 K. This is only slightly less than the uptake of CO_2.

The high uptake of CO_2 by MUF-16 contrasts with its low affinity for hydrocarbons. Adsorption isotherms of CH_4, C_2H_2, C_2H_4, C_2H_6, C_3H_6 and C_3H_8 were measured on MUF-16 at 293 K (Figure 4a and Table 1). MUF-16 takes up just 1.20 cm^3/g of CH_4 at 1 bar and 293 K and 3.99 cm^3/g of C_2H_2. The highest adsorption amount was 5.35 cm^3/g observed for C_3H_6. The Q_{st} values for these gases are much lower than for CO_2 (Table S6). Since only modest quantities of these gases are adsorbed, care was taken to ensure the accuracy of these measurements by using large sample quantities.

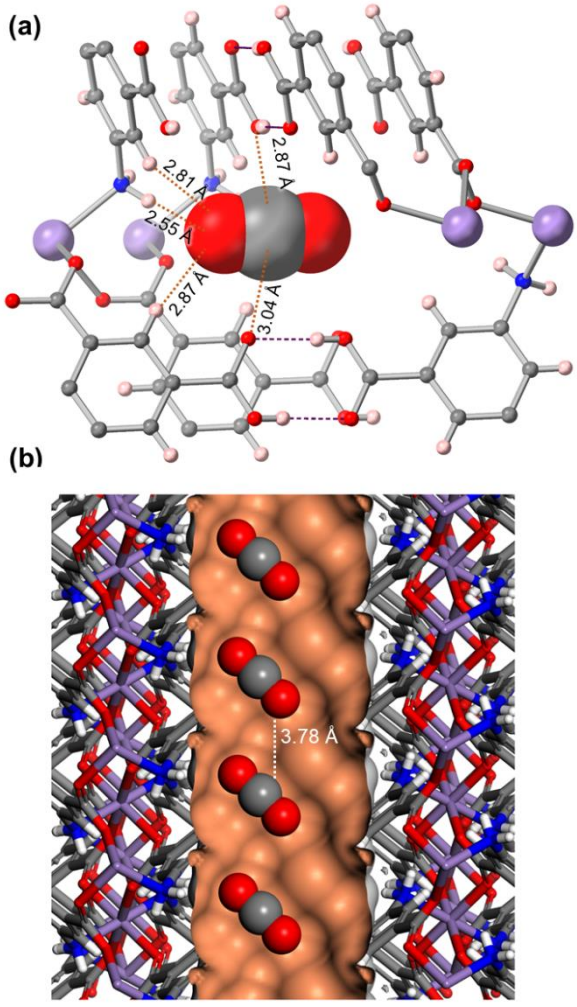

Figure 3. (a) The adsorption sites of CO_2 molecules in the pores of MUF-16(Mn), as determined by single-crystal X-ray diffraction. The CO_2 is depicted in space-filling mode. Key intermolecular distances between MUF-16(Mn) and the adsorbed CO_2 are shown with dashed orange lines. A second, symmetry-equivalent CO_2 adsorption site exists. (b) Adsorbed CO_2 molecules in MUF-16(Mn) highlighting the arrangement of adsorbed CO_2 in the framework channels and potential attractive noncovalent interactions between adjacent guests. The CO_2 molecules are shown in representative orientations in one of two symmetry-related crystallographic orientations. Colour code: manganese = lilac; nitrogen = blue; oxygen = red; carbon = grey; hydrogen = pale pink or white; pore Connolly surface = orange.

Uptake ratios provide a useful indication of the preference of an adsorbent for certain gases over others. For MUF-16, the CO_2/CH_4 uptake ratio is 39.8 (293 K and 1 bar). This is comparable to $[Cd_2L(H_2O)]$ (42.9)[29] and exceeded by only one other reported material (SIFSIX-14-Cu-i, 85) (Table S10).[30] Typical physisorbents show a preference for unsaturated hydrocarbons over CO_2, especially when bonding between the guest's π electrons and open metal sites can occur.[23, 31-45] However, MUF-16 exhibits a uniform preference for CO_2 over all C2 and C3 hydrocarbons at 293 K and 1 bar (Table 1). Here, the uptake ratios fall between 12 (acetylene), 15.6 (ethane) and 8.9 (propene). While the limited uptake of CH_4 is a well-established function of

its small size and low polarizability, the low affinity of MUF-16 for larger and more polar/polarizable hydrocarbon guests is notable. Inverted selectivity of this kind, that is, a preference for CO_2 over small hydrocarbons, is a sought after yet seldom reported phenomenon.[23, 46-52] With an uptake ratio of 12, MUF-16 surpasses all reported materials that preferentially adsorb CO_2 over C_2H_2, including SIFSIX-3-Ni (1.2 at 298 K and 0.1 bar)[23], CD-MOF-2 (1.3 at 298 K and 1 bar)[46], $K_2[Cr_3O(OOCH)_6(4\text{-ethylpyridine})_3]_2[\alpha\text{-}SiW_{12}O_{40}]$ (4.5 at 278 K and 1 bar)[50] and [Mn(bdc)(dpe)] (6.4 at 273 K and 1 bar)[47] (Table S11). The diminished affinity of MUF-16 for C_2H_2 may result from the reversed quadrupole moment of this guest *vis-à-vis* CO_2. Specifically, electropositive regions around the C_2H_2 termini may induce repulsive interactions with the framework pore surface, as illustrated by a hypothetical loading model (Figure S10).

Table 1. Summary of gas adsorption data and IAST-calculated selectivities for the MUF-16 family at 1 bar and 293 K.

	MUF-16	MUF-16(Mn)	MUF-16(Ni)
Q_{st}			
CO_2 [a]	32.3	36.6	37.3
Uptake [b]			
CO_2	47.78	50.5	47.97
CH_4	1.20	3.10	2.77
C_2H_2	3.99	9.69	7.53
C_2H_4	3.17	8.31	5.42
C_2H_6	3.06	8.81	5.67
C_3H_6	5.35	-	-
C_3H_8	4.82	-	-
IAST selectivity			
CO_2/CH_4 [c]	6690	470	1220
CO_2/C_2H_2 [c]	510	31	46
CO_2/C_2H_4 [c]	600	150	130
CO_2/C_2H_6 [c]	600	55	110
CO_2/C_3H_6 [c]	260	-	-
CO_2/C_3H_8 [c]	84	-	-

[a] In kJ/mol at zero loading. [b] In cm^3/g. [c] 50/50 ratio at 1 bar and 293 K as calculated by IAST.

Building on the preferential affinity indicated by the uptake ratios, we quantified the selectivity of MUF-16 by Ideal Adsorbed Solution Theory (IAST) calculations.[53] At 293 K and 1 bar, the IAST selectivity of MUF-16 for CO_2 over CH_4 (50/50 mixture) is 6690 (Figure 4b). MUF-16 is thus the best physisorbents known for this separation (Figure 5 and Table S10). For equimolar mixtures of CO_2 and C_2H_2, C_2H_4, C_2H_6, C_3H_6 and C_3H_8 the selectivity of MUF-16 is also high (Table 1). Here, MUF-16 sets a new benchmark for the separation of CO_2/C_2H_2 (50/50) with a selectivity of 510. As recognised in the literature for related systems,[15, 16, 54] high selectivities emerge by suppressing the uptake of the hydrocarbon gases while maintaining proficient CO_2 capture.

While the pore characteristics of MUF-16 clearly favour the uptake of CO_2 over other gases, its affinity could potentially rely on molecular sieving if the larger adsorbates are excluded from the framework on the basis of their size. This was ruled out by measuring hydrocarbon adsorption isotherms at 195 K, which showed that MUF-16 is able to take up significant amounts of CH_4, C_2H_2 and C_2H_6 (Figure S15). Guest molecules of this size can freely enter the pore network of MUF-16. However, since

their uptake is low at ambient temperatures their interactions with the framework must be weak. Further, the kinetics of adsorption of several guest molecules were measured (Figure S16). All gases display a similar kinetic profile and reach their equilibrium uptake in well under one minute. Therefore, thermodynamic – rather than kinetic – effects have the most decisive impact on the differential affinity of these gases for MUF-16.

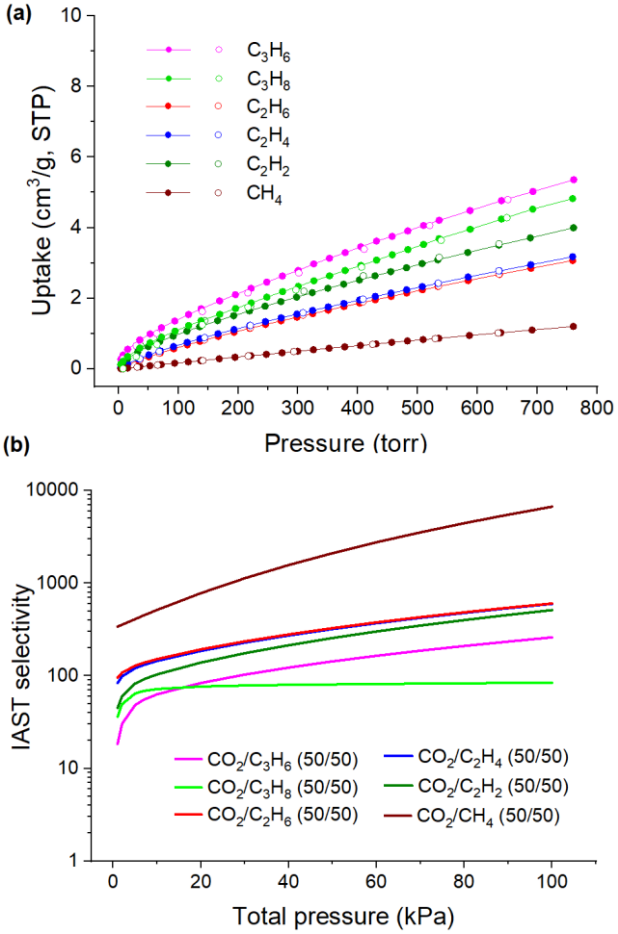

Figure 4. (a) Experimental CH_4, C_2H_2, C_2H_4, C_2H_6, C_3H_6 and C_3H_8 adsorption (solid spheres) and desorption (open spheres) isotherms of MUF-16 measured at 293 K. (b) Predicted IAST selectivities, displayed with a log scale, of MUF-16 for various gas mixtures at 293 K.

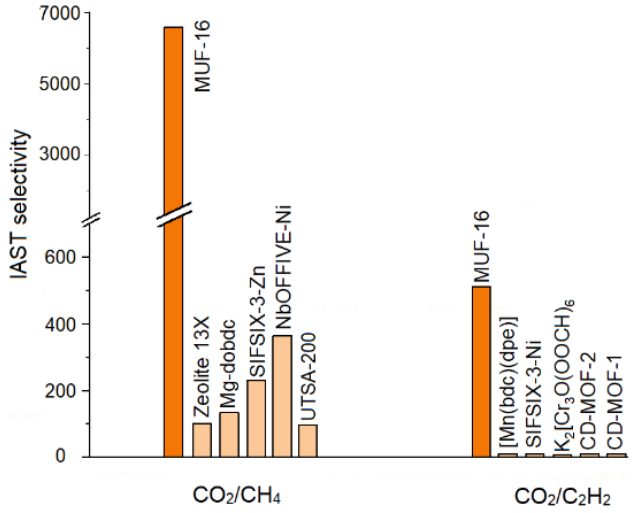

Figure 5. IAST selectivity of MUF-16 in comparison to a selection of top-performing physisorbents for CO_2/CH_4 (50/50) and CO_2/C_2H_2 (50/50) mixtures at ambient temperature and 1 bar. For clarity, the y axis is broken in two parts with different scales.

Invigorated by these results, we then investigated the feasibility of CO_2/hydrocarbon separations under dynamic conditions. Experimental breakthrough curves were measured for various gas mixtures at 293 K and 1.1 bar: CO_2/C_2H_6 (50/50), CO_2/C_2H_4 (50/50) and CO_2/C_2H_2 (50/50 and 5/95) (Figures 6a,b S44 and S51). Figure 6a,b shows the dimensionless concentration of CO_2 and the hydrocarbons (measured independently) exiting an adsorbent bed packed with MUF-16 (0.9 gram) as a function of time.

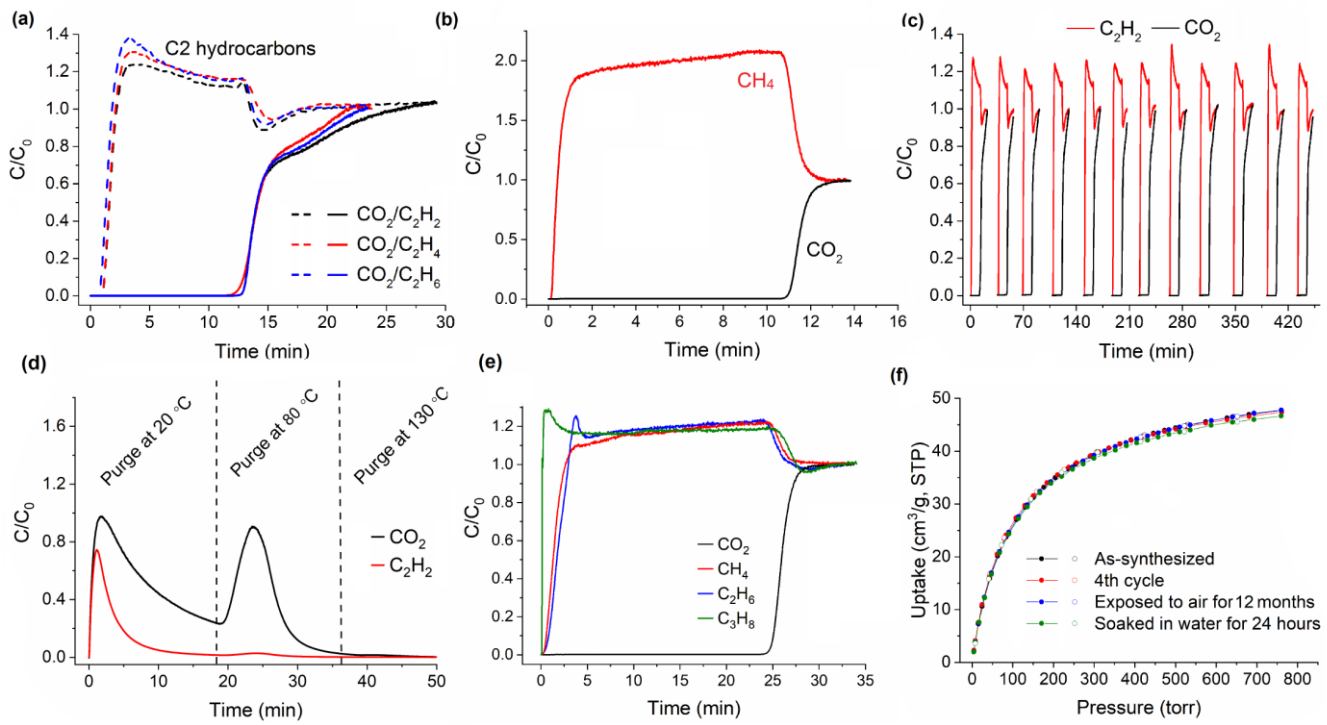

Figure 6. (a) Experimental breakthrough curves for 50/50 mixtures of CO_2 and the three C2 hydrocarbons (measured independently) at 293 K and 1.1 bar in an adsorption column packed with MUF-16. (b) Experimental breakthrough curves for 50/50 mixtures of CO_2 and CH_4 at 293 K and 1.1 bar in an adsorption column packed with MUF-16. (c) Twelve separation cycles for a CO_2/C_2H_2 mixture (50/50 mixture). Each separation process was carried out at 293 K and 1.1 bar. MUF-16 was regenerated between cycles by placing it under vacuum at ambient temperature for 20-25 min. (d) Experimental desorption profile of MUF-16 following the separation of CO_2 and C_2H_2 upon heating under a helium flow of 5 ml_N/min at 1.1 bar. No adsorbates were removed upon further heating at 130 °C indicating that they had been fully expelled at lower temperatures. (e) Experimental breakthrough curves for a 15/80/4/1 $CO_2/CH_4/C_2H_6/C_3H_8$ mixture at 1.1 bar and 293 K in an adsorption column packed with MUF-16. (f) CO_2 adsorption isotherms (293 K) of as-synthesized MUF-16 after four consecutive adsorption-desorption cycles, after exposing it to air with ~80% humidity for 12 months, and after immersion in water for 48 hours.

Complete separation was realized by MUF-16, whereby the hydrocarbons broke through from the column at an early stage because of their low affinity for the framework. Conversely, the signal of CO_2 was not detected for at least 10 minutes due to its adsorption by MUF-16. The dynamic adsorption capacity for CO_2 fell in the range 1.2 – 1.5 mmol/g which is nearly identical to the equilibrium capacity at the relevant partial pressures of CO_2 (Table S7). Significant volumes of pure hydrocarbons can be obtained in this way. Productivity calculations showed 1 kg of MUF-16 produces 27 L of the hydrocarbons from an equimolar mixture with CO_2 at 293 K and 1 bar. The ability of MUF-16 to selectively adsorb CO_2 is an important advantage of this MOF as pure hydrocarbons can be produced directly in a single adsorption. In literature reports to date, the capture of CO_2 over C2 hydrocarbons has so far largely been restricted to cryogenic temperatures and/or static conditions.[47-50, 52, 55] With respect to CO_2/C_2H_2 mixtures at ambient temperatures, we are aware of only three reported materials, CD-MOF-1[46], CD-MOF-2[46] and SIFSIX-3-Ni,[23] for which CO_2 trapping has been verified by experimental breakthrough measurements. Since these MOFs adsorb C_2H_2 (in addition to CO_2) strongly at moderate pressures, their uptake ratios are modest. They are limited to very low partial pressures of CO_2 and suffer from low productivity.

Subsequent multiple breakthrough tests revealed that MUF-16 maintains its CO_2 uptake and the complete removal of CO_2 over at least 12 separation cycles (Figure 6c). MUF-16 was regenerated between cycles by placing it under vacuum or by purging with an inert gas (Figure 6d). Virtually all of the adsorbed acetylene and around half of the CO_2 can be removed from the bed by purging at room temperature. The remainder can be fully desorbed at 80 °C.

To investigate separations involving trace CO_2, we simulated breakthrough curves of feed gases with low CO_2 partial pressures. First, a mass transfer coefficient was empirically determined based on measured breakthrough results. This

produces an excellent match between simulated and experimental breakthrough curves.[24, 56] With this realistic mass transfer coefficient in hand, we predicted breakthrough curves using feeds containing 0.1% CO_2 in C_2H_2 (Figure S57). These calculations revealed that MUF-16 is capable of eliminating trace quantities of CO_2, as often required in industrial processes.

We then turned our attention to the separation of more complex gas mixtures. Using $CO_2/CH_4/C_2H_6/C_3H_8$ (15/80/4/1) as a feed mixture, we observed complete CO_2 capture by MUF-16. CH_4, C_2H_6 and C_3H_8 broke through quickly with steep elution profiles (Figure 6e). Crucially, the relatively large adsorbates C_2H_6 and C_3H_8, do not diminish the CO_2 capture capabilities of MUF-16. This is an important observation for the removal of CO_2 from both biogas and natural gas, which often contain these hydrocarbons.[17] To further probe its applicability to natural gas sweeting, we conducted breakthrough measurements at higher pressure (9 bar). CO_2 was cleanly removed from the gas stream (Figures S45 and S46). Breakthrough simulations at pressures relevant to natural gas processing (50 bar) led to the prediction that MUF-16 can competently capture CO_2 from natural gas (Figure S50). Water vapour is a component of crude natural gas streams and it can affect gas adsorption by physisorbents.[57, 58] To test the moisture resistance of MUF-16, we measured its CO_2 adsorption properties after exposure to air and immersion in water (Figure 6f). The framework retains its CO_2 adsorption capacity following these mistreatments. More detailed analysis, including the resistance of MUF-16 to other common natural gas impurities such as H_2S, is an important next step.

Conclusion

The pores in MUF-16 are complementary to CO_2 in size and electrostatic potential. This underlies its high affinity for molecular CO_2 guests. Fortuitously, its pores have a low affinity for methane and C2 and C3 hydrocarbons. The intersection of these characteristics imbues the material with a high selectivity for CO_2 over hydrocarbon guests. Benchmark selectivities were determined for CO_2/CH_4 and CO_2/C_2H_2 separations. MUF-16 operates efficiently across a range of CO_2/hydrocarbon mixtures and pressures. These data highlight the performance improvements that are embodied in MUF-16. These findings are relevant to the practical challenges of purifying both natural gas and industrial feedstocks. MUF-16 has the potential to be produced economically on large scales and its chemical stability meets the demands of a long-lived physisorbent. Given these characteristics, MUF-16 has promise for applications involving the capture of CO_2 from hydrocarbon streams.

Supporting Information

Crystallographic data and files of MUF-16 as synthesized, under vacuum and loaded with CO_2 (CCDC 1948901, 1948905 and 1948904), additional structural plot, TG curves, PXRD, multiple cycle sorption isotherm, dual site Langmuir isotherm model fitting, isosteric heat of adsorption calculation, BET surface area calculations, IAST calculations of adsorption selectivities, breakthrough curves simulations and models used and column breakthrough test setup with procedures and measurements (PDF). This material is available free of charge via the Internet at…

Author Contributions

The manuscript was written through contributions of all authors. All authors have given approval to the final version of the manuscript.

Notes

A patent on MUF-16 has been lodged (WO 2020/130856 A1).

ACKNOWLEDGMENTS

We would like to thank Seok June (Subo) Lee and Adil Alkas for useful discussions and assistance with X-ray crystallography and Steve Denby for expert engineering assistance. We gratefully acknowledge the MacDiarmid Institute and RSNZ Marsden Fund (contract 14-MAU-024) for financial support.

References

1. Sholl, D. S.; Lively, R. P., Seven chemical separations: to change the world: purifying mixtures without using heat would lower global energy use, emissions and pollution--and open up new routes to resources. *Nature* **2016,** *532* (7600), 435-438.
2. Ravanchi, M. T.; Sahebdelfar, S., Carbon dioxide capture and utilization in petrochemical industry: potentials and challenges. *Appl. Petrochem. Res.* **2014,** *4* (1), 63-77.
3. Rochelle, G. T., Amine scrubbing for CO2 capture. *Science* **2009,** *325* (5948), 1652-1654.
4. Yu, C.-H.; Huang, C.-H.; Tan, C.-S., A review of CO_2 capture by absorption and adsorption. *Aerosol Air Qual. Res.* **2012,** *12* (5), 745-769.
5. Kohl, A.; Nielsen, R., *Gas Purification*. 5th ed.; Gulf Publishing Company: Houston, 1997.
6. Oschatz, M.; Antonietti, M., A search for selectivity to enable CO_2 capture with porous adsorbents. *Energ. Environ. Sci.* **2018,** *11* (1), 57-70.
7. Sreenivasulu, B.; Sreedhar, I.; Suresh, P.; Raghavan, K. V., Development trends in porous adsorbents for carbon capture. *Environ. Sci. Technol.* **2015,** *49* (21), 12641-12661.
8. Yang, R. T., *Gas separation by adsorption processes*. Butterworth-Heinemann: 2013.
9. Lu, A.-H.; Dai, S., *Porous materials for carbon dioxide capture*. Springer: 2014.
10. Lin, R.-B.; Xiang, S.; Xing, H.; Zhou, W.; Chen, B., Exploration of porous metal–organic frameworks for gas separation and purification. *Coord. Chem. Rev.* **2019,** *378*, 87-103.
11. Li, H.; Li, L.; Lin, R.-B.; Zhou, W.; Zhang, Z.; Xiang, S.; Chen, B., Porous metal-organic frameworks for gas storage and separation: Status and challenges. *EnergyChem* **2019,** *1* (1), 100006.

12. Ding, M.; Flaig, R. W.; Jiang, H.-L.; Yaghi, O. M., Carbon capture and conversion using metal–organic frameworks and MOF-based materials. *Chem. Soc. Rev.* **2019,** *48* (10), 2783-2828.
13. Mukherjee, S.; Kumar, A.; Zaworotko, M. J., 2 - Metal-organic framework based carbon capture and purification technologies for clean environment. In *Metal-Organic Frameworks (MOFs) for Environmental Applications*, Ghosh, S. K., Ed. Elsevier: 2019; pp 5-61.
14. Qazvini, O. T.; Telfer, S. G., A robust metal–organic framework for post-combustion carbon dioxide capture. *J. Mater. Chem. A* **2020,** *8* (24), 12028-12034.
15. Balashankar, V. S.; Rajagopalan, A. K.; Pauw, R. d.; Avila, A. M.; Rajendran, A., Analysis of a Batch Adsorber Analogue for Rapid Screening of Adsorbents for Postcombustion CO_2 Capture. *Ind. Eng. Chem. Res.* **2019,** *58*, 3314−3328.
16. Rajagopalan, A. K.; Avila, A. M.; Rajendran, A., Do adsorbent screening metrics predict process performance? A process optimisation based study for post-combustion capture of CO2. *Int. J. Greenh. Gas. Con.* **2016,** *46*, 76-85.
17. Rufford, T. E.; Smart, S.; Watson, G. C.; Graham, B.; Boxall, J.; Da Costa, J. D.; May, E., The removal of CO_2 and N_2 from natural gas: A review of conventional and emerging process technologies. *J. Petrol. Sci. Eng.* **2012,** *94*, 123-154.
18. Madden, D. G.; O'Nolan, D.; Chen, K.-J.; Hua, C.; Kumar, A.; Pham, T.; Forrest, K. A.; Space, B.; Perry, J. J.; Khraisheh, M., Highly selective CO_2 removal for one-step liquefied natural gas processing by physisorbents. *Chem. Commun.* **2019,** *55* (22), 3219-3222.
19. Belmabkhout, Y.; Bhatt, P. M.; Adil, K.; Pillai, R. S.; Cadiau, A.; Shkurenko, A.; Maurin, G.; Liu, G.; Koros, W. J.; Eddaoudi, M., Natural gas upgrading using a fluorinated MOF with tuned H 2 S and CO 2 adsorption selectivity. *Nature Energy* **2018,** *3* (12), 1059-1066.
20. Matar, S.; Hatch, L. F., *Chemistry of Petrochemical Processes*. Gulf Professional Publishing: 2001.
21. Hort, E. V.; Taylor, P., Acetylene‐Derived Chemicals. *Kirk‐Othmer Encyclopedia of Chemical Technology* **2000**.
22. Pässler, P.; Hefner, W.; Buckl, K.; Meinass, H.; Meiswinkel, A.; Wernicke, H. J.; Ebersberg, G.; Müller, R.; Bässler, J.; Behringer, H., Acetylene. *Ullmann's Encyclopedia of Industrial Chemistry* **2008,** *1*, 177-227.
23. Chen, K.-J.; Scott, H. S.; Madden, D. G.; Pham, T.; Kumar, A.; Bajpai, A.; Lusi, M.; Forrest, K. A.; Space, B.; Perry, J. J.; Zaworotko, M. J., Benchmark C_2H_2/CO_2 and CO_2/C_2H_2 Separation by Two Closely Related Hybrid Ultramicroporous Materials. *Chem* **2016,** *1* (5), 753-765.
24. Qazvini, O. T.; Babarao, R.; Shi, Z.-L.; Zhang, Y.-B.; Telfer, S. G., A Robust Ethane-Trapping Metal–Organic Framework with a High Capacity for Ethylene Purification. *J. Am. Chem. Soc.* **2019**.
25. Qazvini, O. T.; Babarao, R.; Telfer, S. G., Multipurpose Metal–Organic Framework for the Adsorption of Acetylene: Ethylene Purification and Carbon Dioxide Removal. *Chem. Mater.* **2019,** *31* (13), 4919-4926.
26. Tang, E.; Dai, Y.-M.; Zhang, J.; Li, Z.-J.; Yao, Y.-G.; Zhang, J.; Huang, X.-D., Two Cobalt(II) 5-Aminoisophthalate Complexes and Their Stable Supramolecular Microporous Frameworks. *Inorg. Chem.* **2006,** *45* (16), 6276-6281.
27. Tian, C.-B.; He, C.; Han, Y.-H.; Wei, Q.; Li, Q.-P.; Lin, P.; Du, S.-W., Four New MnII Inorganic–Organic Hybrid Frameworks with Diverse Inorganic Magnetic Chain's Sequences: Syntheses, Structures, Magnetic, NLO, and Dielectric Properties. *Inorg. Chem.* **2015,** *54* (6), 2560-2571.
28. Sumida, K.; Rogow, D. L.; Mason, J. A.; McDonald, T. M.; Bloch, E. D.; Herm, Z. R.; Bae, T.-H.; Long, J. R., Carbon Dioxide Capture in Metal–Organic Frameworks. *Chem. Rev.* **2012,** *112* (2), 724-781.
29. Hou, L.; Shi, W.-J.; Wang, Y.-Y.; Guo, Y.; Jin, C.; Shi, Q.-Z., A rod packing microporous metal–organic framework: unprecedented ukv topology, high sorption selectivity and affinity for CO_2. *Chem. Commun.* **2011,** *47* (19), 5464-5466.
30. Jiang, M.; Li, B.; Cui, X.; Yang, Q.; Bao, Z.; Yang, Y.; Wu, H.; Zhou, W.; Chen, B.; Xing, H., Controlling Pore Shape and Size of Interpenetrated Anion-Pillared Ultramicroporous Materials Enables Molecular Sieving of CO_2 Combined with Ultrahigh Uptake Capacity. *ACS Appl. Mater. Interfaces* **2018,** *10* (19), 16628-16635.
31. Moreau, F.; da Silva, I.; Al Smail, N. H.; Easun, T. L.; Savage, M.; Godfrey, H. G. W.; Parker, S. F.; Manuel, P.; Yang, S.; Schröder, M., Unravelling exceptional acetylene and carbon dioxide adsorption within a tetra-amide functionalized metal-organic framework. *Nat. Commun.* **2017,** *8*, 14085.
32. Xiang, S.; Zhou, W.; Gallegos, J. M.; Liu, Y.; Chen, B., Exceptionally High Acetylene Uptake in a Microporous Metal−Organic Framework with Open Metal Sites. *J. Am. Chem. Soc.* **2009,** *131* (34), 12415-12419.
33. Li, P.; He, Y.; Zhao, Y.; Weng, L.; Wang, H.; Krishna, R.; Wu, H.; Zhou, W.; O'Keeffe, M.; Han, Y.; Chen, B., A Rod-Packing Microporous Hydrogen-Bonded Organic Framework for Highly Selective Separation of C_2H_2/CO_2 at Room Temperature. *Angew. Chem., Int. Ed.* **2015,** *54* (2), 574-577.
34. Lee, J.; Chuah, C. Y.; Kim, J.; Kim, Y.; Ko, N.; Seo, Y.; Kim, K.; Bae, T. H.; Lee, E., Separation of Acetylene from Carbon Dioxide and Ethylene by a Water-Stable Microporous Metal–Organic Framework with Aligned Imidazolium Groups inside the Channels. *Angewandte Chemie International Editions* **2018,** *57* (26), 7869-7873.
35. Luo, F.; Yan, C.; Dang, L.; Krishna, R.; Zhou, W.; Wu, H.; Dong, X.; Han, Y.; Hu, T.-L.; O'Keeffe, M.; Wang, L.; Luo, M.; Lin, R.-B.; Chen, B., UTSA-74: A MOF-74 Isomer with Two Accessible Binding Sites per Metal Center for Highly Selective Gas Separation. *J. Am. Chem. Soc.* **2016,** *138* (17), 5678-5684.
36. Zhang, J.-P.; Chen, X.-M., Optimized Acetylene/Carbon Dioxide Sorption in a Dynamic Porous Crystal. *J. Am. Chem. Soc.* **2009,** *131* (15), 5516-5521.
37. Zhang, L.; Jiang, K.; Li, L.; Xia, Y.-P.; Hu, T.-L.; Yang, Y.; Cui, Y.; Li, B.; Chen, B.; Qian, G., Efficient separation of C_2H_2 from C_2H_2/CO_2 mixtures in an acid–base resistant metal–organic framework. *Chem. Commun.* **2018,** *54* (38), 4846-4849.
38. Peng, Y.-L.; Pham, T.; Li, P.; Wang, T.; Chen, Y.; Chen, K.-J.; Forrest, K. A.; Space, B.; Cheng, P.; Zaworotko, M. J.; Zhang, Z., Robust Ultramicroporous Metal–Organic Frameworks with Benchmark Affinity for Acetylene. *Angew. Chem., Int. Ed.* **2018,** *57* (34), 10971-10975.
39. Scott, H. S.; Shivanna, M.; Bajpai, A.; Madden, D. G.; Chen, K.-J.; Pham, T.; Forrest, K. A.; Hogan, A.; Space, B.; Perry Iv, J. J.; Zaworotko, M. J., Highly Selective Separation of C_2H_2 from CO_2 by a New Dichromate-Based Hybrid Ultramicroporous Material. *ACS Appl. Mater. Interfaces* **2017,** *9* (39), 33395-33400.
40. Matsuda, R.; Kitaura, R.; Kitagawa, S.; Kubota, Y.; Belosludov, R. V.; Kobayashi, T. C.; Sakamoto, H.; Chiba, T.; Takata, M.; Kawazoe, Y.; Mita, Y., Highly controlled acetylene accommodation in a metal–organic microporous material. *Nature* **2005,** *436*, 238.
41. Duan, X.; Wang, H.; Ji, Z.; Cui, Y.; Yang, Y.; Qian, G., A novel metal-organic framework for high storage and separation of acetylene at room temperature. *J. Solid State Chem.* **2016,** *241*, 152-156.
42. Duan, X.; Zhang, Q.; Cai, J.; Yang, Y.; Cui, Y.; He, Y.; Wu, C.; Krishna, R.; Chen, B.; Qian, G., A new metal–organic framework with potential for adsorptive separation of methane from carbon dioxide, acetylene, ethylene, and ethane established by simulated breakthrough experiments. *J. Mat. Chem. A* **2014,** *2* (8), 2628-2633.
43. Gao, J.; Qian, X.; Lin, R.-B.; Krishna, R.; Wu, H.; Zhou, W.; Chen, B., Mixed Metal–Organic Framework with Multiple Binding Sites for Efficient C2H2/CO2 Separation. *Angew. Chem. Int. Ed.* **2020,** *59* (11), 4396-4400.
44. Ye, Y.; Ma, Z.; Lin, R.-B.; Krishna, R.; Zhou, W.; Lin, Q.; Zhang, Z.; Xiang, S.; Chen, B., Pore Space Partition within a Metal–Organic Framework for Highly Efficient C_2H_2/CO_2 Separation. *J. Am. Chem. Soc.* **2019,** *141* (9), 4130-4136.

45. Fan, W.; Yuan, S.; Wang, W.; Feng, L.; Liu, X.; Zhang, X.; Wang, X.; Kang, Z.; Dai, F.; Yuan, D.; Sun, D.; Zhou, H.-C., Optimizing Multivariate Metal–Organic Frameworks for Efficient C2H2/CO2 Separation. *J. Am. Chem. Soc.* **2020**.
46. Li, L.; Wang, J.; Zhang, Z.; Yang, Q.; Yang, Y.; Su, B.; Bao, Z.; Ren, Q., Inverse Adsorption Separation of CO2/C2H2 Mixture in Cyclodextrin-Based Metal–Organic Frameworks. *ACS Appl. Mater. Interfaces* **2019,** *11* (2), 2543-2550.
47. Foo, M. L.; Matsuda, R.; Hijikata, Y.; Krishna, R.; Sato, H.; Horike, S.; Hori, A.; Duan, J.; Sato, Y.; Kubota, Y.; Takata, M.; Kitagawa, S., An Adsorbate Discriminatory Gate Effect in a Flexible Porous Coordination Polymer for Selective Adsorption of CO_2 over C_2H_2. *J. Am. Chem. Soc.* **2016,** *138* (9), 3022-3030.
48. Duan, J.; Higuchi, M.; Foo, M. L.; Horike, S.; Rao, K. P.; Kitagawa, S., A Family of Rare Earth Porous Coordination Polymers with Different Flexibility for CO_2/C_2H_4 and CO_2/C_2H_6 Separation. *Inorg. Chem.* **2013,** *52* (14), 8244-8249.
49. Yang, W.; Davies, A. J.; Lin, X.; Suyetin, M.; Matsuda, R.; Blake, A. J.; Wilson, C.; Lewis, W.; Parker, J. E.; Tang, C. C.; George, M. W.; Hubberstey, P.; Kitagawa, S.; Sakamoto, H.; Bichoutskaia, E.; Champness, N. R.; Yang, S.; Schröder, M., Selective CO2 uptake and inverse CO2/C2H2 selectivity in a dynamic bifunctional metal–organic framework. *Chemical Science* **2012,** *3* (10), 2993-2999.
50. Eguchi, R.; Uchida, S.; Mizuno, N., Inverse and High CO_2/C_2H_2 Sorption Selectivity in Flexible Organic–Inorganic Ionic Crystals. *Angew. Chem., Int. Ed.* **2012,** *51* (7), 1635-1639.
51. Horike, S.; Kishida, K.; Watanabe, Y.; Inubushi, Y.; Umeyama, D.; Sugimoto, M.; Fukushima, T.; Inukai, M.; Kitagawa, S., Dense coordination network capable of selective CO2 capture from C1 and C2 hydrocarbons. *J. Am. Chem. Soc.* **2012,** *134* (24), 9852-5.
52. Noro, S.-i.; Tanaka, D.; Sakamoto, H.; Shimomura, S.; Kitagawa, S.; Takeda, S.; Uemura, K.; Kita, H.; Akutagawa, T.; Nakamura, T., Selective Gas Adsorption in One-Dimensional, Flexible CuII Coordination Polymers with Polar Units. *Chem. Mater.* **2009,** *21* (14), 3346-3355.
53. Krishna, R., Methodologies for evaluation of metal–organic frameworks in separation applications. *RSC Adv.* **2015,** *5* (64), 52269-52295.
54. Subraveti, S. G.; Pai, K. N.; Rajagopalan, A. K.; Wilkins, N. S.; Rajendran, A.; Jayaraman, A.; Alptekin, G., Cycle design and optimization of pressure swing adsorption cycles for pre-combustion CO_2 capture. *Appl. Energy* **2019,** *254*, 113624.
55. Yanai, N.; Kitayama, K.; Hijikata, Y.; Sato, H.; Matsuda, R.; Kubota, Y.; Takata, M.; Mizuno, M.; Uemura, T.; Kitagawa, S., Gas detection by structural variations of fluorescent guest molecules in a flexible porous coordination polymer. *Nat. Mater.* **2011,** *10*, 787.
56. Qazvini, O. T.; Fatemi, S., Modeling and simulation pressure–temperature swing adsorption process to remove mercaptan from humid natural gas; a commercial case study. *Sep. Purif. Technol.* **2015,** *139*, 88-103.
57. Mukherjee, S.; Sikdar, N.; O'Nolan, D.; Franz, D. M.; Gascón, V.; Kumar, A.; Kumar, N.; Scott, H. S.; Madden, D. G.; Kruger, P. E., Trace CO2 capture by an ultramicroporous physisorbent with low water affinity. *Sci. Adv.* **2019,** *5* (11), eaax9171.
58. Masala, A.; Vitillo, J. G.; Mondino, G.; Grande, C. A.; Blom, R.; Manzoli, M.; Marshall, M.; Bordiga, S., CO2 Capture in Dry and Wet Conditions in UTSA-16 Metal–Organic Framework. *ACS Appl. Mater. Interfaces* **2017,** *9* (1), 455-463.

Entry for the Table of Contents

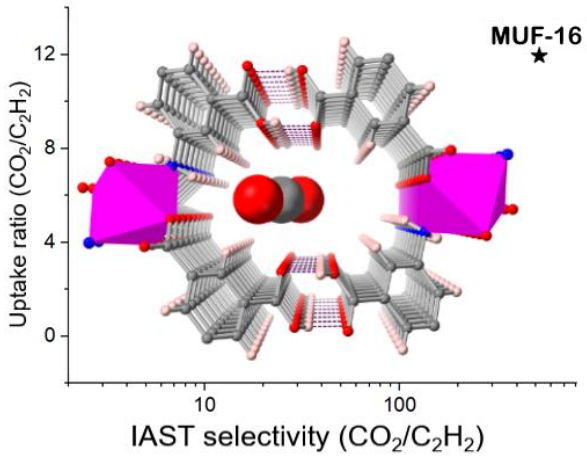

Supplementary Materials for

Selective Capture of Carbon Dioxide from Hydrocarbons Using a Metal-Organic Framework: Relevance to the Purification of Natural Gas and Acetylene

Omid T. Qazvini[1,2] and Shane G. Telfer[*,1]

[1]MacDiarmid Institute for Advanced Materials and Nanotechnology, School of Fundamental Sciences, Massey University, Palmerston North, New Zealand.

[2]Department of Chemical Engineering and Analytical Science, The University of Manchester, Oxford Road, Manchester M13 9PL, UK.

Contents

1. General procedures and information

All starting compounds and solvents were used as received from commercial sources without further purification unless otherwise noted. Elemental analyses were performed by the Campbell Microanalytical Laboratory at the University of Otago, New Zealand.

2. Synthesis

2.1 MUF-16 ([Co(Haip)$_2$])

Small-scale synthesis:

A mixture of $Co(OAc)_2 \cdot 4H_2O$ (0.625 g, 2.5 mmol), 5-aminoisophthalic acid (1.8 g, 10 mmol), methanol (80 mL) and water (5 ml) were sonicated for 20 min in a sealed 1000 mL Schott bottle, which was then heated in a pre-heated oven at 85 °C for 2 hours under autogenous pressure. After cooling the oven to room temperature, the resulting pink crystals were isolated by decanting off the mother liquor, washed with methanol several times and dried under vacuum at 130 °C for 20 h. Yield: 0.98 g (94% based on cobalt) of guest-free MUF-16.

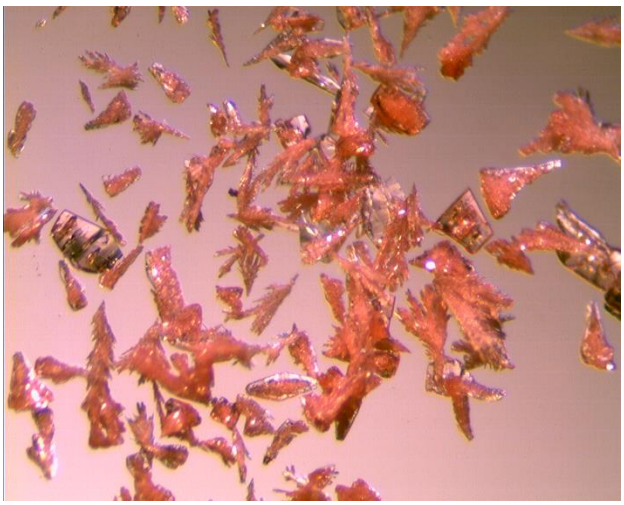

Fig. S1. Crystal of MUF-16.

2.2 MUF-16(Mn) and MUF-16(Ni) ([Mn(Haip)$_2$] and [Ni(Haip)$_2$])

A mixture of $M(ClO_4)_2 \cdot 6H_2O$ (where M = Mn or Ni) (1.25 mmol), 5-aminoisophthalic acid (2.50 mmol, 0.45 g), and NH_4NO_3 (2.50 mmol, 0.20 g) with a mixed-solvent of CH_3CN (20 mL) and CH_3OH (15 mL) were sonicated for 20 min and sealed in a 100 mL Teflon-lined stainless-steel reaction vessel and heated at 160 °C for two days under autogenous pressure. After cooling the oven to room temperature, the resulting brownish-coloured crystals were isolated by decanting off the mother liquor, then washed

with methanol several times and dried under vacuum at 130 °C for 20 h. Yields: 0.21 g (40% based on Mn) of guest free MUF-16(Mn), and 0.28 g (53% based on Ni) of guest-free MUF-16(Ni).

2.3 Elemental analyses of the MUF-16 frameworks.

	C: calcd./found	H: calcd./found	N: calcd./found
MUF-16·H_2O	43.95/43.49	3.23/3.23	6.41/6.40
MUF-16(Mn)·H_2O	44.36/44.05	3.26/3.42	6.47/6.64
MUF-16(Ni)·H_2O	43.98/44.18	3.23/3.57	6.41/6.90

3. Thermogravimetric Analysis (TGA)

Freshly prepared MOF samples were washed with MeOH, and then activated at 130 °C under vacuum for 10 hours. Samples were exposed to air for one hour and then transferred to an aluminium sample pan. Measurements were then commenced under an N_2 flow with a heating rate of 5 °C /min.

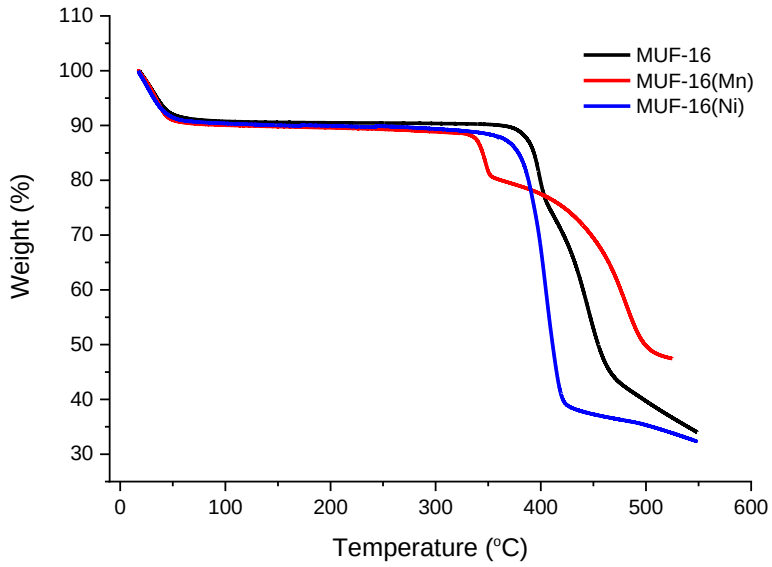

Fig. S2. TGA curves of MUF-16, MUF-16(Mn), and MUF-16(Ni) under N_2.

4. Single crystal X-ray diffraction

A Rigaku Spider diffractometer equipped with a MicroMax MM007 rotating anode generator (Cu_α radiation, 1.54180 Å), high-flux Osmic multilayer mirror optics, and a curved image plate detector was used to collect SCXRD data.

4.1 As-synthesized MUF-16, MUF-16(Ni) and MUF-16(Mn)

General

MOF crystals were analysed after removing them from methanol. Room temperature data collections produced better refinement statistics than low temperature data collections. All atoms were found in the electron density difference map. All atoms were refined anisotropically, except hydrogen atoms and certain of the water molecules in the pores (as specified below). The structures of solvated MUF-16[1] and MUF-16(Mn)[2] have been reported previously.

MUF-16

O15 of an occluded H_2O molecule was refined isotropically. Despite numerous data collections, the wR_2 value remained high due to an inherent lack of precise ordering in the material. A small (1.95 eA^{-3}) electron density peak remained near the Co site.

MUF-16(Ni)

The crystals diffracted to a resolution of just 1.0 Å thus the calculated $\sin(\theta_{max})$/wavelength is 0.4999. This limited the number of data and produced a relatively low data: parameter ratio (7.3) and low precision on the C-C bonds. Despite numerous data collections, the wR_2 value remained high due to an inherent lack of precise ordering in the material. And a small (1.55 eA^{-3}) electron density peak remained near the Ni site.

A solvent mask was calculated and 124 electrons were found in a volume of 308 $Å^3$ in one void per unit cell. This is consistent with the presence of three disordered water molecules per asymmetric unit, which account for 120 electrons per unit cell.

Table S1. Crystal data and structure refinement details for MUF-16, MUF-16(Mn) and MUF-16(Ni).

	MUF-16	**MUF-16(Mn)**	**MUF-16(Ni)**
Formula	$Co(Haip)_2 \cdot 2H_2O$	$Mn(Haip)_2 \cdot 3H_2O$	$Ni(Haip)_2 \cdot 3H_2O$
CCDC deposition no.	1948901	1948902	1948903
Empirical formula	$C_{16}H_{16}CoN_2O_{10}$	$C_{16}H_{18}MnN_2O_{11}$	$C_{16}H_{18}N_2NiO_{11}$
Formula weight	455.24	471.28	473.3
Temperature / K	292	292	293.0
Crystal system	monoclinic	monoclinic	monoclinic
Space group	I2/a	*I*2/*a*	I2/a
a / Å	15.3514(15)	25.2367(14)	15.4963(11)
b / Å	4.4232(4)	4.57990(10)	4.5780(2)
c / Å	25.614(4)	15.4895(11)	25.230(2)
α / °	90	90	90
β / °	94.294(10)	96.046(8)	96.177(8)
γ / °	90	90	90
Volume / $Å^3$	1734.4(4)	1780.34(17)	1779.5(2)
Z	4	4	4
ρ_{calc} / g cm^{-3}	1.743	1.758	1.564
μ / mm^{-1}	8.357	6.682	2.020
F(000)	932.0	972.0	856.0
Resolution range for data/ Å	0.81	0.81	1.0
Reflections collected	7472	14132	6610
Independent reflections	1594 [R_{int} = 0.0918, R_{sigma} = 0.0917]	1668 [R_{int} = 0.1054, R_{sigma} = 0.1158]	925 [R_{int} = 0.0917, R_{sigma} = 0.0852]
Data/restraints/parameters	1594/2/136	1668/1/149	925/0/126
Goodness-of-fit on F2	1.301	1.152	1.649
Final R indices [I>2σ(I)]	R_1 = 0.1185, wR_2 = 0.3035	R_1 = 0.0740, wR_2 = 0.1821	R_1 = 0.1517, wR_2 = 0.3672
Final R indices [all data]	R_1 = 0.1576, wR_2 = 0.3785	R_1 = 0.1350, wR_2 = 0.2421	R_1 = 0.2061, wR_2 = 0.4467
Largest diff. peak/hole / e $Å^{-3}$	0.93/-1.26	0.57/-0.51	0.77/-0.83

4.2 Single crystal X-ray crystallography under vacuum and loaded with CO_2

Capillary SCXRD was performed for a single crystal of MUF-16(Mn) both under vacuum and loaded with CO_2 at around 1.1 bar and 20 °C based on the following steps:
First a single crystal was chosen with an appropriate size (~ 0.1 × 0.1 × 0.1 mm) and soaked in ethanol. A small capillary tube with around 0.2 mm in diameter and 50 mm in length (which is open at both ends) was made by burning and shaping the neck of a glass pipette (referred to as the 'home-made capillary'). The home-made capillary was then used to trap the crystal inside it. Normally, the crystal flowed through the capillary carried by the ethanol stream.

The home-made capillary was then transferred into a standard 0.3 mm capillary. A long capillary (0.2 mm in diameter) was used to push the home-made capillary to the very bottom of the 0.3 mm capillary.

Around 6 or 7 crystals of cobalt chloride hydrate were then transferred to the 0.3 mm capillary and placed on the top of the home-made capillary. The cobalt chloride was used a visual indicator of the level of water vapour in the capillary based on its pink → blue colour change upon dehydration.

The top of the 0.3 mm capillary was then covered by glass wool to avoid the elutriation of cobalt chloride crystals during activation.

The capillary assembly was then connected to an adsorption apparatus (Quantachrome-Autosorb-iQ2) using appropriate Swagelok fittings (Fig. S3) and was kept under vacuum and a temperature of 140 °C for around 5 hours so that the vacuum level reached 0.0008 torr. At this point the cobalt chloride crystals were blue in colour (anhydrous).

The capillary was flame sealed to trap the crystal under vacuum. Alternatively, the capillary was filled with CO_2 to a pressure of 1.2 bar and then flame sealed.

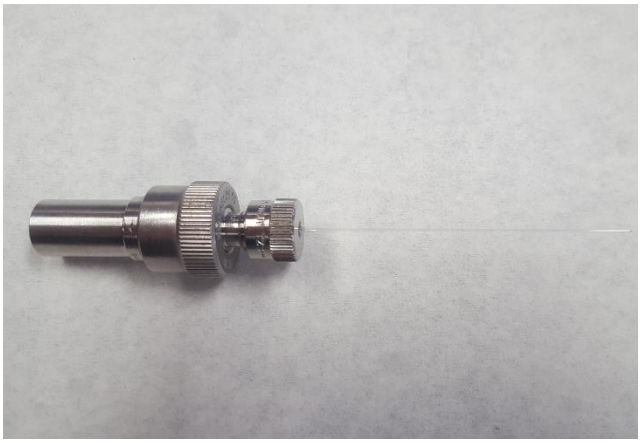

Fig. S3. Swagelok fittings for connecting capillary to Quantachrome-Autosorb-iQ2.

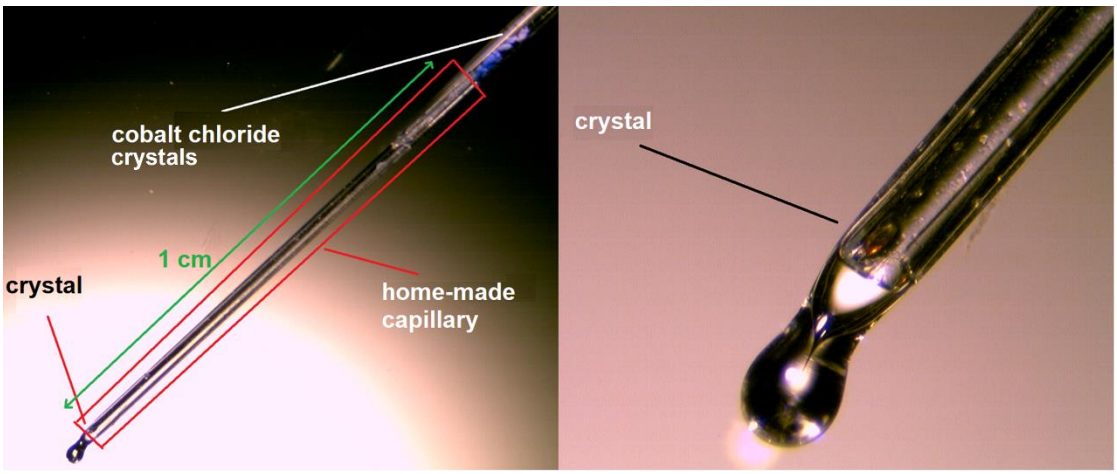

Fig. S4. Schematic and dimensions of capillaries used for SCXRD.

4.3 Refinement details for guest-free and CO_2-loaded MUF-16(Mn)

General

Certain reflections were omitted from the refinement process since they were mismeasured due to the presence of the glass capillary. All non-hydrogen atoms were found in the Fourier difference map.

MUF-16(Mn) in vacuo

The crystals diffracted to a resolution of just 0.90 Å thus the calculated $\sin(\theta_{max})$/wavelength is 0.555.

MUF-16(Mn) under CO_2

The crystals diffracted to a resolution of just 1.08 Å thus the calculated $\sin(\theta_{max})$/wavelength is 0.463. This limited the number of data and produced a relatively low data: parameter ratio (5.3) and low precision on the C-C bonds.

A strong electron density peak was observed in the middle of the pore and two weaker areas of electron density towards the pore surface. The central dense area was assigned to be an oxygen (O15) with a fixed occupancy of 1 (lowing for its location on a special position), while the other two areas were ascribed to oxygen (O16) and carbon (C17) atoms with fixed occupancies of 0.5. This describes two disordered CO_2 molecules that occupy one of two sites. The two molecules share an O atom. Overall, this equates to one CO_2 molecule per Mn centre which is in agreement with the adsorption isotherm. The C=O bond lengths were restrained to 1.16 Å and the O=C=O angle to 180°. The C and O atoms of the CO_2 were refined isotropically.

Table S2. SCXRD data and refinement details of guest-free and CO_2-loaded MUF-16(Mn).

	MUF-16(Mn) *in vacuo*	**MUF-16(Mn) under CO_2 (1.1 bar)**
Formula	$Mn(Haip)_2$	$Mn(Haip)_2 \cdot CO_2$
CCDC deposition no.	1948905	1948904
Empirical formula	$C_{16}H_{12}MnN_2O_8$	$C_{17}H_{12}MnN_2O_{10}$
Formula weight	415.22	459.23
Temperature/K	292	292
Crystal system	monoclinic	monoclinic
Space group	*I*2/a	*I*2/a
a/Å	15.4872(11)	15.5719(10)
b/Å	4.51930(10)	4.52010(10)
c/Å	25.4913(13)	25.438(2)
α/°	90	90
β/°	97.080(16)	97.108(8)
γ/°	90	90
Volume/Å^3	1770.56(17)	1776.7(2)
Z	4	4
ρ_{calc} /g cm^{-3}	1.558	1.717
μ/mm^{-1}	6.512	6.646
F(000)	844.0	932.0
Data range for refinement/ Å	0.90	1.08
Reflections collected/ind.	7515/1214 [R_{int} = 0.1632, R_σ = 0.1964]	8177/713 [R_{int} = 0.1104, R_σ = 0.0804]
Data/restraints/parameters	1214/0/129	713/90/136
Goodness-of-fit on F^2	0.862	1.216
Final R indexes [I>=2σ (I)]	R_1 = 0.0510, wR_2 = 0.0954	R_1 = 0.0868, wR_2 = 0.2280
Final R indexes [all data]	R_1 = 0.1341, wR_2 = 0.1112	R_1 = 0.1278, wR_2 = 0.2915
Largest diff. peak/hole / e Å^{-3}	0.35/-0.48	0.56/-0.58

5. Powder X-ray diffraction patterns

The data were obtained from freshly prepared MOF samples that had been washed several times with MeOH. MOF crystals were analysed right after removing them from MeOH. The two-dimensional images of the Debye rings were integrated with 2DP to give 2θ vs I diffractograms. Predicted powder patterns were generated from single crystal structures using Mercury.

For aging experiments on the frameworks, after washing as-synthesized samples several times with MeOH, they were activated and were aged in air at 70-85% relative humidity or water at 20 °C.

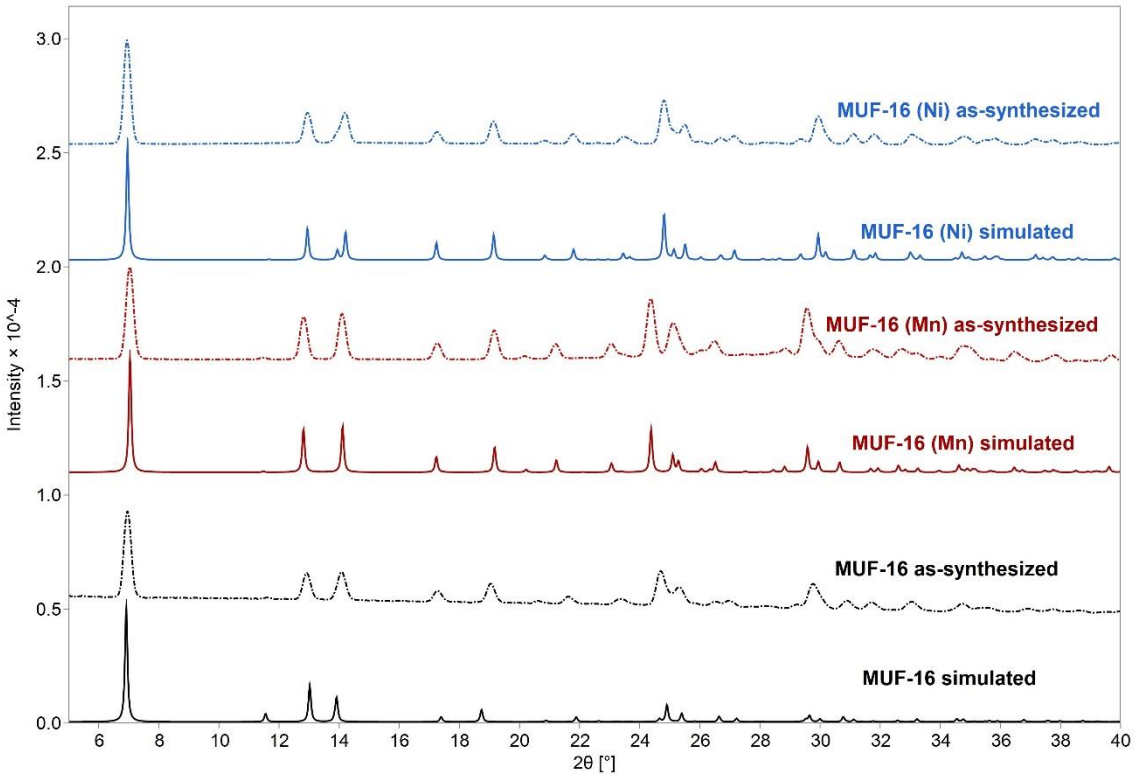

Fig. S5. PXRD patterns of MUF-16, MUF-16(Mn) and MUF-(Ni) with comparisons between measurements on as-synthesized bulk samples and diffractograms predicted from SCXRD structures.

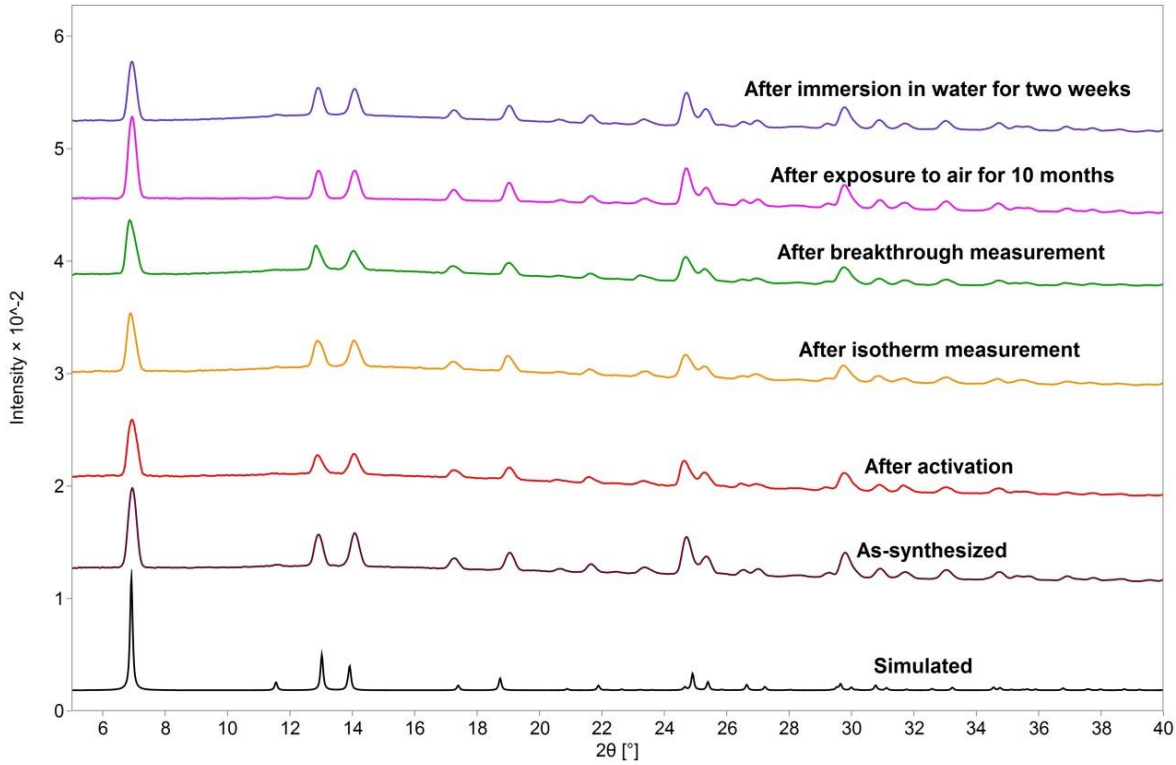

Fig. S6. PXRD patterns of MUF-16 showing that its structure remains unchanged after activation at 130 °C under vacuum, after isotherm measurements, after breakthrough experiments, after exposure to an air with relative humidity of >80% for at least 12 months and after immersion in water for two weeks.

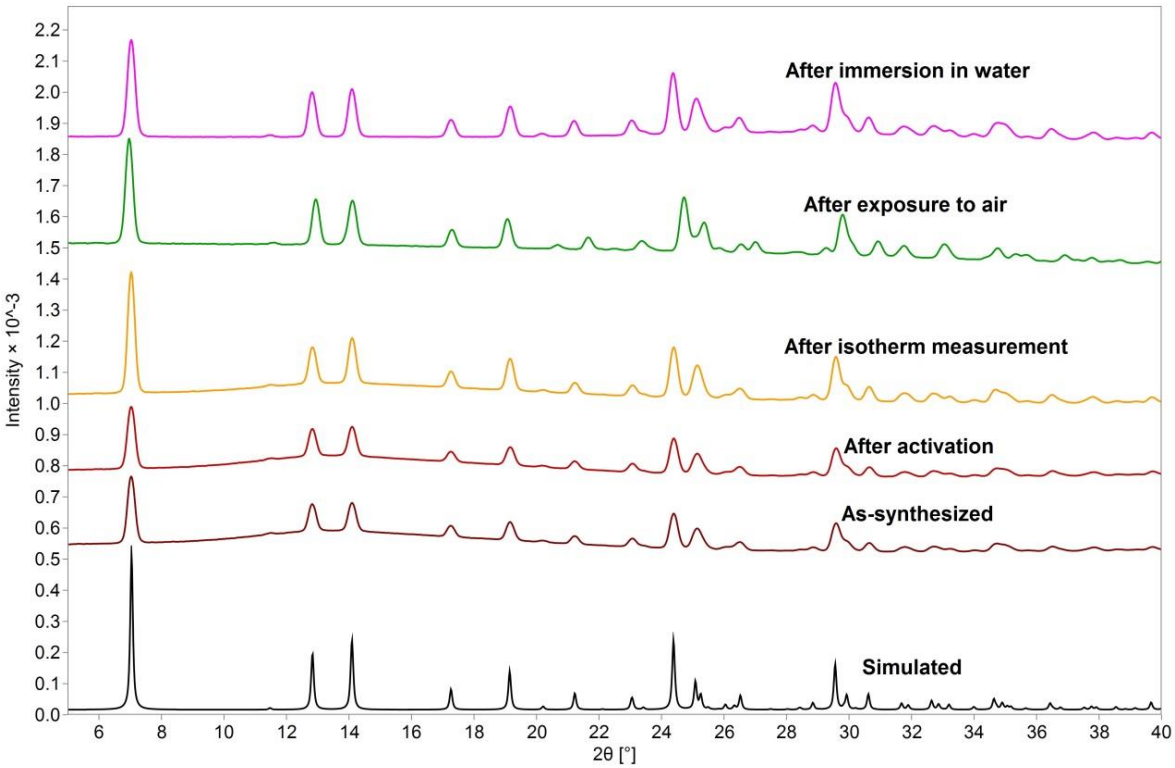

Fig. S7. PXRD patterns of MUF-16(Mn) showing that its structure remains unchanged after activation at 130 °C under vacuum, after isotherm measurements, after exposure to an air with relative humidity of >80% for at least 12 months and after immersion in water for 2 weeks.

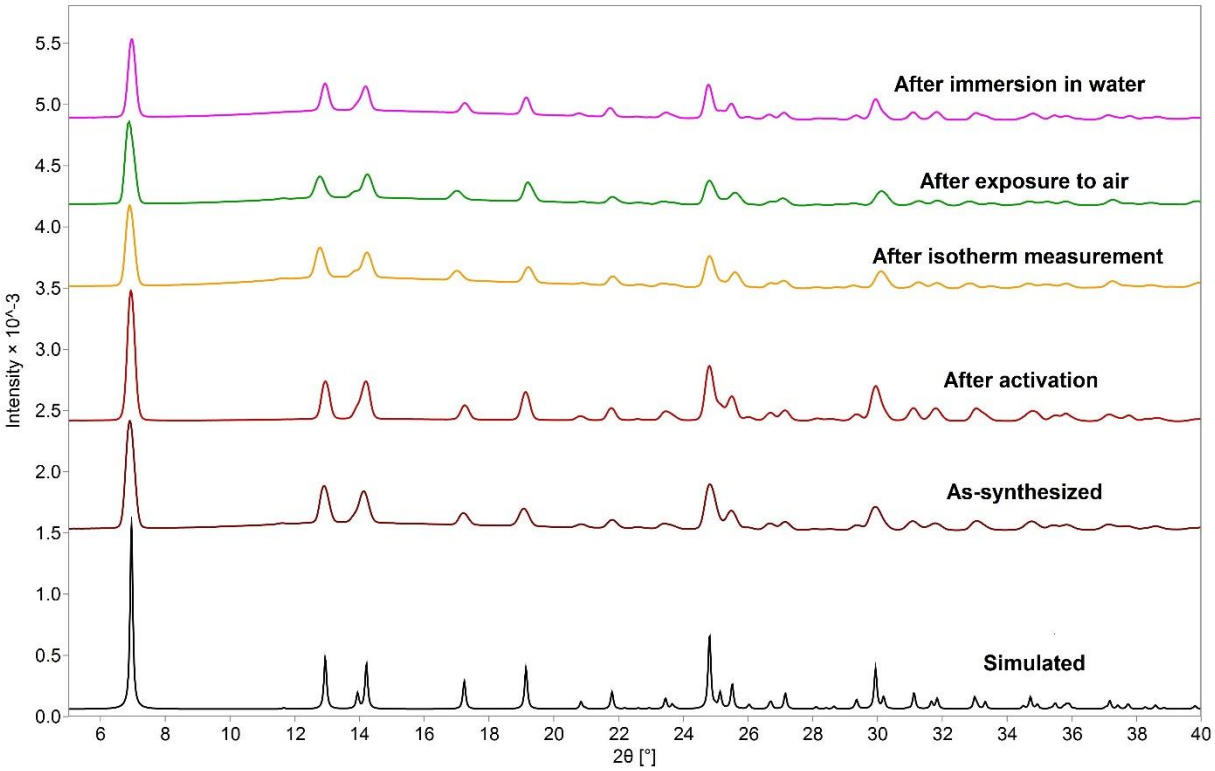

Fig. S8. PXRD patterns of MUF-16(Ni) showing that its structure remains unchanged after activation at 130 °C under vacuum, after isotherm measurements, after exposure to an air with relative humidity of >80% for at least 12 months and after immersion in water for 2 weeks.

6. Textural properties and low-pressure gas adsorption measurements

Single crystal structures of MUF-16, MUF-16(Mn) and MUF-16(Ni) were used directly for all the calculations and simulations without modification except removal of occluded solvent, where relevant. The Zeo++[3] code and RASPA2[4] were used to calculate their pore volumes and surface areas with the use of H_2 and He probes, respectively.

Table S3. Some calculated and experimentally determined properties of the MUF-16 family.

	MUF-16	MUF-16(Mn)	MUF-16(Ni)
Geometric surface area (m^2/g, Zeo++)	313	315	313
BET surface area (m^2/g, from experimental N_2 isotherm/77 K)	214	205	204
Calculated void fraction (%, RASPA2)	17.3	17.0	16.7
Calculated pore volume (cm^3/g, RASPA2)	0.10	0.11	0.11
Pore volume (cm^3/g, from experimental N_2 isotherm/77 K)	0.11	0.12	0.11

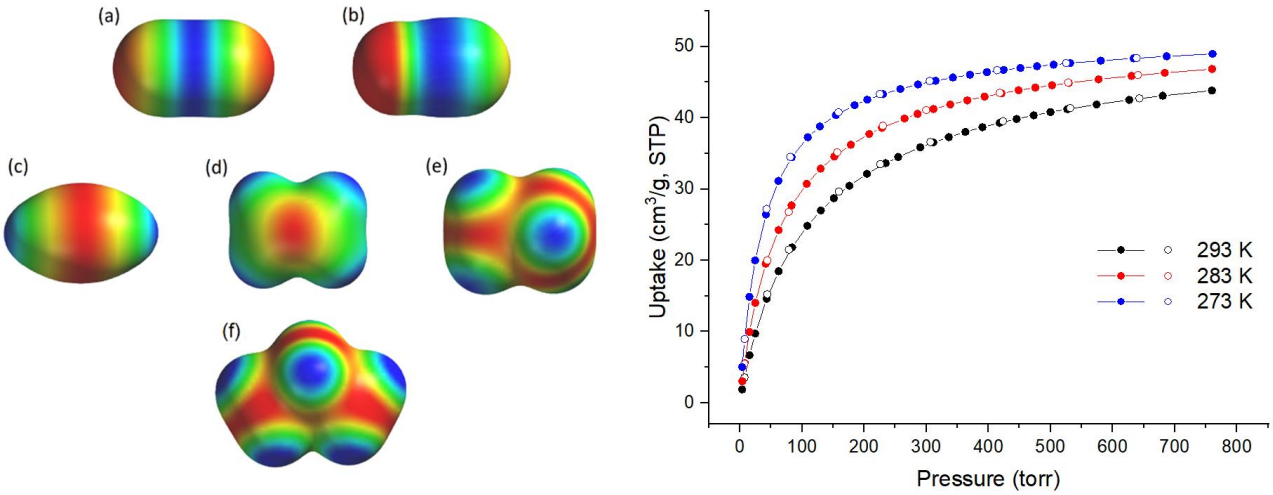

Fig. S9. Left: Electrostatic potential maps of (a) CO_2, (b) (N_2O) (c) C_2H_2, (d) C_2H_4, (e) C_2H_6 and (f) C_3H_8 Blue/green = positive; red/orange = negative; Right: Volumetric adsorption isotherms of N_2O measured at different temperatures for MUF-16.

Table S4. Physicochemical characteristics of different gasses relevant to their separation.[5-8]

	Boiling point (K)	Molecular dimensions (Å)	Polarizability ($Å^3$)	Dipole moment $\times 10^{18}$/esu cm^2	Quadrupole moment $\times 10^{26}$/esu cm^2
CO_2	216.5	3.18×3.33×5.36	2.91	0	-4.3
CH_4	111.66	3.82×3.94×4.10	2.59	0	0
C_2H_2	188.4	3.32×3.34×5.7	3.33-3.93	0	+7.5
C_2H_4	169.4	3.28×4.18×4.84	4.25	0	+1.5
C_2H_6	184.5	3.81×4.82×4.08	4.43-4.47	0	+0.65
C_3H_8	231.0	6.80×4.20×3.80	6.29-6.37	0.084	-
C_3H_6	225.4	-	6.26	0.366	-

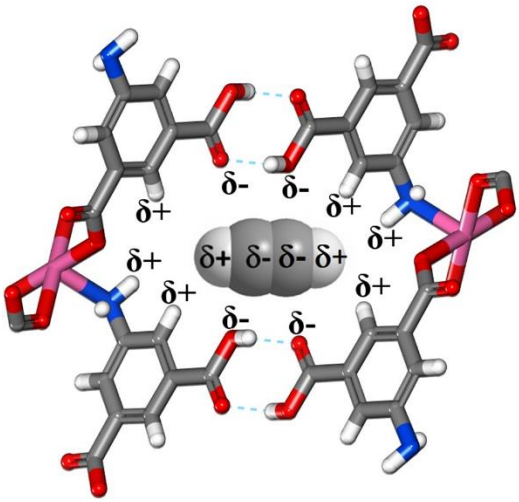

Fig. S10. Schematic of electrostatic potential distribution on the pore surface of MUF-16 leads to repulsive interactions with guest C_2H_2 molecules if they occupy the sites crystallographically observed for the binding of CO_2.

For adsorption measurements, as-synthesized samples were washed with anhydrous methanol several times and 50-1000 mg was transferred into a pre-dried and weighed sample tube. Large sample quantities (~1 g) were used to measure isotherms of the weakly-adsorbing gases to ensure that the recorded uptake measurements were reliable. To activate the sample, it was heated at rate of 10°C/min to a temperature of 130 °C under a dynamic vacuum with a turbomolecular pump for 20 hours.

Table S5. Uptake capacity of MUF-16 for CO_2 at 293 K and 1 bar.

	Uptake (wt%)	**Molecules of CO_2 per unit cell**	**Molecules of CO_2 per metal**	**Fraction of void volume occupied by CO_2***
MUF-16	9.38	3.57	0.89	0.67
MUF-16(Ni)	9.41	3.58	0.89	0.68
MUF-16(Mn)	9.90	3.74	0.93	0.70

*The fraction of the total free volume of MUF-16 that is occupied by adsorbate molecules. This was calculated from the accessible void fraction given by RASPA2 software (Table S3), the molecular volume of the CO_2 adsorbates (56.75 $Å^3$/molecule) and the total number of adsorbate molecules.

Fig. S11. Volumetric adsorption (filled circles) and desorption (open circles) isotherms of CO_2 at different temperatures for MUF-16.

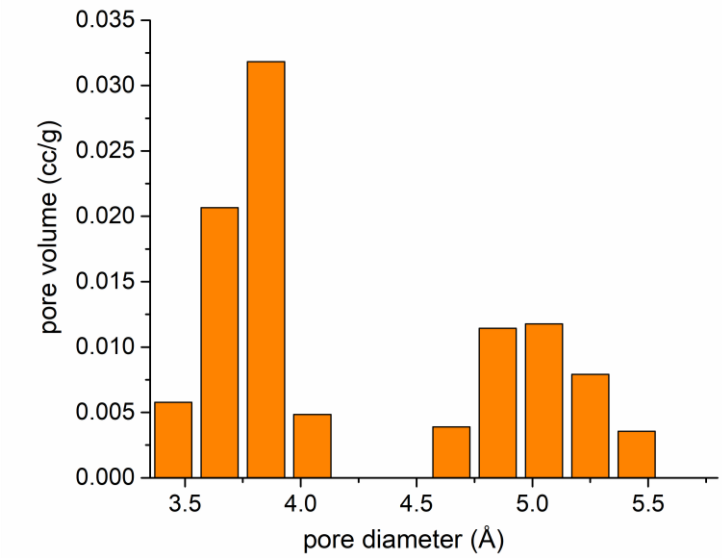

Fig. S12. Pore size distribution of MUF-16 calculated from its CO_2 adsorption isotherm at 273 K using a NLDFT method.

Fig. S13. CO_2 adsorption isotherms (293 K) of as-synthesized MUF-16 after four consecutive adsorption-desorption cycles, after exposing it to air with ~80% humidity for 6 months, and after immersion in water for 48 hours.

Fig. S14. Volumetric adsorption (filled circles) and desorption (open circles) isotherms of N_2 for MUF-16 (black), MUF-16(Mn) (red) and MUF-16(Ni) (blue) measured at 77 K.

Fig. S15. Volumetric adsorption (filled circles) and desorption (open circles) isotherms C_2H_2 (red), C_2H_6 (blue) and CH_4 (purple) measured at 195 K for MUF-16.

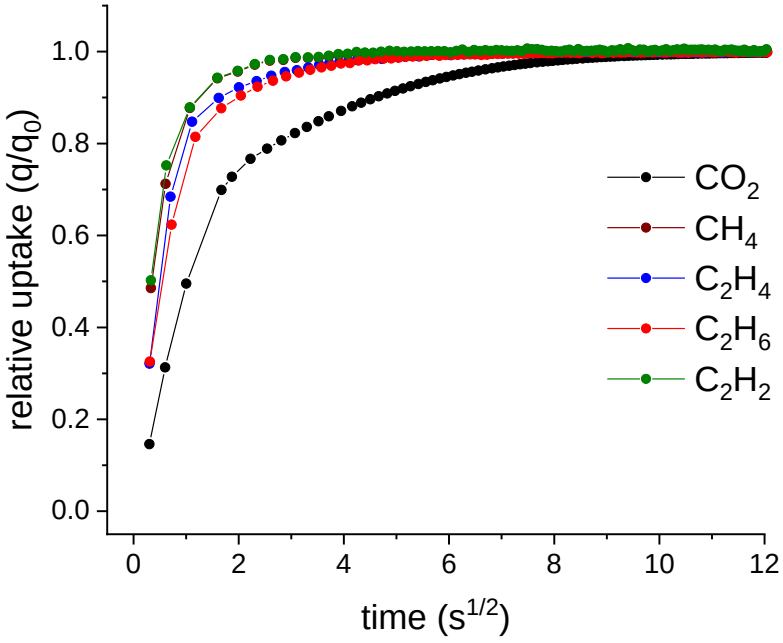

Fig. S16. Kinetic profiles of different gas uptake by MUF-16 at 293 K upon exposing an evacuated sample to a dose of gas equal to its measured total adsorption of that gas at 1 bar. q is the amount of uptake at time t and q_0 is the final uptake amount.

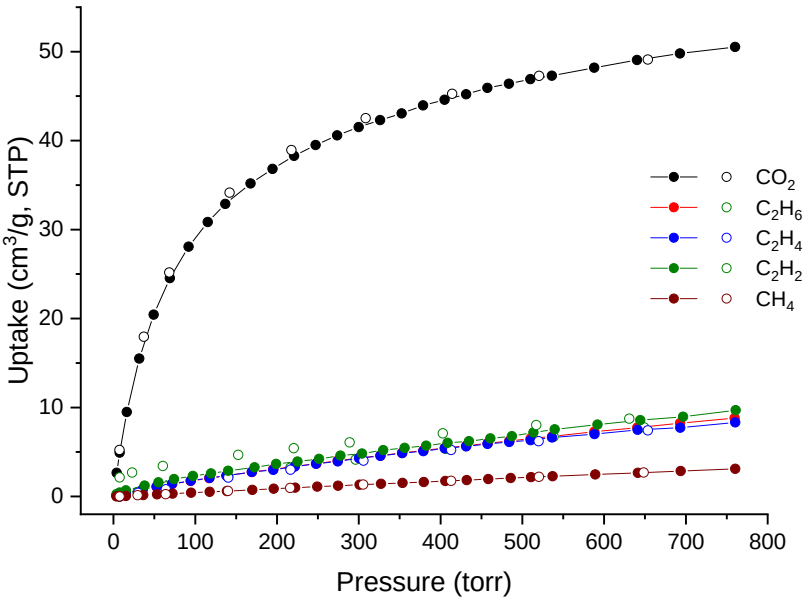

Fig. S17. Volumetric adsorption (filled circles) and desorption (open circles) isotherms of different gases by MUF-16(Mn) at 293 K.

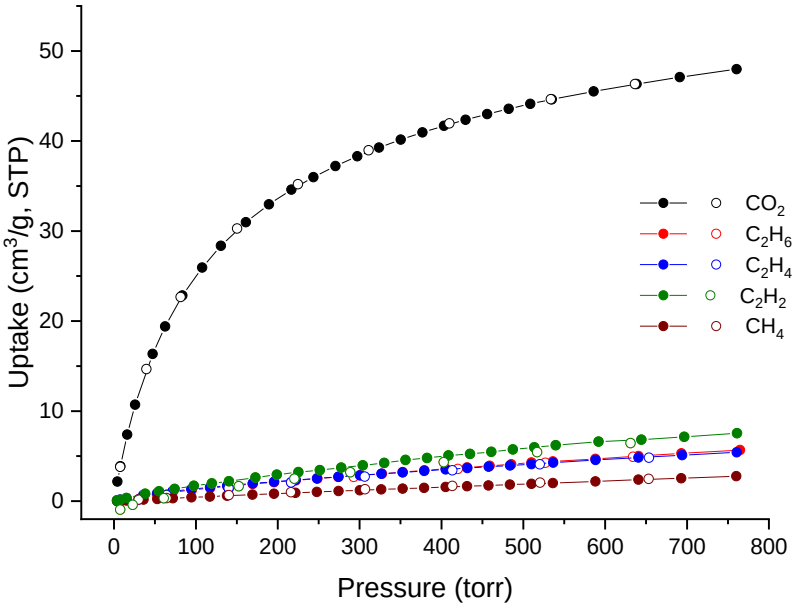

Fig. S18. Volumetric adsorption (filled circles) and desorption (open circles) isotherms of different gases by MUF-16(Ni) at 293 K.

7. Calculation of BET surface areas

BET surface areas were calculated from N_2 adsorption isotherms at 77 K according to the following procedures[9]:

1) The isotherm region where $v(1 - P/P_0)$ increases versus P/P_0, where v is the amount of N_2 adsorbed, was identified.

2) Within this isotherm region, sequential data points that led to a positive intercept in the plot of $\frac{P/P_0}{v(1-P/P_0)}$ against P/P_0, were found. This plot yields a slope a, and a positive intercept b. The amount of gas molecules adsorbed in the initial monolayer is $v_m = \frac{1}{a+b}$.

3) The BET surface area was calculated according to the following equation:

$$A_{BET} = v_m(cm^3g^{-1}) * \frac{1\ (mol)}{22400\ (cm^3)} * \sigma_0(\text{Å}^2) * N_A(mol^{-1}) * 10^{-20}(\frac{m^2}{\text{Å}^2})$$

Where N_A is Avogadro's constant, and σ_0 is the cross-sectional area of a N_2 molecule, which is 16.2 Å^2.

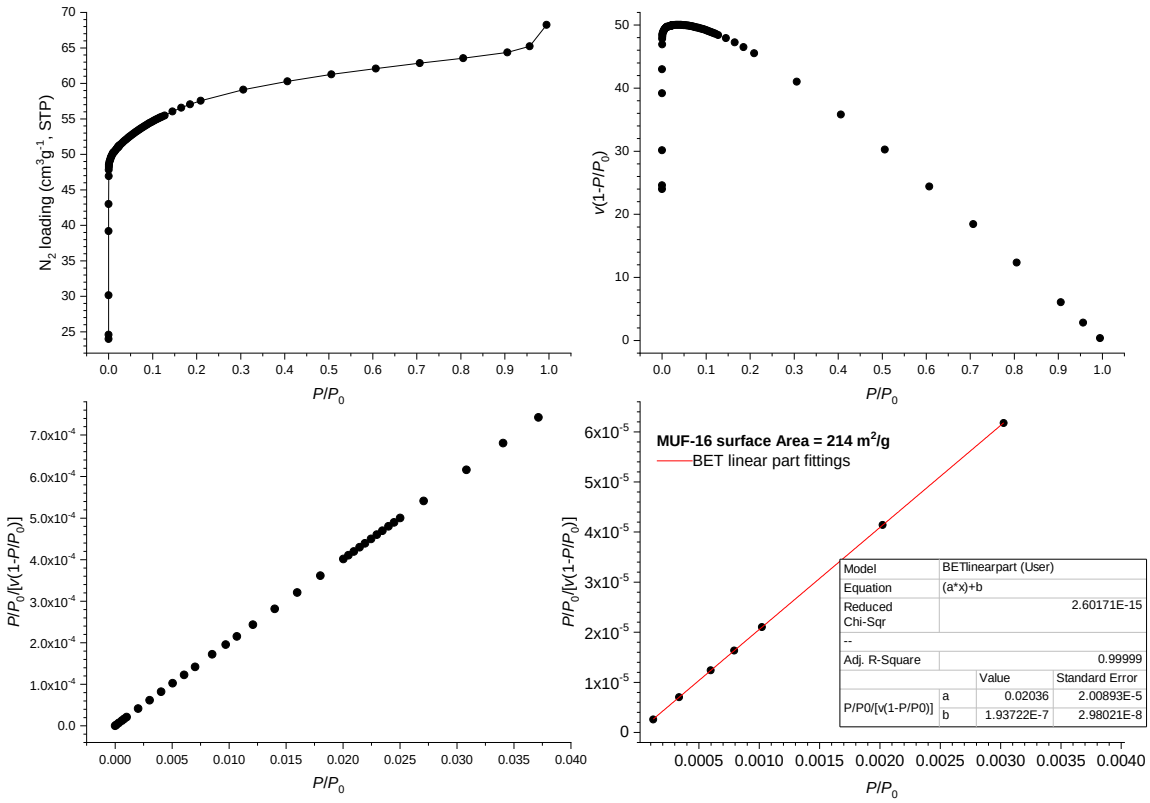

Fig. S19. N_2 adsorption isotherm at 77 K and BET surface area plots for MUF-16.

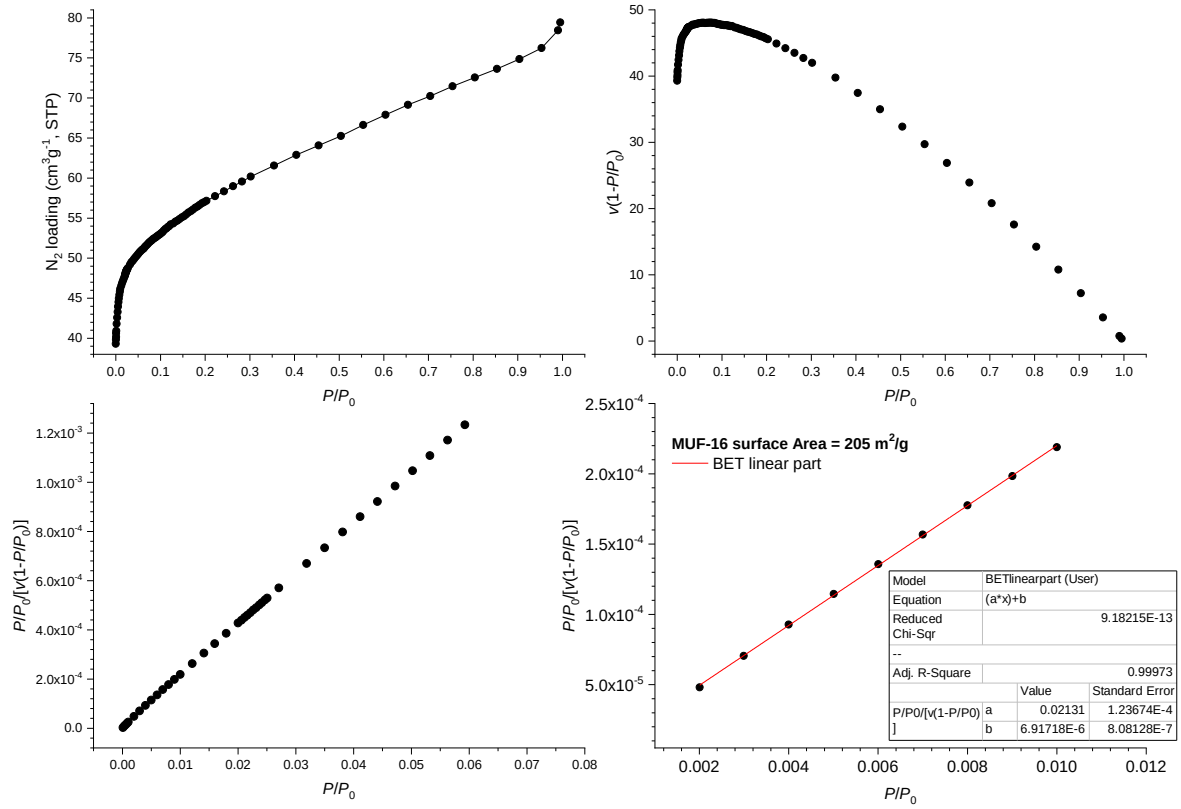

Fig. S20. N_2 adsorption isotherm at 77 K and BET surface area plots for MUF-16(Mn).

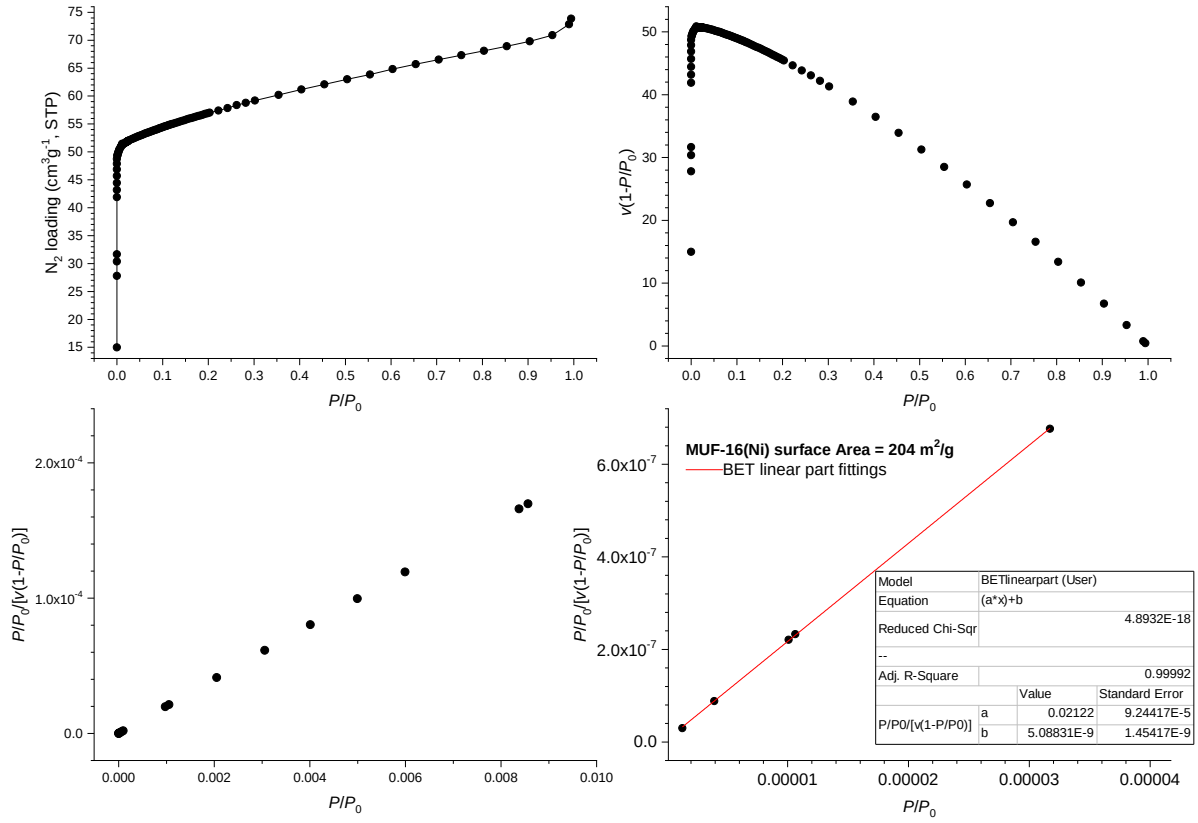

Fig. S21. N_2 adsorption isotherm at 77 K and BET surface area plots for MUF-16(Ni).

8. Heat of adsorption

Isosteric heat of adsorption (Q_{st})[10] values were calculated from isotherms measured at 293K, 298K and 303 K for CO_2. The isotherms were first fit to a viral equation:

$$\ln P = \ln N + \frac{1}{T}\sum_{i=0}^{m} a_i N^i + \sum_{i=0}^{n} b_i N^i$$

Where N is the amount of gas adsorbed at the pressure P, a and b are virial coefficients, m and n are the number of coefficients require to adequately describe the isotherm. To calculate Q_{st}, the fitting parameters from the above equation were input in to the following equation:

$$Q_{st} = -R\sum_{i=0}^{m} a_i N^i$$

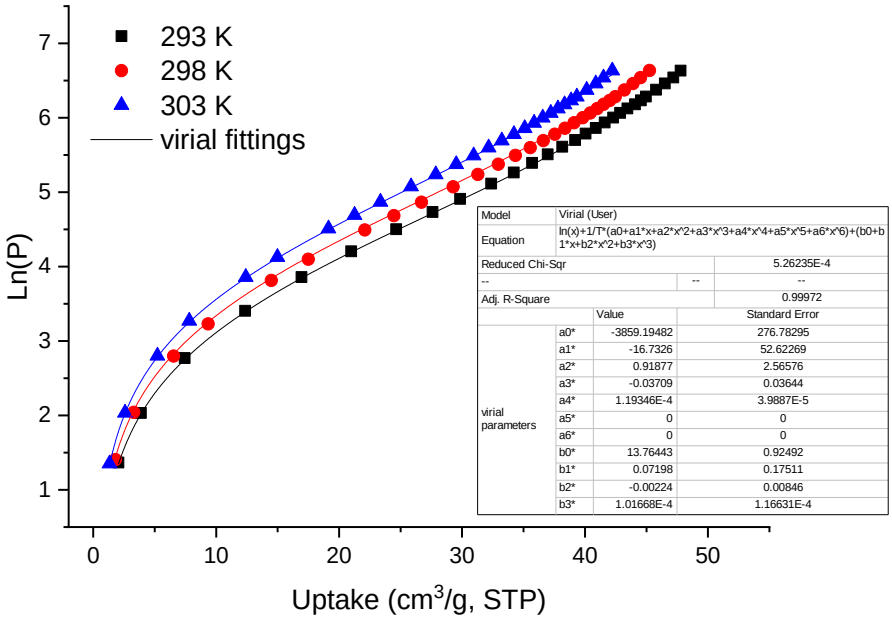

Fig. S22. Virial equation fits for CO_2 adsorption isotherms of MUF-16.

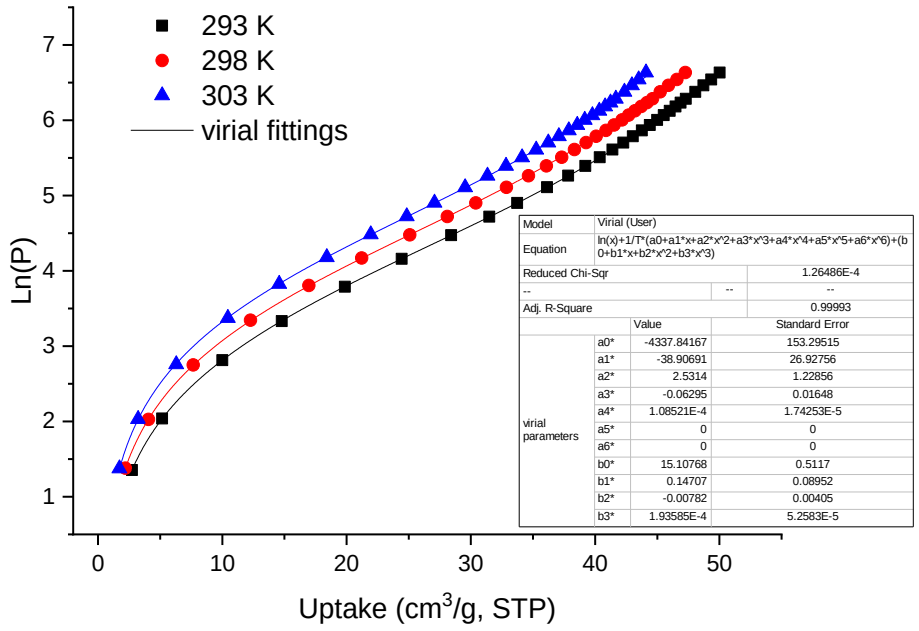

Fig. S23. Virial equation fits for CO_2 adsorption isotherms of MUF-16(Mn).

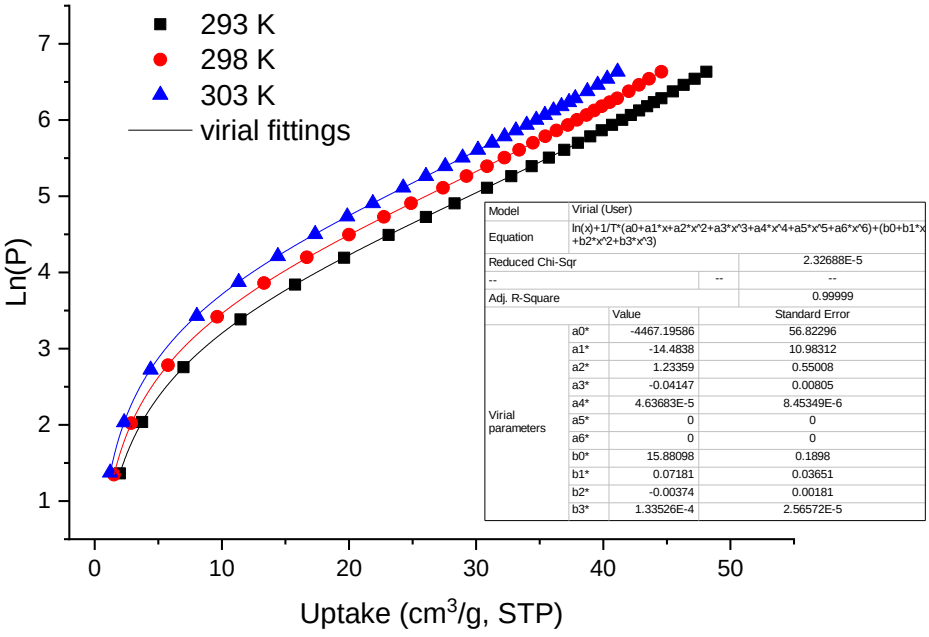

Fig. S24. Virial equation fits for CO_2 adsorption isotherms of MUF-16(Ni).

Table S6. Q_{st} values at low coverage for MUF-16 with various gases.

gas	**CO_2**	**C_2H_6**	**C_2H_4**	**C_2H_2**	**CH_4**
Q_{st} (kJ/mol)	32.3	24.8	24.9	25.8	18.6

9. IAST calculations

Mixed gas adsorption isotherms and gas selectivities for different mixtures of CO_2/C_2H_2, CO_2/C_2H_4, CO_2/C_2H_6, CO_2/N_2, CO_2/CH_4 and CO_2/H_2 at 293 K were calculated based on the ideal adsorbed solution theory (IAST) proposed by Myers and Prausnitz[11]. In order to predict the sorption performance of MUF-16 toward the separation of binary mixed gases, the single-component adsorption isotherms were first fit to a Dual Site Langmuir or a Dual Site Langmuir Freundlich model, as below:

$$q = \frac{q_1 b_1 P}{1 + b_1 P} + \frac{q_2 b_2 P}{1 + b_2 P}$$

$$q = \frac{q_1 b_1 P^{1/t_1}}{1 + b_1 P^{1/t_1}} + \frac{q_2 b_2 P^{1/t_2}}{1 + b_2 P^{1/t_2}}$$

Where q is the uptake of a gas; P is the equilibrium pressure and q_1, b_1, t_1, q_2, b_2 and t_2 are constants. These parameters were subsequently used for the IAST calculations.

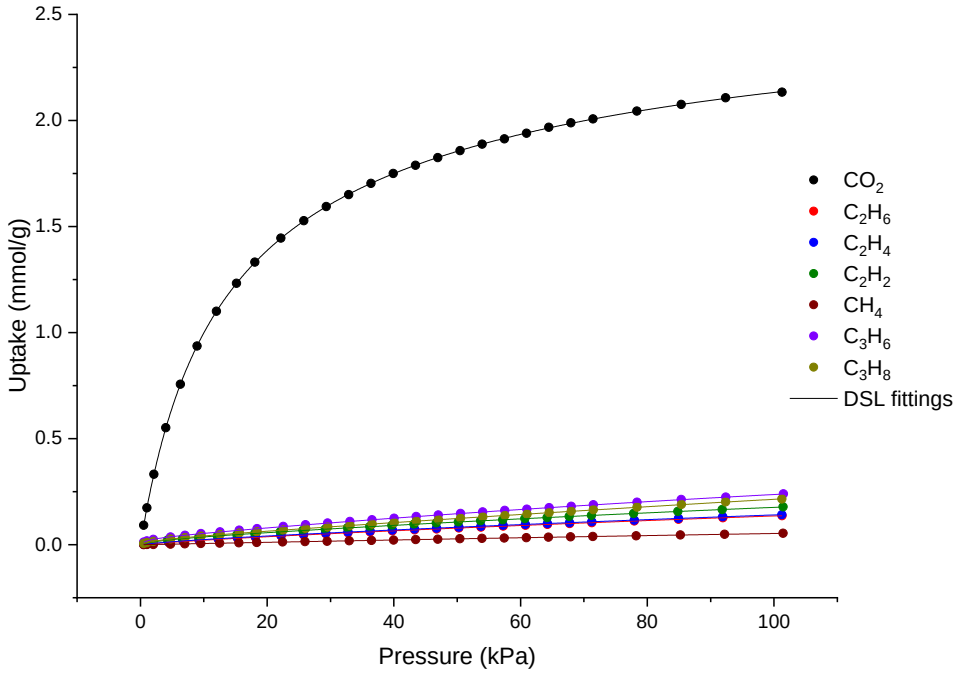

Model	DSL (User)						
Equation	q1*b1*x/(1+b1*x)+q2*b2*x/(1+b2*x)						
Plot	CO2	C2H6	C2H4	C2H2	CH4	C3H6	C3H8
q1	1.92197 ± 0.03622	0.01903 ± 7.58427E-4	0.90455 ± 0.02194	0.84858 ± 0.02172	-1.37048E-4 ± 2.62012E-5	0.92327 ± 0.02031	0.02582 ± 8.46918E-4
b1	0.09147 ± 0.00142	0.06919 ± 0.00295	0.00155 ± 4.83418E-5	0.00219 ± 7.32671E-5	2.40335 ± 2.41269	0.00289 ± 8.52827E-5	0.38985 ± 0.03262
q2	0.71591 ± 0.02029	0.91643 ± 0.02976	0.02077 ± 4.66874E-4	0.02486 ± 4.712E-4	0.63958 ± 0.01292	0.03023 ± 4.69954E-4	2.11273 ± 0.21651
b2	0.01264 ± 0.0014	0.00149 ± 6.32966E-5	0.09736 ± 0.00278	0.29065 ± 0.01171	9.04454E-4 ± 2.00076E-5	0.92871 ± 0.04824	9.83565E-4 ± 1.13365E-4
Reduced Chi-Sqr	2.547E-6	4.27057E-9	4.09689E-9	3.87189E-8	1.11837E-9	1.63183E-7	2.34956E-7
R-Square (COD)	0.99999	1	1	0.99999	1	0.99997	0.99994
Adj. R-Square	0.99999	1	1	0.99998	1	0.99996	0.99994

Fig. S25 Dual-site Langmuir fits of various adsorption isotherms for MUF-16 at 293 K.

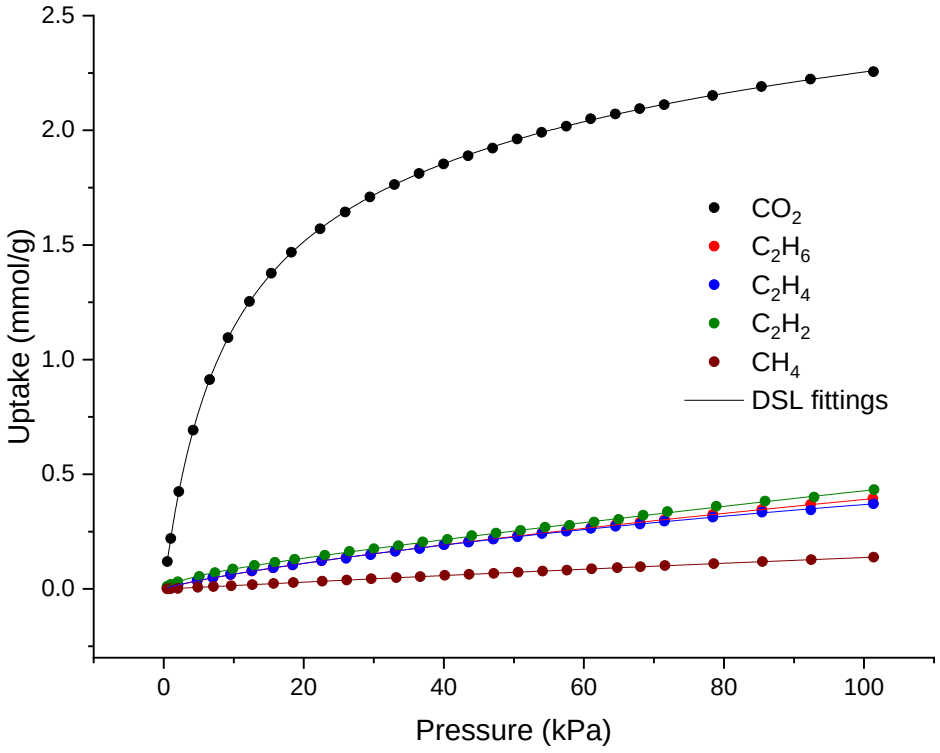

Model	DSL (User)				
Equation	q1*b1*x/(1+b1*x)+q2*b2*x/(1+b2*x)				
Plot	CO2	C2H6	C2H4	C2H2	CH4
q1	1.94289 ± 0.0227	0.04806 ± 0.00391	1.11314 ± 0.0652	3.94913 ± 1.20449	1.20612 ± 0.06748
b1	0.12229 ± 0.00169	0.09141 ± 0.009	0.00448 ± 4.81593E-	0.00102 ± 3.53725E-	0.00129 ± 8.15601E-5
q2	1.14216 ± 0.04571	2.04938 ± 0.09902	0.02464 ± 0.00777	0.06637 ± 0.00631	-8.32165E-4 ± 2.43966E
b2	0.0067 ± 8.46612E-	0.00204 ± 1.38007E-	0.20141 ± 0.10616	0.24669 ± 0.04921	10.03567 ± 38.12063
Reduced Chi-Sq	6.81414E-6	2.15657E-7	3.7049E-6	6.09794E-6	1.33437E-7
R-Square (COD)	0.99998	0.99999	0.99973	0.99963	0.99993
Adj. R-Square	0.99998	0.99998	0.99969	0.99958	0.99992

Fig. S26. Dual-site Langmuir fits of various adsorption isotherms for MUF-16(Mn) at 293 K.

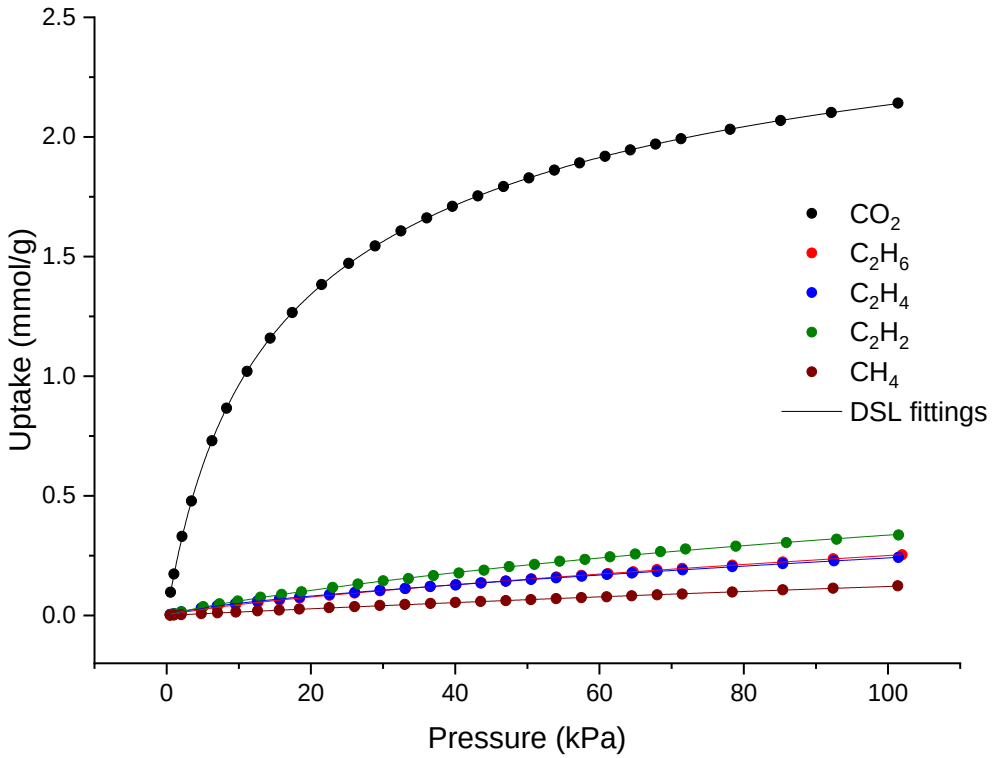

Model	DSL (User)				
Equation	q1*b1*x/(1+b1*x)+q2*b2*x/(1+b2*x)				
Plot	CO2	C2H6	C2H4	C2H2	CH4
q1	1.57274 ± 0.02824	0.05244 ± 0.00708	1.27493 ± 0.09994	0.88496 ± 0.04798	0.74301 ± 0.05154
b1	0.10503 ± 0.00153	0.07063 ± 0.01023	0.00176 ± 1.81686E-4	0.0056 ± 6.32939E-4	0.00195 ± 1.53031E-4
q2	1.12788 ± 0.01983	1.38112 ± 0.20289	0.05362 ± 0.00249	0.01883 ± 0.00847	0 ± 0
b2	0.01624 ± 7.28604E-4	0.00174 ± 3.48805E-4	0.1148 ± 0.00734	0.23099 ± 0.18081	0 ± 0
Reduced Chi-Sqr	1.49036E-6	3.73129E-7	1.65794E-7	5.0543E-6	7.98591E-7
R-Square (COD)	1	0.99994	0.99997	0.99956	0.99946
Adj. R-Square	1	0.99993	0.99997	0.99951	0.99939

Fig. S27. Dual-site Langmuir fits of various adsorption isotherms for MUF-16(Ni) at 293 K.

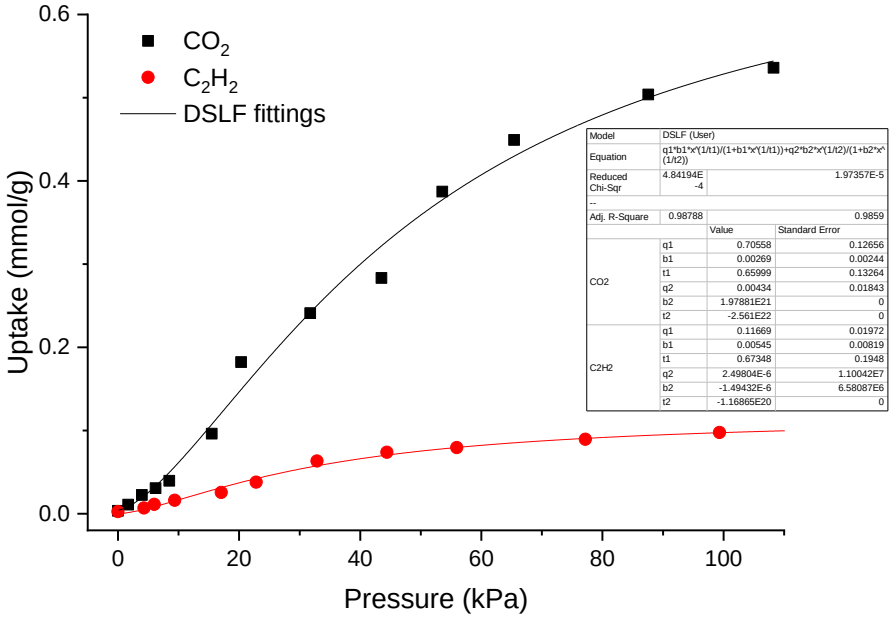

Fig. S28. Dual-site Langmuir Freundlich fits for $K_2[Cr_3O(OOCH)_6(4\text{-ethylpyridine})_3]_2[\alpha\text{-}SiW_{12}O_{40}]$ at 278 K. Isotherm data were extracted from [6] using a digitizer software.

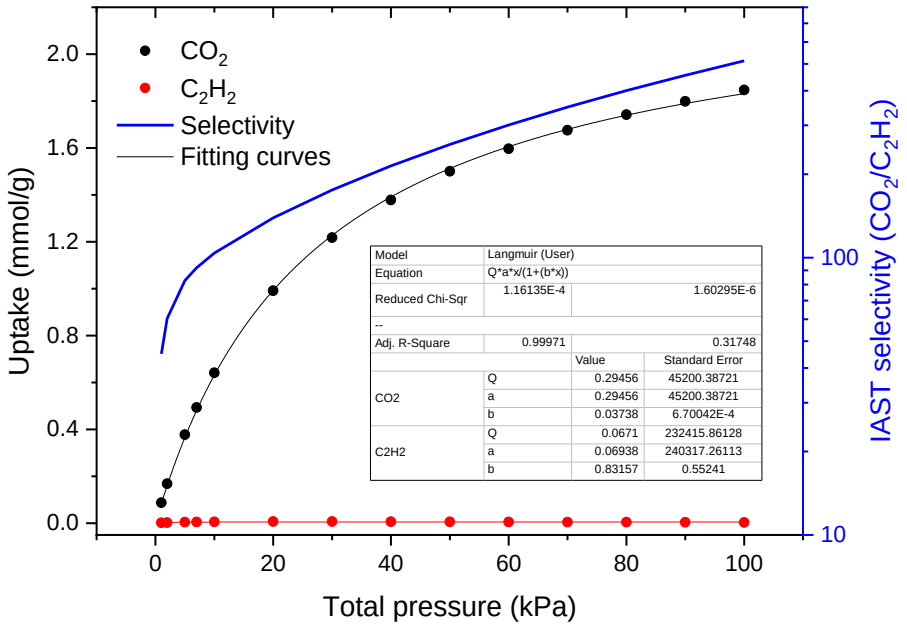

Fig. S29. Mixed-gas isotherms and selectivity of MUF-16 predicted by IAST for a mixture of 50/50 CO_2/C_2H_2 at 293 K.

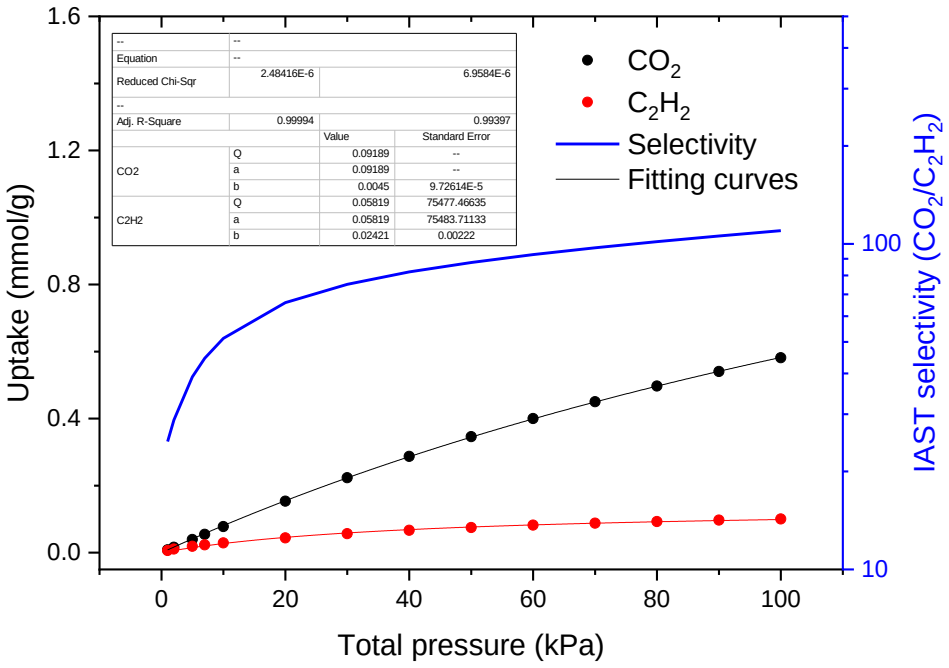

Fig. S30. Mixed-gas isotherms and selectivity of MUF-16 predicted by IAST for a mixture of 5/95 CO_2/C_2H_2 at 293 K.

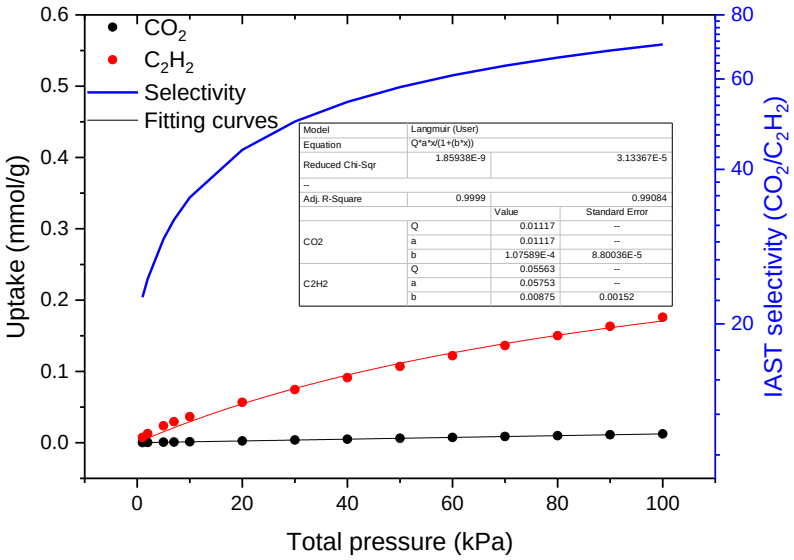

Fig. S31. Mixed-gas isotherms and selectivity of MUF-16 predicted by IAST for a mixture of 0.1/99.9 CO_2/C_2H_2 at 293 K.

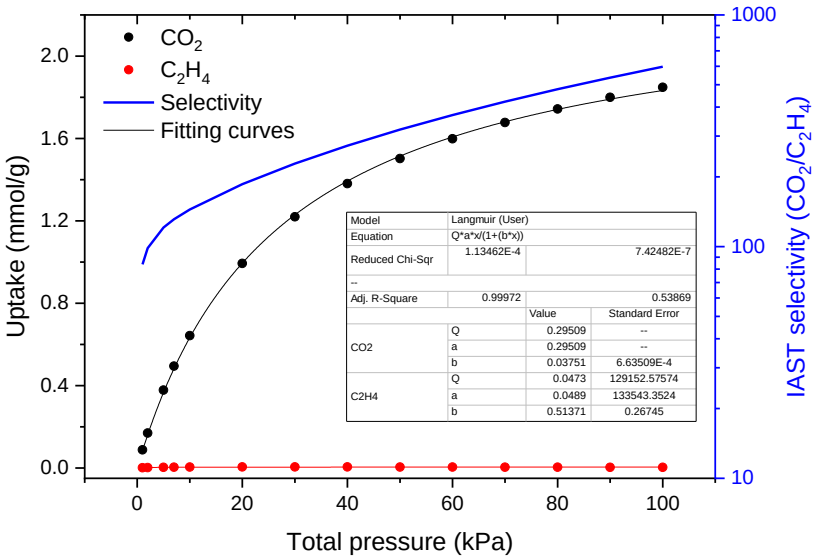

Fig. S32. Mixed-gas isotherms and selectivity of MUF-16 predicted by IAST for a mixture of 50/50 CO_2/C_2H_4 at 293 K.

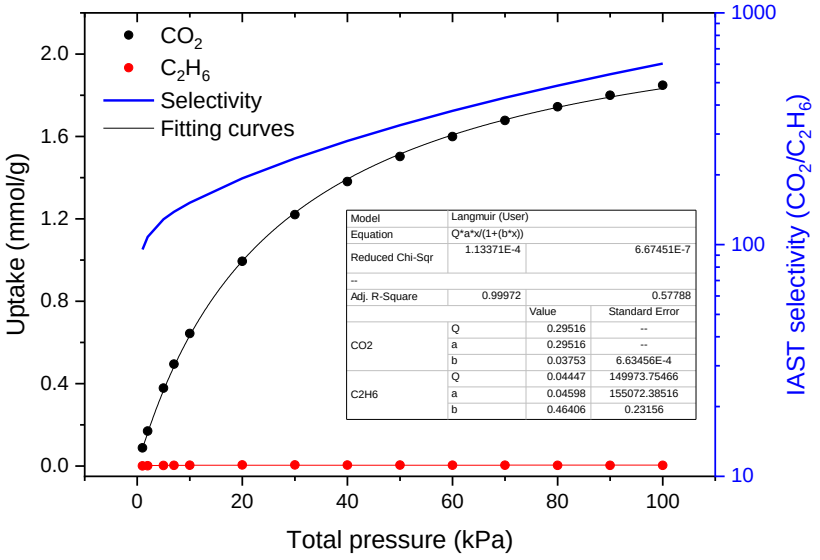

Fig. S33. Mixed-gas isotherms and selectivity of MUF-16 predicted by IAST for a mixture of 50/50 CO_2/C_2H_6 at 293 K.

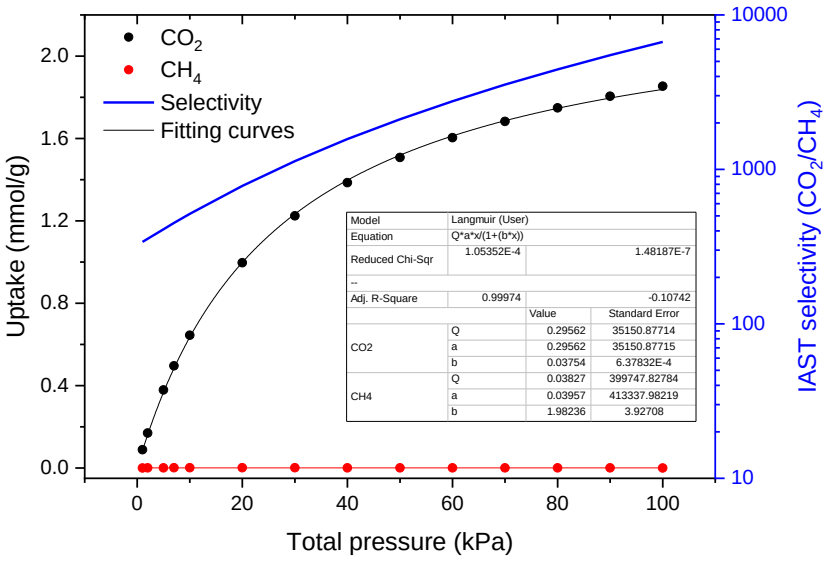

Fig. S34. Mixed-gas isotherms and selectivity of MUF-16 predicted by IAST for a mixture of 50/50 CO_2/CH_4 at 293 K.

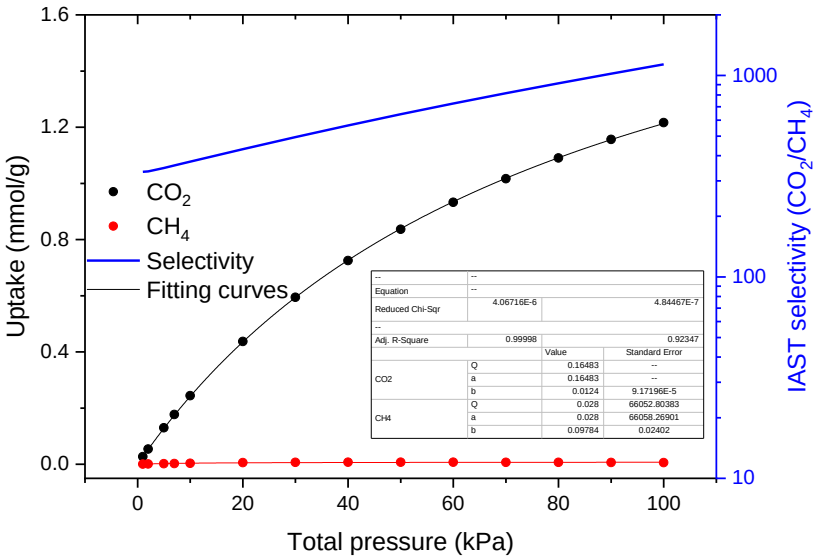

Fig. S35. Mixed-gas isotherms and selectivity of MUF-16 predicted by IAST for a mixture of 15/85 CO_2/CH_4 at 293 K.

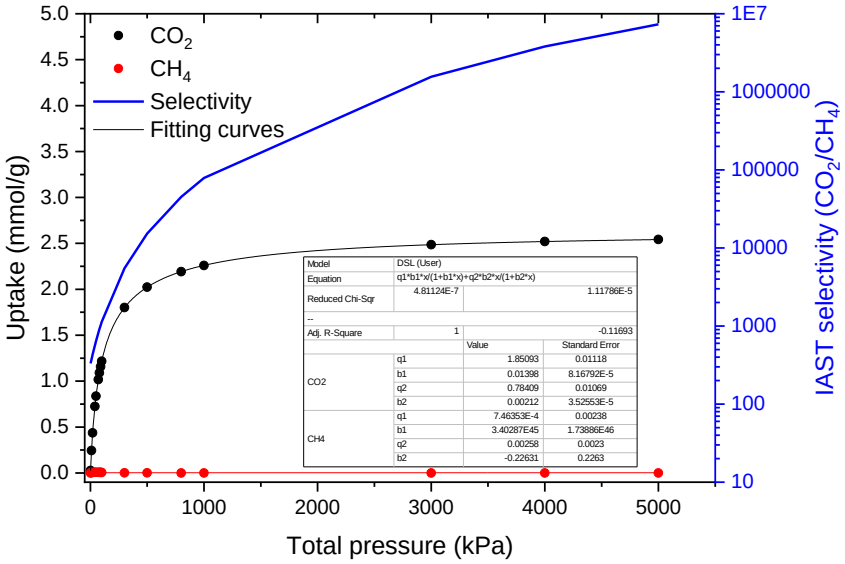

Fig. S36. Mixed-gas isotherms and selectivity of MUF-16 predicted by IAST for a mixture of 15/85 CO_2/CH_4 at 293 K up to 50 bar.

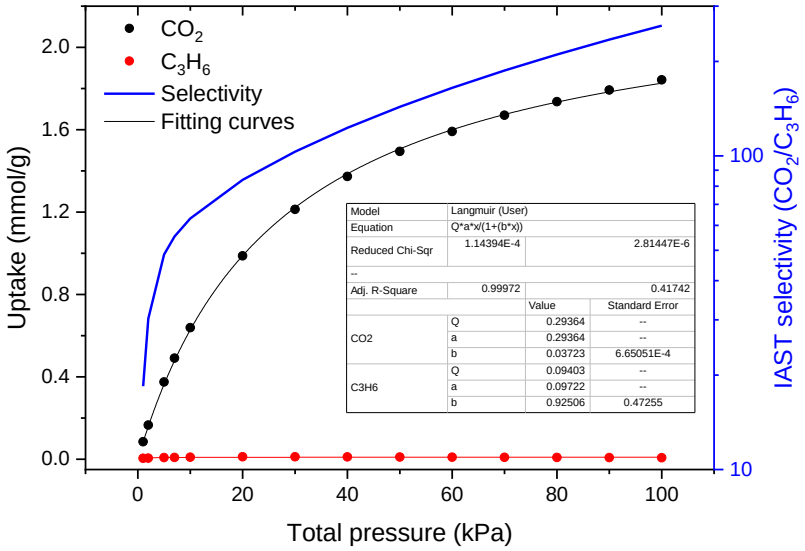

Fig. S37. Mixed-gas isotherms and selectivity of MUF-16 predicted by IAST for a mixture of 50/50 CO_2/C_3H_6 at 293 K.

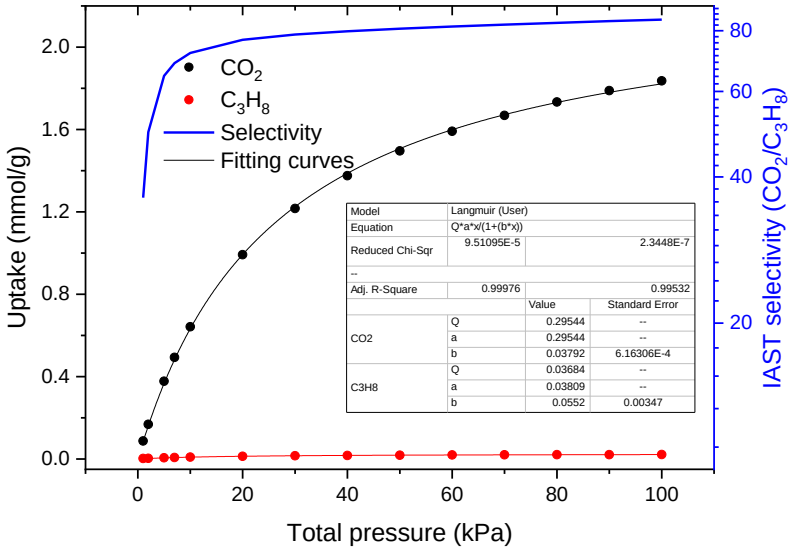

Fig. S38. Mixed-gas isotherms and selectivity of MUF-16 predicted by IAST for a mixture of 50/50 CO_2/C_3H_8 at 293 K.

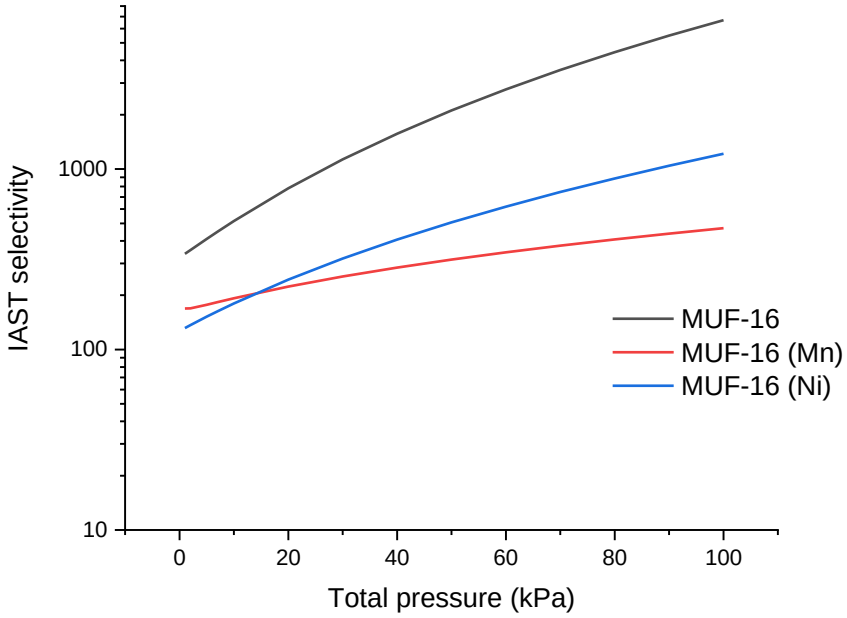

Fig. S39. IAST selectivity for a 50/50 mixture of CO_2/CH_4 at 293 K for the MUF-16 family.

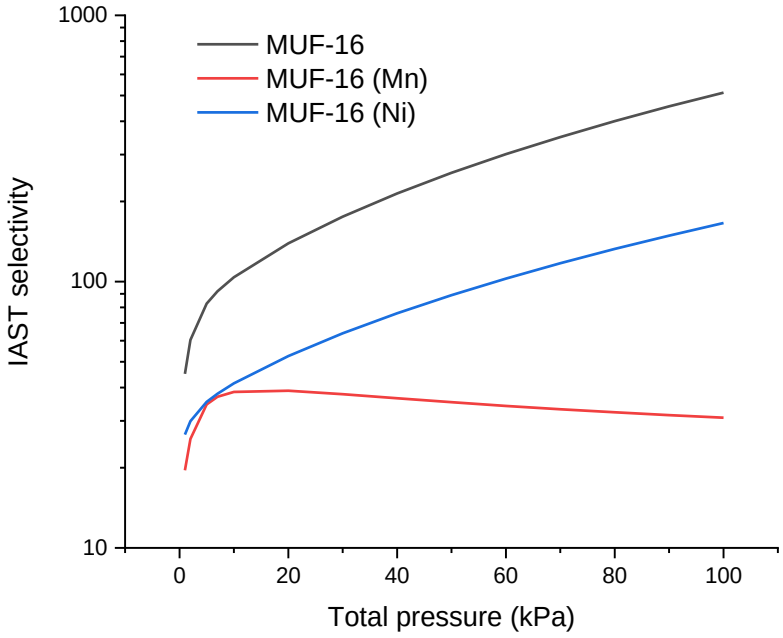

Fig. S40. IAST selectivity for a 50/50 mixture of CO_2/C_2H_2 at 293 K for the MUF-16 family.

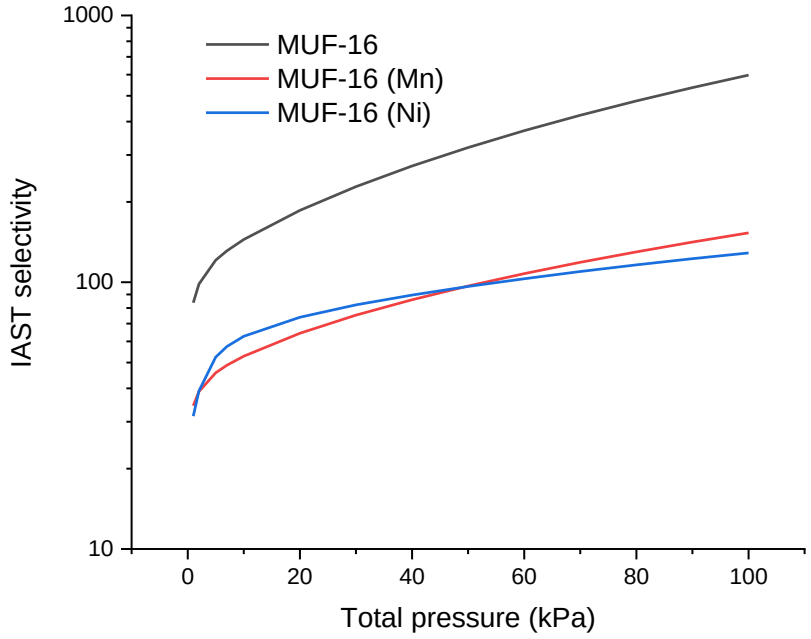

Fig. S41. IAST selectivity for a 50/50 mixture of CO_2/C_2H_4 at 293 K for the MUF-16 family.

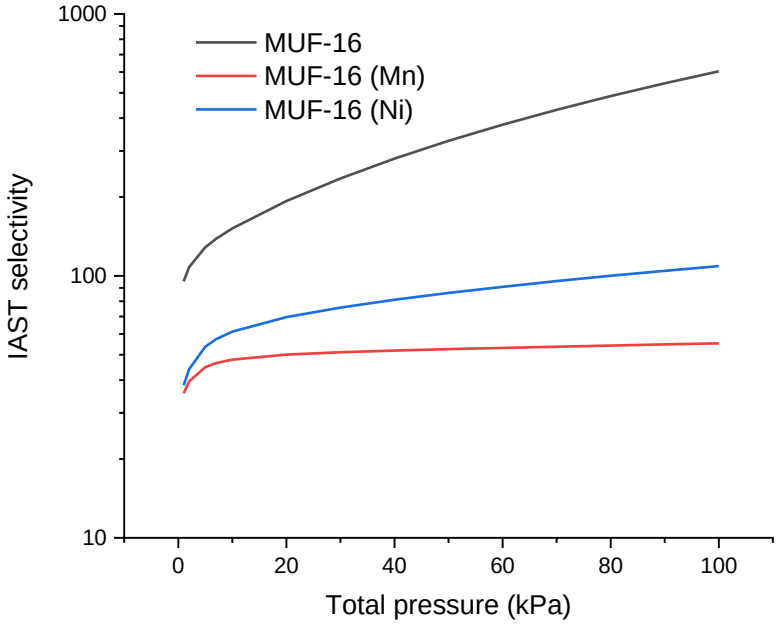

Fig. S42. IAST selectivity for a 50/50 mixture of CO_2/C_2H_6 at 293 K for the MUF-16 family.

10. Breakthrough separation experiments and simulations

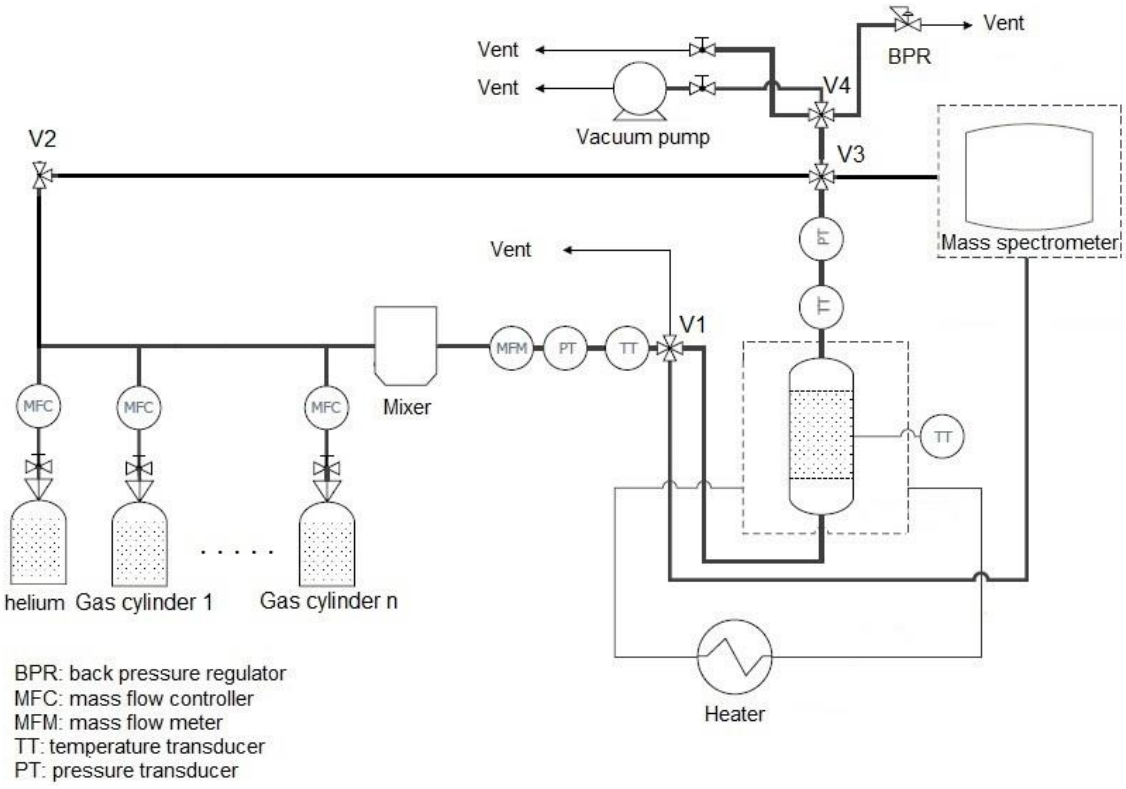

Fig. S43. A schematic of the experimental column breakthrough setup.

Table S7. Summary of inlet gas feed streams, outlet compositions and associated data for experimental breakthrough tests using a MUF-16 adsorbent bed.

Gas mixture	Total pressure (bar)	Inlet CO_2 partial pressure (bar)	Flowrate (mL_N/min)	Upper limit for CO_2 concentration in effluent (ppmv)	Breakthrough point of CO_2 (min)	CO_2 concentration in effluent at breakthrough point (ppmv)	Dynamic adsorption capacity (mmol/g)	Equilibrium adsorption capacity (mmol/g)
CO_2/CH_4 (50/50)	1	0.5	6	500	10.6	600	1.53	1.85
CO_2/CH_4 (15/85)	1	0.15	6	520	25.6	600	1.13	1.23
CO_2/CH_4 (15/85)	9	0.15	6	360	44.8	600	2.01	-
$CO_2/CH_4+C_2H_6+C_3H_8$ (15/80/4/1)	1	0.15	6	520	24.6	600	1.09	1.23
$CO_2/CH_4+C_2H_6+C_3H_8$ (15/80/4/1)	9	0.15	6	390	42.5	600	1.93	-
CO_2/C_2H_2 (50/50)*	1	0.33	6	500	12.3	600	1.23	1.64
CO_2/C_2H_2 (5/95)	1	0.035	6.85	540	15.1	600	0.18	0.46
CO_2/C_2H_4 (50/50)*	1	0.33	6	500	11.9	600	1.19	1.64
CO_2/C_2H_6 (50/50)*	1	0.33	6	500	12.2	600	1.22	1.64

* 2 mL_N/min of helium was used as carrier gas in this experiment.

10.1. CO_2/CH_4 and $CO_2/CH_4+C_2H_6+C_3H_8$ breakthrough separations

Activated MUF-16 (0.9 g) was placed in an adsorption column (6.4 mm in diameter × 11 cm in length) to form a fixed bed. The adsorbent was activated at 130 °C under high vacuum for 7 hours and then the column was left under vacuum for another 3 hours while being cooled to 20 °C. The column was then purged under a 20 mL_N/min flow of He gas for 1 hr at 1.1 bar prior to the breakthrough experiment. A gas mixture containing CO_2/CH_4 or $CO_2/ CH_4+ C_2H_6+C_3H_8$ was introduced to the column at 1.1 bar and 9 bar for CO_2/CH_4 and $CO_2/CH_4+C_2H_6+C_3H_8$) and 20 °C.

A feed flowrate of 6 mL_N/min was set. The operating pressure was controlled at 1.1 or 9 bar with a back-pressure regulator. The outlet composition was continuously monitored by a SRS UGA200 mass spectrometer. The CO_2 was deemed to have broken through from the column when its concentration reached 600 ppmv.

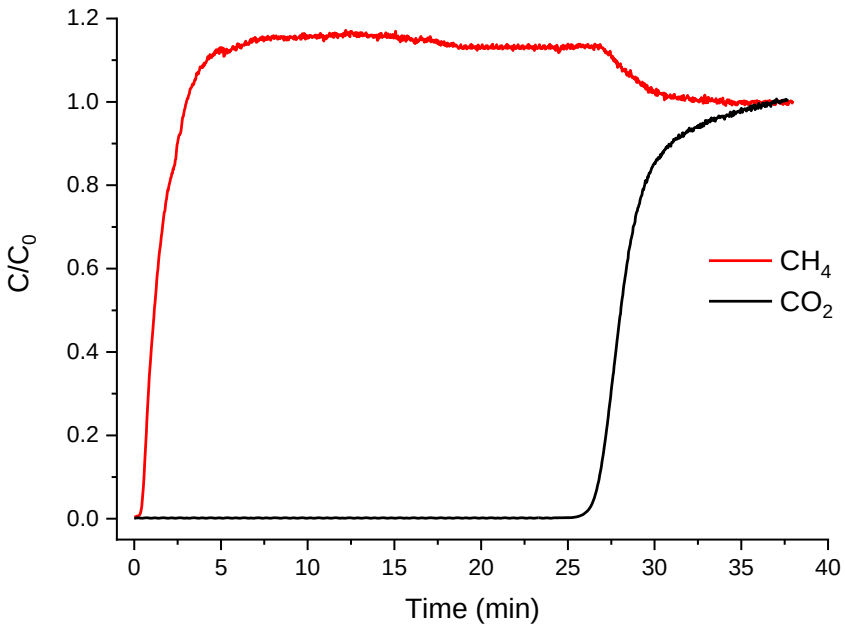

Fig. S44. Experimental breakthrough curves for a mixture of 15/85 CO_2/CH_4 at 1.1 bar and 293 K in an adsorption column packed with MUF-16.

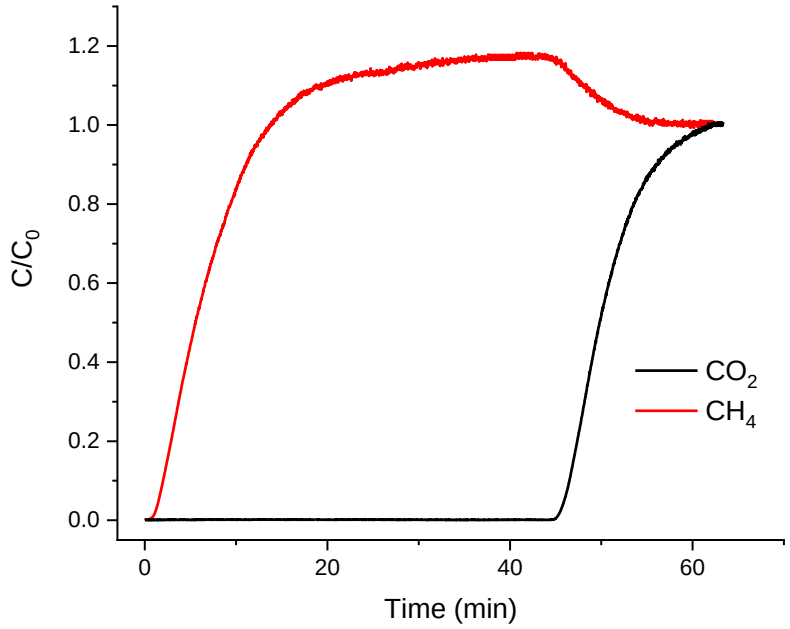

Fig. S45. Experimental breakthrough curves for a mixture of 15/85 CO_2/CH_4 at 9 bar and 293 K in an adsorption column packed with MUF-16.

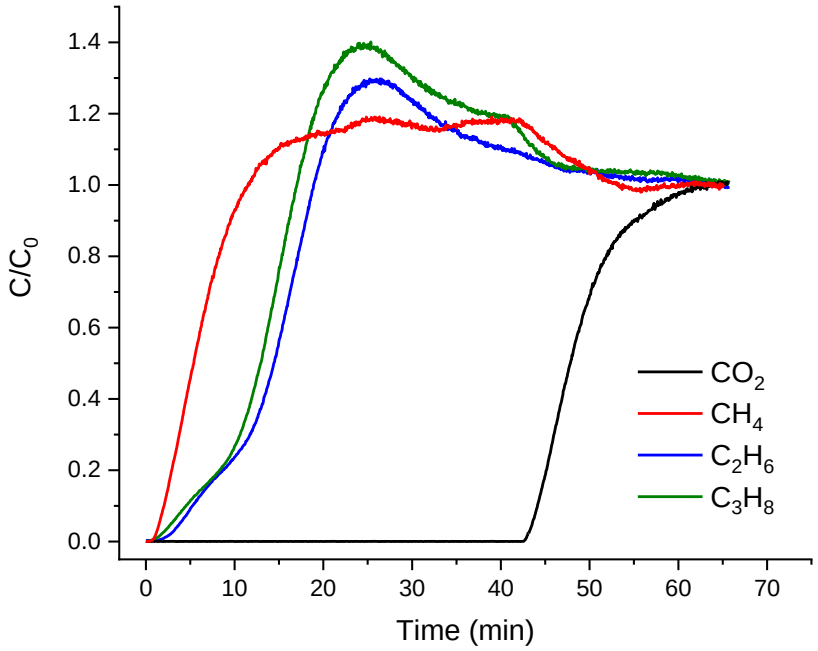

Fig. S46. Experimental breakthrough curves for a mixture of 15/80/4/1 $CO_2/CH_4/C_2H_6/C_3H_8$ at 9 bar and 293 K in an adsorption column packed with MUF-16.

10.1.4. Simulations of CO_2/CH_4 breakthrough curves

The simulation of breakthrough curves was carried out using a previously reported method.[12, 13] A value for the mass transfer coefficient (k) was obtained by empirical tuning the steepness of the predicted breakthrough curves to match the experimental curve. The mass transfer coefficient tuned in this way was later used to predict breakthrough curves for other feed mixtures and operating pressures. A summary of adsorption column parameters and feed characterizations are presented in Table S8.

Table S8. Adsorption column parameters and feed characterizations used for the simulations for MUF-16.

Adsorption bed	**Feed**
Length: 110 mm Diameter: 6.4 mm Amount of adsorbent in the bed: 0.9 g Adsorbent density: 1.674 g/cm^3 Adsorbent average radius: 0.2 mm k_{CO2}: 0.029 s^{-1} k_{CH4}: 0.00021 s^{-1}	Flow rate: 6 mL$_N$/min Temperature: 293 K Pressure: 1.1 bar Carrier gas flow rate: No carrier gas was used

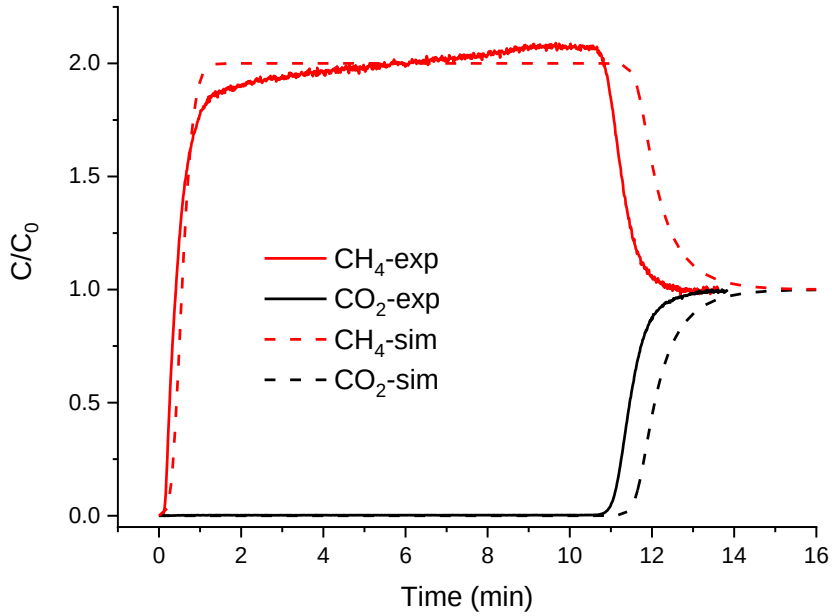

Fig. S47. Experimental breakthrough curves in comparison to simulated one for a mixture of 50/50 CO_2/CH_4 at 1.1 bar and 293 K in an adsorption column packed with MUF-16.

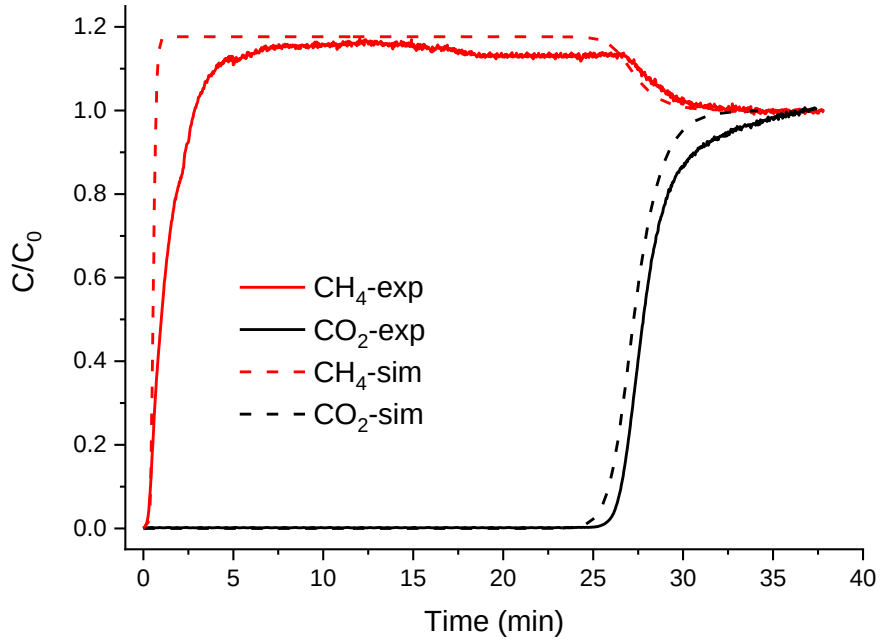

Fig. S48. Experimental breakthrough curves in comparison to simulated one for a mixture of 15/85 CO_2/CH_4 at 1.1 bar and 293 K in an adsorption column packed with MUF-16.

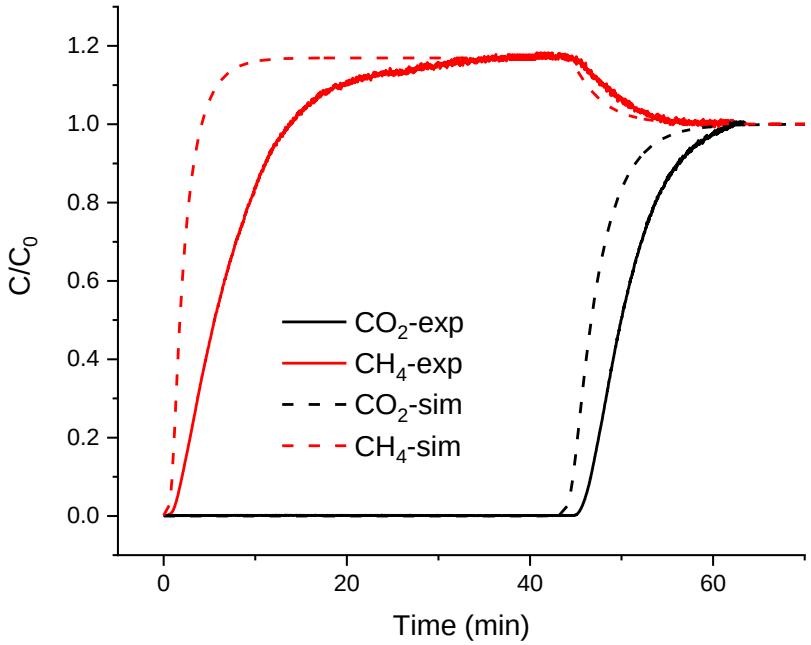

Fig. S49. Experimental breakthrough curves in comparison to simulated one for a mixture of 15/85 CO_2/CH_4 at 9 bar and 293 K in an adsorption column packed with MUF-16.

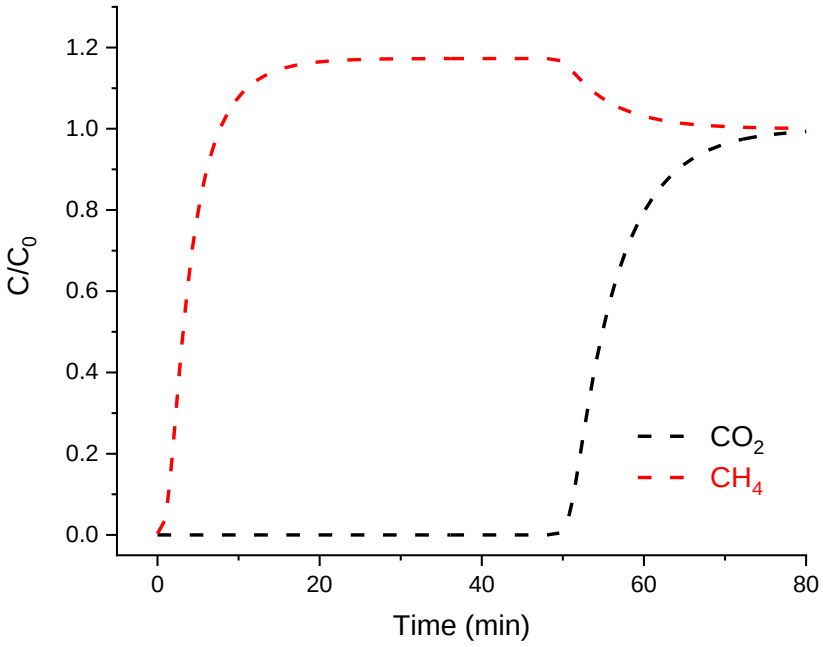

Fig. S50. Simulated breakthrough curves for a mixture of 15/85 CO_2/CH_4 at 50 bar and 293 K in an adsorption column packed with MUF-16.

10.2 CO_2/C2 hydrocarbon separations

In a typical breakthrough experiment, 0.9 g of activated MUF-16 was placed in an adsorption column (6.4 mm in diameter × 11 cm in length) to form a fixed bed. The adsorbent was activated at 130 °C under high vacuum for 7 hours and then the column was left under vacuum for another 3 hours while being cooled to 20 °C. The column was then purged under a 20 mL_N/min flow of He gas for 1 hr at 1.1 bar prior to the breakthrough experiment. A gas mixture containing different gas pairs of CO_2 and C_2H_2, C_2H_6 or C_2H_4 along with He as a carrier gas was introduced to the column at 1.1 bar and 20 °C. A feed flowrate of 6.0 or 6.85 mL_N/min (including helium) was set for the experiments with 50/50 and 5/95 mixture of gases, respectively, and the flowrate of He in the feed was kept constant at 2 mL_N/min for all the experiments. The operating pressure was controlled at 1.1 bar with a back-pressure regulator. The outlet composition was continuously monitored by a SRS UGA200 mass spectrometer. The CO_2 was deemed to have broken through from the column when its concentration reached 600 ppmv.

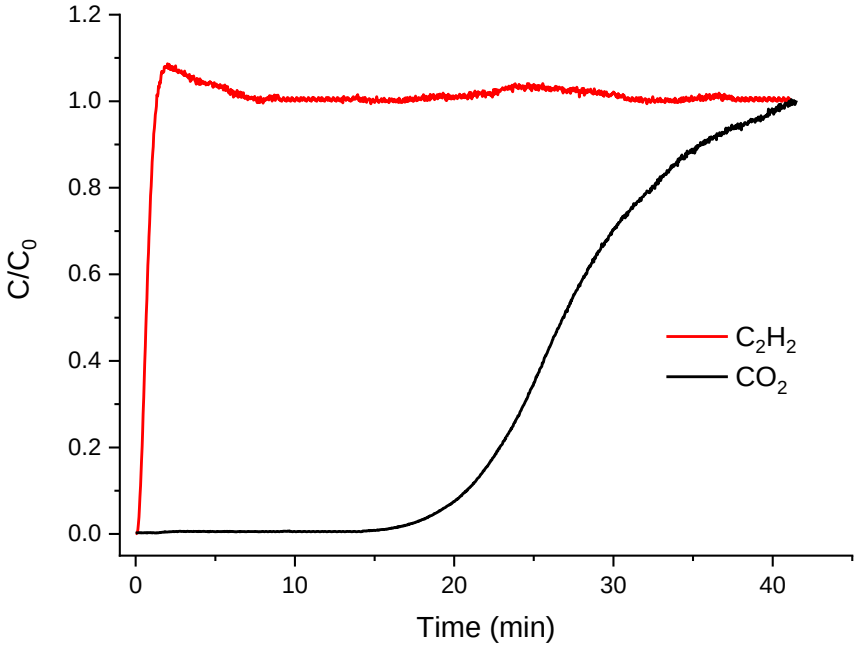

Fig. S51. Experimental breakthrough curves for a mixture of 5/95 CO_2/C_2H_2 at 1.1 bar and 293 K in an adsorption column packed with MUF-16.

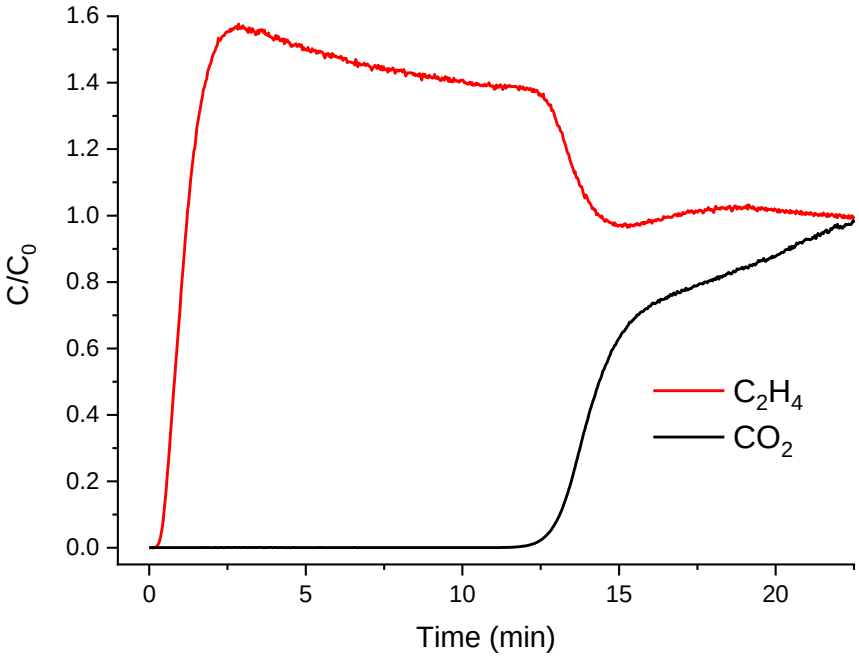

Fig. S52. Experimental breakthrough curves for a mixture of 50/50 CO_2/C_2H_4 at 1.1 bar and 293 K in an adsorption column packed with MUF-16.

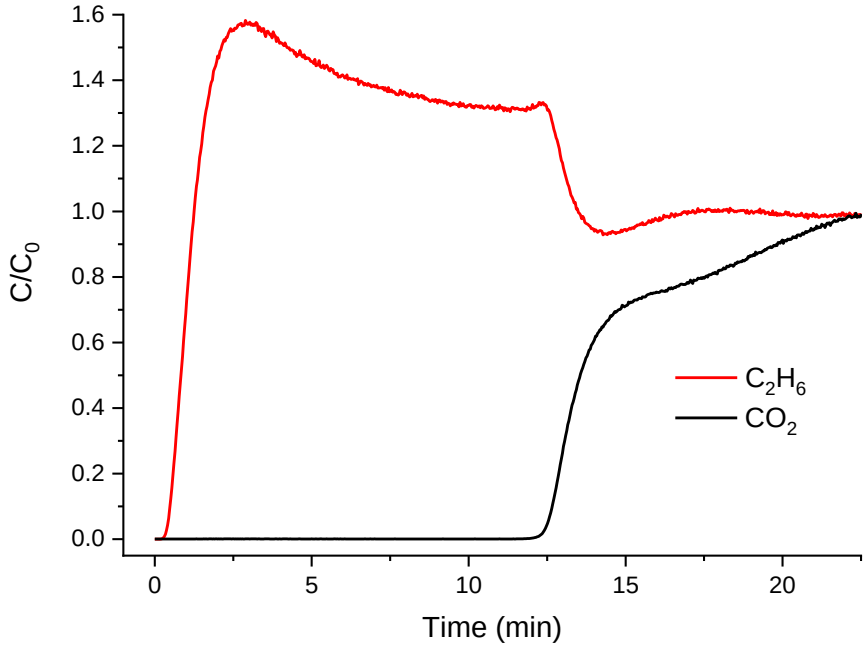

Fig. S53. Experimental breakthrough curves for a mixture of 50/50 CO_2/C_2H_6 at 1.1 bar and 293 K in an adsorption column packed with MUF-16.

Adsorbent regeneration

The desorption behaviour of CO_2 and C_2H_2 from the adsorption column was also investigated. Once the adsorbent was saturated with an equimolar mixture of CO_2 and C_2H_2, the column was purged with a helium flow of 5 mL_N/min for 18 mins at 20 °C at 1 bar while monitoring the effluent gas. Then the column was then heated to 80 °C with a ramp of 10 °C/min for 20 mins. Finally, the column was heated to 130 °C with the same ramping for 15 min before cooling to 20 °C. A breakthrough measurement was then performed, which showed that the absorbent had been fully regenerated.

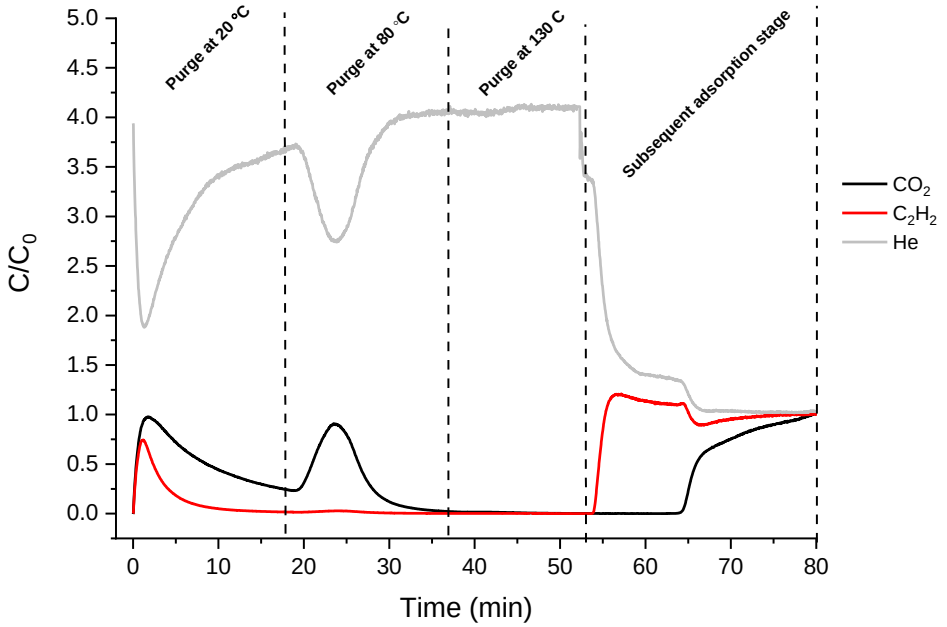

Figure S54. Desorption behaviour of the adsorbates through heating the column at 1 bar under a helium flow of 5 mL_N/min. C_2H_2 is fully removed from the bed by purging with helium at room temperature. CO_2 is completely desorbed from the column upon heating to 80 °C with a flow of helium. No adsorbates remained to be removed upon further heating to 130 °C.

10.2.1. Simulations of CO_2/C_2H_2 breakthrough curves

The simulation of breakthrough curves for CO_2/C2 hydrocarbons was carried out using the method reported above. A summary of adsorption column parameters and feed characterizations are presented in Table S9.

Table S9. Adsorption column parameters and feed characterizations used for the simulations for MUF-16.

Adsorption bed	***Feed***
Length: 110 mm Diameter: 6.4 mm Amount of adsorbent in the bed: 0.9 g Bed voidage: 0.84 Adsorbent average radius: 0.2 mm k_{CO2}: 0.021 s^{-1} k_{C2H2}: 0.024 s^{-1}	Flow rates: 6 mL_N/min for equimolar and 0.1/99.9 mixtures, and 6.85 mL_N/min for the 5/95 mixture. Temperature: 293 K Pressure: 1.1 bar Carrier gas (He) flow rate: 2 mL_N/min.

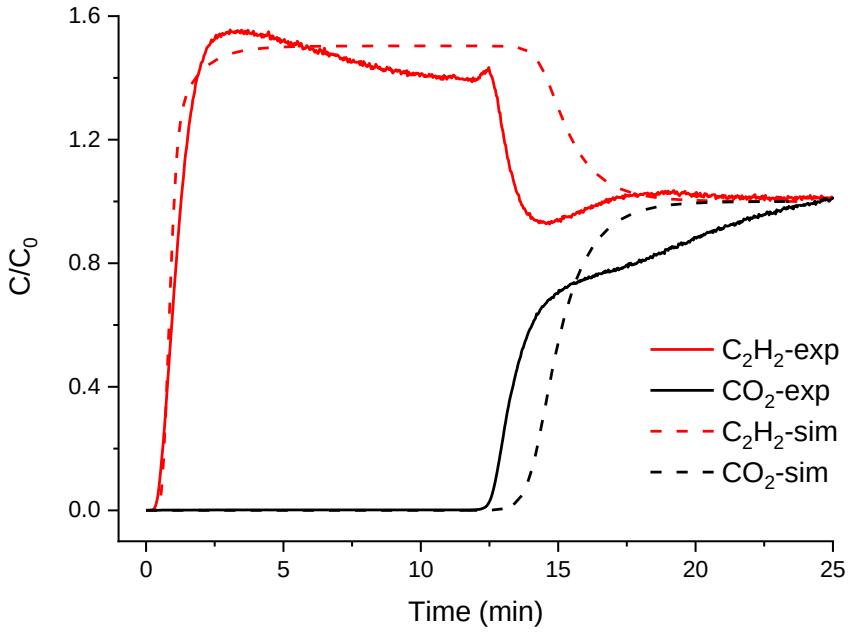

Fig. S55. Experimental breakthrough curves in comparison to simulated one for a mixture of 50/50 CO_2/C_2H_2 at 1.1 bar and 293 K in an adsorption column packed with MUF-16.

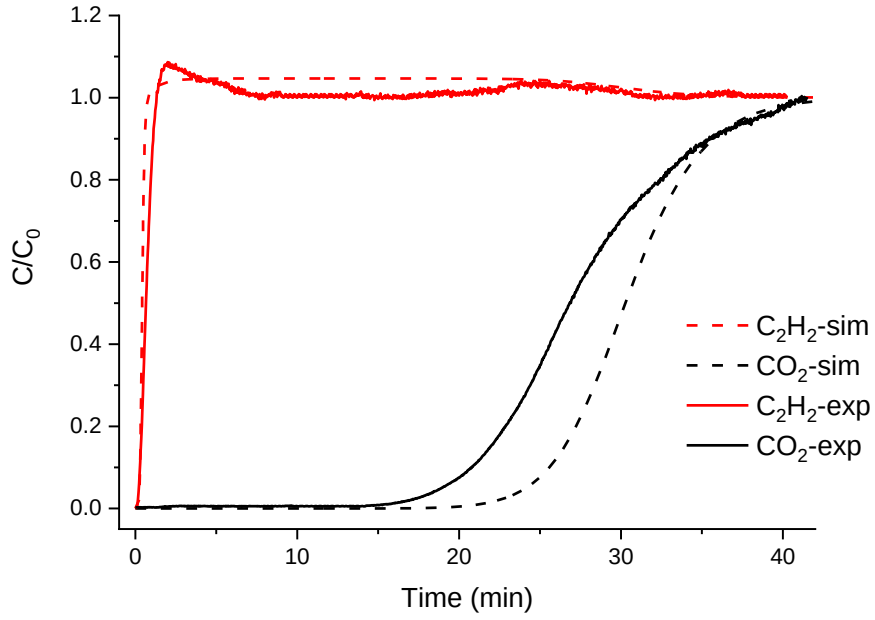

Fig. S56. Experimental breakthrough curves in comparison to simulated one for a mixture of 5/95 CO_2/C_2H_2 at 1.1 bar and 293 K in an adsorption column packed with MUF-16.

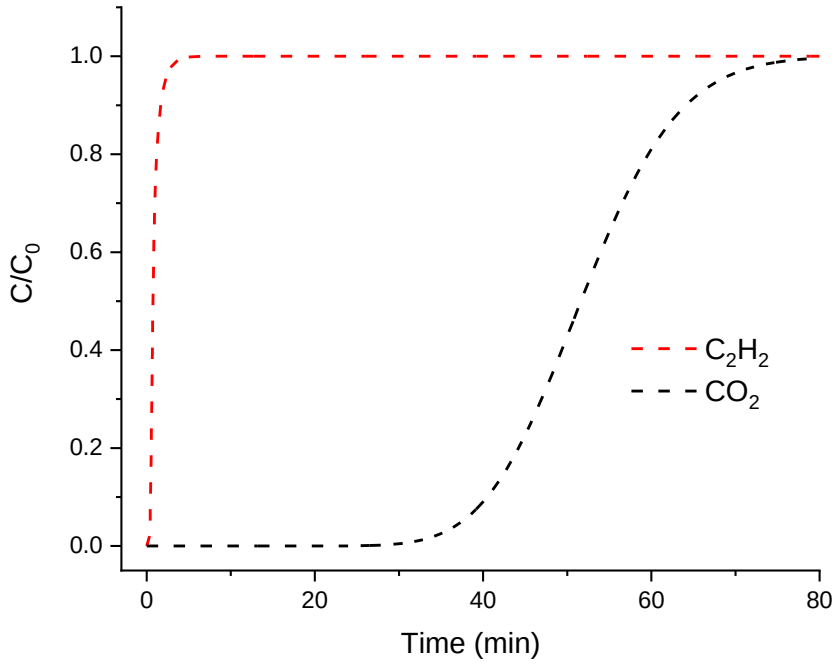

Fig. S57. Simulated breakthrough curves for a mixture of 0.1/99.9 CO_2/C_2H_2 at 1.1 bar and 293 K in an adsorption column packed with MUF-16.

11. Tabulated separation metrics

The CO_2/CH_4 and CO_2/C_2H_2 separation parameters of MUF-16 in comparison to top-performing MOFs and related materials are presented in Tables S9 and S10. Materials with molecular sieving mechanisms are excluded from this analysis. IAST selectivities are presented for a 50/50 CO_2/CH_4 and CO_2/C_2H_2 at 1 bar, unless otherwise stated. Q_{st} values are reported at low loading, unless otherwise stated. Uptake ratios are calculated by dividing the uptake of CO_2 by that of CH_4 or C_2H_2 (all at 1 bar and the specified temperature in the Table S9 and S10). These were taken from either a direct statement of relevant details in the manuscript or were extracted from Figs. by a digitizer software.

Table S10. Metrics relevant to $CO_2/N_2/CH_4$ separations for MUF-16 in comparison to a selection of materials reported in the literature.

	Material	T (°C)	P (bar)	CO_2 | CH_4 uptakes (cc/g)	$Q_{st}(CO_2)$ (kJ/mol)	Uptake ratio	IAST selectivity (50/50)
This work	**MUF-16**	**20**	**1**	**47.8 | 1.2**	**32**	**39.8**	**6686**
	MUF-16(Mn)	**20**	**1**	**50.5 | 3.1**	**37**	**16.3**	**470**
	MUF-16(Ni)	**20**	**1**	**48.0 | 2.8**	**37**	**17.3**	**1215**
Selected MOFs, carbons and zeolites	Zeolite 13X[14, 15]	25	1	112 | 13	44-54	8.6	103
	Zeolite 5A[16, 17]	30	1	75.5 | 11.8	23[c]	6.4	n/a
	Zeolite 4A[18, 19]	30-32	1	105.3 | 15	39	7	n/a
	BPL Activated carbon[20, 21]	25	1	46.2 | 20.2	21[c]	2.3	4
	SIFSIX-3-Zn[15]	25	1	57 | 17.6	45	3.2	230
	$[Cd_2L(H_2O)]_2.5H_2O$[22]	20	1	47.2 | 1.1	37	42.9	n/a
	UTSA-120[23]	23	1	112 | 20.8	27	5.4	96
	UTSA-16[24, 25]	23	1	96 | 13.2	33	7.3	38
	HKUST-1[25-27]	25	1	103 | 18.7	35[c]	7.4	5.5
	Mg-dobdc[15, 25, 28, 29]	23	1	190 | 25	47-52	7.6	130
	IITKGP-5a[30]	22	1	49 | 13.6	23	3.6	24
	WOFOUR-1-Ni[31]	25	1	52 | 11.5	66	4.5	26[a]
	SIFSIX-2-Cu-i[15]	25	1	121.2 | 10.5	32	11.5	33
	CAU-1[32]	0	1	165 | 27	48	6.1	28[b]
	NbOFFIVE-Ni[33, 34]	25	1	51.7 | 2.2	54	23.1	366
	TIFSIX-3-Ni[33, 34]	25	1	48.6 | 4.8	50	10.2	158
	SIFSIX-14-Cu-i[35]	20	1	110.5 | 1.3 |	38	85	n/a
	SIFSIX-3-Ni[33, 34]	25	1	64.5 | 6.6	51	8.9	130

Values were generally taken from either a direct statement in the manuscript or were extracted from relevant Figs. by a digitizer software. Materials with molecular sieving mechanisms are excluded from this analysis. [a] IAST is calculated for a 10/90 mixture. [b] Selectivity was calculated from the slope of isotherms at low pressures (Henry constants).[c] Heat of adsorption averaged over CO_2 uptakes.

Table S11. Separation metrics relevant to C_2H_2/CO_2 separations for MUF-16 in comparison to other top-performing materials reported in the literature.

MOF	T (°C)	P (bar)	CO_2 uptake (mmol/g)	C_2H_2 uptake (mmol/g)	Q_{st} of CO_2[a] (kJ/mol)	Q_{st} of C_2H_2[a] (kJ/mol)	Uptake ratio*	IAST selectivity (50/50)*
CO_2-selective MOFs								
MUF-16	20	1	2.14	0.18	32	25.8	12.0	510
[Mn(bdc)(dpe)][36]	0	1	2.08	0.32	29.5	27.8	6.4	9.0
SIFSIX-3-Ni[37]	25	1	2.80	3.30	51	36.5	0.8	7.5[&]
$K_2[Cr_3O(OOCH)_6$[6]	5	1	0.50	0.10	38	30	4.5	5.6[##]
CD-MOF-1[38]	25	1	2.87	2.23	41	17	1.3	3.4[&]
CD-MOF-2[38]	25	1	2.67	2.03	67.5	25	1.3	6.1[&]
C_2H_2-selective MOFs								
UTSA-300a[39]	25	1	0.15	3.10	-	57	20.6	700
NKMOF-1-Ni[40]	25	1	2.27	2.67	41	60	1.2	22
HOF-3a[41]	23	1	0.93	2.14	42	19.5	2.3	21
$[Ni_3(HCOO)_6]$[42]	25	1	3.00	4.20	24.5	41	1.4	21
SNNU-45[43]	25	1	4.34	5.98	27.1	40	1.37	4.5
ZJU-196a[44]	25	1	0.35	3.70	-	39	10.6	18
JCM-1[45]	25	1	1.69	3.34	33	36.5	2.0	14
DICRO-4-Ni-i[46]	25	1	1.02	1.91	34	38	1.9	13.5
UTSA-74a[47]	25	1	3.00	4.80	25.5	31.5	1.6	8
TIFSIX-2-Cu-i[37]	25	1	4.20	4.10	36	46	0.97	6
Cu-BTC[25, 41, 48]	25	1	5.10	8.90	26.9	30	1.7	5.5
MAF-2[49]	25	1	0.82	3.90	27	33	4.7	5
UTSA-50a[41]	23	1	3.10	4.10	27.8	32	1.3	5
FJU-90a[50]	25	1	4.92	8.03	21	25	1.6	4.3
ZJU-60a[51]	23	1	3.12	6.69	15.5	17.5	2.1	4
ZJU-10a[52]	25	1	3.66	7.58	26	39	2.1	4
MFM-188[53]	25	1	5.35	10.20	20.8	32.5	1.9	3.7
FeNi-M'MOF[54]	25	1	2.72	4.29	24.5	32.8	1.6	22.5

Values were taken from either a direct statement in the manuscript or were extracted from relevant Figs. by a digitizer software. [a] Q_{st} at low coverage. * Uptake ratios and IAST selectivities are given with respect to the ratio of the highly adsorbed component to the weakly adsorbed component from an equimolar mixture. [&] isotherm from taken from literatures for 3-Ni[37] and for CD-MOFs[38] and to calculate IAST selectivity for an equimolar mixture. [##] Isotherm data were extracted from [6] using a digitizer software and so we could calculate IAST selectivity for an equimolar mixture.

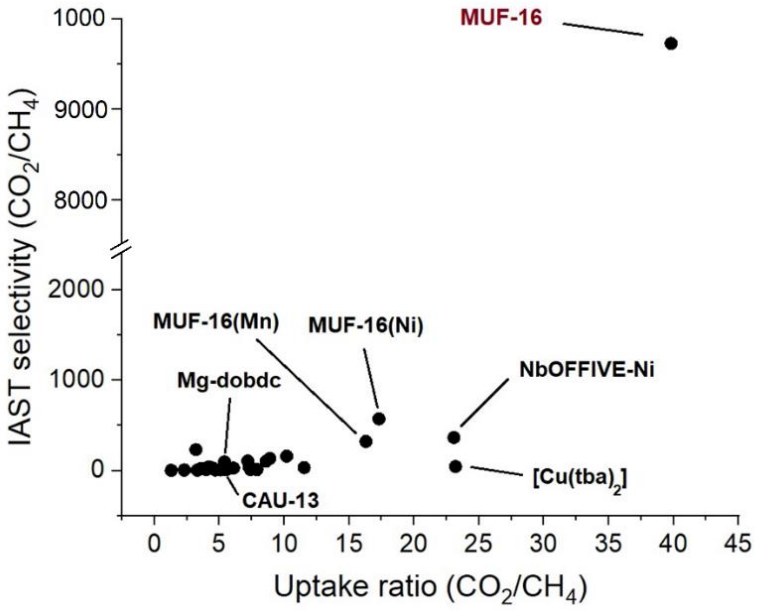

Fig. S58. IAST selectivity of MUF-16 family for an equimolar mixture of CO_2/CH_4 in comparison to top top-performing MOFs at 1 bar and ambient temperature versus their uptake ratio at 1 bar.

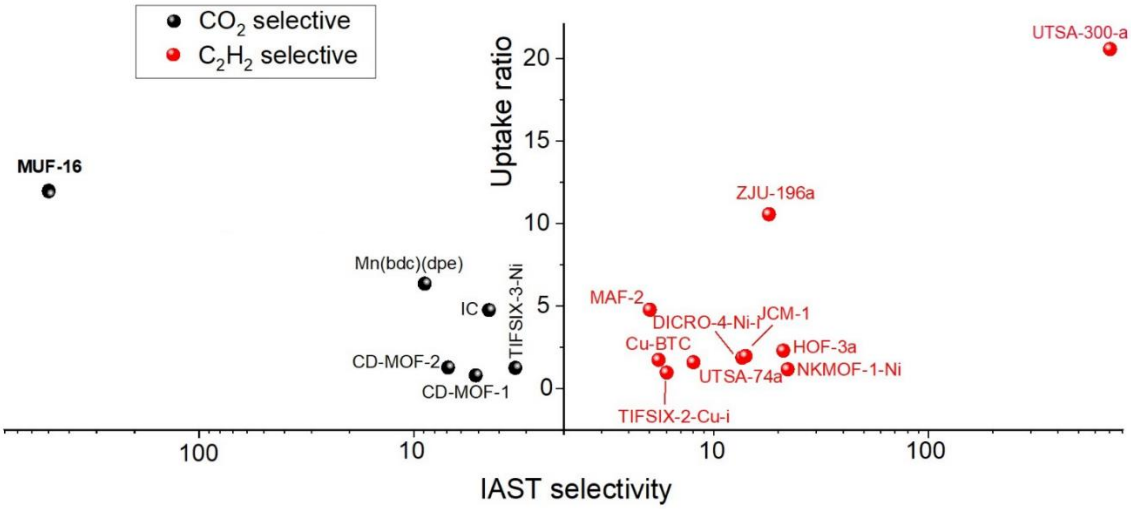

Fig. S59. Predicted IAST selectivity (log scale) from an equimolar mixture of CO_2/C_2H_2 plotted against uptake ratio at 1 bar and 293-298 K (except for IC (278 K) and [Mn(bdc)(dpe)] (273 K)) for MUF-16 in comparison to the best materials reported to date. Selectivity and uptake ratios are defined as CO_2/C_2H_2 and C_2H_2/CO_2 for CO_2-selective and C_2H_2-selective materials, respectively.

12. References

1. Tang, E.; Dai, Y.-M.; Zhang, J.; Li, Z.-J.; Yao, Y.-G.; Zhang, J.; Huang, X.-D., Two Cobalt(II) 5-Aminoisophthalate Complexes and Their Stable Supramolecular Microporous Frameworks. *Inorg. Chem.* **2006,** *45*, 6276-6281.
2. Tian, C.-B.; He, C.; Han, Y.-H.; Wei, Q.; Li, Q.-P.; Lin, P.; Du, S.-W., Four New MnII Inorganic–Organic Hybrid Frameworks with Diverse Inorganic Magnetic Chain's Sequences: Syntheses, Structures, Magnetic, NLO, and Dielectric Properties. *Inorg. Chem.* **2015,** *54*, 2560-2571.
3. Willems, T. F.; Rycroft, C. H.; Kazi, M.; Meza, J. C.; Haranczyk, M., Algorithms and tools for high-throughput geometry-based analysis of crystalline porous materials. *Microporous Mesoporous Mater.* **2012,** *149*, 134-141.
4. Dubbeldam, D.; Calero, S.; Ellis, D. E.; Snurr, R. Q., RASPA: molecular simulation software for adsorption and diffusion in flexible nanoporous materials. *Mol. Simul.* **2016,** *42*, 81-101.
5. Li, J.-R.; Kuppler, R. J.; Zhou, H.-C., Selective gas adsorption and separation in metal–organic frameworks. *Chem. Soc. Rev.* **2009,** *38*, 1477-1504.
6. Eguchi, R.; Uchida, S.; Mizuno, N., Inverse and High CO_2/C_2H_2 Sorption Selectivity in Flexible Organic–Inorganic Ionic Crystals. *Angew. Chem., Int. Ed.* **2012,** *51*, 1635-1639.
7. Reid, C. R.; Thomas, K. M., Adsorption Kinetics and Size Exclusion Properties of Probe Molecules for the Selective Porosity in a Carbon Molecular Sieve Used for Air Separation. *J. Phys. Chem. B* **2001,** *105*, 10619-10629.
8. Li, L.; Lin, R.-B.; Wang, X.; Zhou, W.; Jia, L.; Li, J.; Chen, B., Kinetic separation of propylene over propane in a microporous metal-organic framework. *Chem. Eng. J.* **2018,** *354*, 977-982.
9. Walton, K. S.; Snurr, R. Q., Applicability of the BET Method for Determining Surface Areas of Microporous Metal-Organic Frameworks. *J. Am. Chem. Soc.* **2007,** *129*, 8552-8558.
10. Dincă, M.; Dailly, A.; Liu, Y.; Brown, C. M.; Neumann, D. A.; Long, J. R., Hydrogen Storage in a Microporous Metal−Organic Framework with Exposed Mn2+ Coordination Sites. *J. Am. Chem. Soc.* **2006,** *128*, 16876-16883.
11. Myers, A.; Prausnitz, J. M., Thermodynamics of mixed-gas adsorption. *AIChE J.* **1965,** *11*, 121-127.
12. Qazvini, O. T.; Babarao, R.; Shi, Z.-L.; Zhang, Y.-B.; Telfer, S. G., A Robust Ethane-Trapping Metal–Organic Framework with a High Capacity for Ethylene Purification. *J. Am. Chem. Soc.* **2019**.
13. Qazvini, O. T.; Babarao, R.; Telfer, S. G., Multipurpose Metal–Organic Framework for the Adsorption of Acetylene: Ethylene Purification and Carbon Dioxide Removal. *Chem. Mater.* **2019,** *31*, 4919-4926.
14. Cavenati, S.; Grande, C. A.; Rodrigues, A. E., Adsorption Equilibrium of Methane, Carbon Dioxide, and Nitrogen on Zeolite 13X at High Pressures. *J. Chem. Eng. Data* **2004,** *49*, 1095-1101.
15. Nugent, P.; Belmabkhout, Y.; Burd, S. D.; Cairns, A. J.; Luebke, R.; Forrest, K.; Pham, T.; Ma, S.; Space, B.; Wojtas, L.; Eddaoudi, M.; Zaworotko, M. J., Porous materials with optimal adsorption thermodynamics and kinetics for CO2 separation. *Nature* **2013,** *495*, 80.
16. Saha, D.; Bao, Z.; Jia, F.; Deng, S., Adsorption of CO_2, CH_4, N_2O, and N_2 on MOF-5, MOF-177, and Zeolite 5A. *Environ. Sci. Technol.* **2010,** *44*, 1820-1826.
17. Nam, G.-M.; Jeong, B.-M.; Kang, S.-H.; Lee, B.-K.; Choi, D.-K., Equilibrium Isotherms of CH_4, C_2H_6, C_2H_4, N_2, and H_2 on Zeolite 5A Using a Static Volumetric Method. *J. Chem. Eng. Data* **2005,** *50*, 72-76.

18. Shao, W.; Zhang, L.; Li, L.; Lee, R. L., Adsorption of CO_2 and N_2 on synthesized NaY zeolite at high temperatures. *Adsorption* **2009,** *15*, 497.
19. Ahmed, M. J.; Theydan, S. K., Equilibrium isotherms studies for light hydrocarbons adsorption on 4A molecular sieve zeolite. *Journal of Petroleum Science and Engineering* **2013,** *108*, 316-320.
20. McEwen, J.; Hayman, J.-D.; Ozgur Yazaydin, A., A comparative study of CO_2, CH_4 and N_2 adsorption in ZIF-8, Zeolite-13X and BPL activated carbon. *Chem. Phys.* **2013,** *412*, 72-76.
21. Delgado, J. A.; Águeda, V. I.; Uguina, M. A.; Sotelo, J. L.; Brea, P.; Grande, C. A., Adsorption and Diffusion of H_2, CO, CH_4, and CO_2 in BPL Activated Carbon and 13X Zeolite: Evaluation of Performance in Pressure Swing Adsorption Hydrogen Purification by Simulation. *Ind. Eng. Chem. Res.* **2014,** *53*, 15414-15426.
22. Hou, L.; Shi, W.-J.; Wang, Y.-Y.; Guo, Y.; Jin, C.; Shi, Q.-Z., A rod packing microporous metal–organic framework: unprecedented ukv topology, high sorption selectivity and affinity for CO_2. *Chem. Commun.* **2011,** *47*, 5464-5466.
23. Wen, H.-M.; Liao, C.; Li, L.; Alsalme, A.; Alothman, Z.; Krishna, R.; Wu, H.; Zhou, W.; Hu, J.; Chen, B., A metal–organic framework with suitable pore size and dual functionalities for highly efficient post-combustion CO_2 capture. *J. Mat. Chem. A* **2019,** *7*, 3128-3134.
24. Masala, A.; Vitillo, J. G.; Mondino, G.; Grande, C. A.; Blom, R.; Manzoli, M.; Marshall, M.; Bordiga, S., CO_2 Capture in Dry and Wet Conditions in UTSA-16 Metal–Organic Framework. *ACS Appl. Mater. Interfaces* **2017,** *9*, 455-463.
25. Xiang, S.; He, Y.; Zhang, Z.; Wu, H.; Zhou, W.; Krishna, R.; Chen, B., Microporous metal-organic framework with potential for carbon dioxide capture at ambient conditions. *Nat. Commun.* **2012,** *3*, 954.
26. Liang, Z.; Marshall, M.; Chaffee, A. L., CO2 Adsorption-Based Separation by Metal Organic Framework (Cu-BTC) versus Zeolite (13X). *Energy Fuels* **2009,** *23*, 2785-2789.
27. Liu, B.; Smit, B., Comparative Molecular Simulation Study of CO2/N2 and CH4/N2 Separation in Zeolites and Metal−Organic Frameworks. *Langmuir* **2009,** *25*, 5918-5926.
28. Mason, J. A.; Sumida, K.; Herm, Z. R.; Krishna, R.; Long, J. R., Evaluating metal–organic frameworks for post-combustion carbon dioxide capture via temperature swing adsorption. *Energy Environ. Sci.* **2011,** *4*, 3030-3040.
29. Herm, Z. R.; Swisher, J. A.; Smit, B.; Krishna, R.; Long, J. R., Metal− organic frameworks as adsorbents for hydrogen purification and precombustion carbon dioxide capture. *J. Am. Chem. Soc.* **2011,** *133*, 5664-5667.
30. Pal, A.; Chand, S.; Elahi, S. M.; Das, M. C., A microporous MOF with a polar pore surface exhibiting excellent selective adsorption of CO_2 from CO_2–N_2 and CO_2–CH_4 gas mixtures with high CO_2 loading. *Dalton Trans.* **2017,** *46*, 15280-15286.
31. Mohamed, M. H.; Elsaidi, S. K.; Pham, T.; Forrest, K. A.; Tudor, B.; Wojtas, L.; Space, B.; Zaworotko, M. J., Pillar substitution modulates CO2 affinity in “mmo” topology networks. *Chem. Commun.* **2013,** *49*, 9809-9811.
32. Si, X.; Jiao, C.; Li, F.; Zhang, J.; Wang, S.; Liu, S.; Li, Z.; Sun, L.; Xu, F.; Gabelica, Z.; Schick, C., High and selective CO2 uptake, H2storage and methanol sensing on the amine-decorated 12-connected MOF CAU-1. *Energy Environ. Sci.* **2011,** *4*, 4522-4527.
33. Madden, D. G.; O’Nolan, D.; Chen, K.-J.; Hua, C.; Kumar, A.; Pham, T.; Forrest, K. A.; Space, B.; Perry, J. J.; Khraisheh, M., Highly selective CO_2 removal for one-step liquefied natural gas processing by physisorbents. *Chem. Commun.* **2019,** *55*, 3219-3222.
34. Mukherjee, S.; Sikdar, N.; O’Nolan, D.; Franz, D. M.; Gascón, V.; Kumar, A.; Kumar, N.; Scott, H. S.; Madden, D. G.; Kruger, P. E., Trace CO2 capture by an ultramicroporous physisorbent with low water affinity. *Science Advances* **2019,** *5*, eaax9171.

35. Jiang, M.; Li, B.; Cui, X.; Yang, Q.; Bao, Z.; Yang, Y.; Wu, H.; Zhou, W.; Chen, B.; Xing, H., Controlling Pore Shape and Size of Interpenetrated Anion-Pillared Ultramicroporous Materials Enables Molecular Sieving of CO_2 Combined with Ultrahigh Uptake Capacity. *ACS Appl. Mater. Interfaces* **2018,** *10*, 16628-16635.
36. Foo, M. L.; Matsuda, R.; Hijikata, Y.; Krishna, R.; Sato, H.; Horike, S.; Hori, A.; Duan, J.; Sato, Y.; Kubota, Y.; Takata, M.; Kitagawa, S., An Adsorbate Discriminatory Gate Effect in a Flexible Porous Coordination Polymer for Selective Adsorption of CO_2 over C_2H_2. *J. Am. Chem. Soc.* **2016,** *138*, 3022-3030.
37. Chen, K.-J.; Scott, H. S.; Madden, D. G.; Pham, T.; Kumar, A.; Bajpai, A.; Lusi, M.; Forrest, K. A.; Space, B.; Perry, J. J.; Zaworotko, M. J., Benchmark C_2H_2/CO_2 and CO_2/C_2H_2 Separation by Two Closely Related Hybrid Ultramicroporous Materials. *Chem* **2016,** *1*, 753-765.
38. Li, L.; Wang, J.; Zhang, Z.; Yang, Q.; Yang, Y.; Su, B.; Bao, Z.; Ren, Q., Inverse Adsorption Separation of CO_2/C_2H_2 Mixture in Cyclodextrin-Based Metal–Organic Frameworks. *ACS Appl. Mater. Interfaces* **2019,** *11*, 2543-2550.
39. Lin, R.-B.; Li, L.; Wu, H.; Arman, H.; Li, B.; Lin, R.-G.; Zhou, W.; Chen, B., Optimized separation of acetylene from carbon dioxide and ethylene in a microporous material. *J. Am. Chem. Soc.* **2017,** *139*, 8022-8028.
40. Peng, Y.-L.; Pham, T.; Li, P.; Wang, T.; Chen, Y.; Chen, K.-J.; Forrest, K. A.; Space, B.; Cheng, P.; Zaworotko, M. J.; Zhang, Z., Robust Ultramicroporous Metal–Organic Frameworks with Benchmark Affinity for Acetylene. *Angew. Chem., Int. Ed.* **2018,** *57*, 10971-10975.
41. Li, P.; He, Y.; Zhao, Y.; Weng, L.; Wang, H.; Krishna, R.; Wu, H.; Zhou, W.; O'Keeffe, M.; Han, Y.; Chen, B., A Rod-Packing Microporous Hydrogen-Bonded Organic Framework for Highly Selective Separation of C_2H_2/CO_2 at Room Temperature. *Angew. Chem., Int. Ed.* **2015,** *54*, 574-577.
42. Zhang, L.; Jiang, K.; Zhang, J.; Pei, J.; Shao, K.; Cui, Y.; Yang, Y.; Li, B.; Chen, B.; Qian, G., Low-cost and high-performance microporous metal–organic framework for separation of acetylene from Carbon dioxide. *ACS Sustain Chem Eng* **2018,** *7*, 1667-1672.
43. Tu, B.; Pang, Q.; Wu, D.; Song, Y.; Weng, L.; Li, Q., Ordered vacancies and their chemistry in metal-organic frameworks. *J. Am. Chem. Soc.* **2014,** *136*, 14465-71.
44. Zhang, L.; Jiang, K.; Li, L.; Xia, Y.-P.; Hu, T.-L.; Yang, Y.; Cui, Y.; Li, B.; Chen, B.; Qian, G., Efficient separation of C_2H_2 from C_2H_2/CO_2 mixtures in an acid–base resistant metal–organic framework. *Chem. Commun.* **2018,** *54*, 4846-4849.
45. Lee, J.; Chuah, C. Y.; Kim, J.; Kim, Y.; Ko, N.; Seo, Y.; Kim, K.; Bae, T. H.; Lee, E., Separation of Acetylene from Carbon Dioxide and Ethylene by a Water-Stable Microporous Metal–Organic Framework with Aligned Imidazolium Groups inside the Channels. *Angewandte Chemie International Editions* **2018,** *57*, 7869-7873.
46. Scott, H. S.; Shivanna, M.; Bajpai, A.; Madden, D. G.; Chen, K.-J.; Pham, T.; Forrest, K. A.; Hogan, A.; Space, B.; Perry Iv, J. J.; Zaworotko, M. J., Highly Selective Separation of C_2H_2 from CO_2 by a New Dichromate-Based Hybrid Ultramicroporous Material. *ACS Appl. Mater. Interfaces* **2017,** *9*, 33395-33400.
47. Luo, F.; Yan, C.; Dang, L.; Krishna, R.; Zhou, W.; Wu, H.; Dong, X.; Han, Y.; Hu, T.-L.; O'Keeffe, M.; Wang, L.; Luo, M.; Lin, R.-B.; Chen, B., UTSA-74: A MOF-74 Isomer with Two Accessible Binding Sites per Metal Center for Highly Selective Gas Separation. *J. Am. Chem. Soc.* **2016,** *138*, 5678-5684.
48. Xiang, S.; Zhou, W.; Gallegos, J. M.; Liu, Y.; Chen, B., Exceptionally High Acetylene Uptake in a Microporous Metal−Organic Framework with Open Metal Sites. *J. Am. Chem. Soc.* **2009,** *131*, 12415-12419.

49. Zhang, J.-P.; Chen, X.-M., Optimized Acetylene/Carbon Dioxide Sorption in a Dynamic Porous Crystal. *J. Am. Chem. Soc.* **2009,** *131*, 5516-5521.
50. Ye, Y.; Ma, Z.; Lin, R.-B.; Krishna, R.; Zhou, W.; Lin, Q.; Zhang, Z.; Xiang, S.; Chen, B., Pore Space Partition within a Metal–Organic Framework for Highly Efficient C_2H_2/CO_2 Separation. *J. Am. Chem. Soc.* **2019,** *141*, 4130-4136.
51. Duan, X.; Zhang, Q.; Cai, J.; Yang, Y.; Cui, Y.; He, Y.; Wu, C.; Krishna, R.; Chen, B.; Qian, G., A new metal–organic framework with potential for adsorptive separation of methane from carbon dioxide, acetylene, ethylene, and ethane established by simulated breakthrough experiments. *J. Mat. Chem. A* **2014,** *2*, 2628-2633.
52. Duan, X.; Wang, H.; Ji, Z.; Cui, Y.; Yang, Y.; Qian, G., A novel metal-organic framework for high storage and separation of acetylene at room temperature. *J. Solid State Chem.* **2016,** *241*, 152-156.
53. Moreau, F.; da Silva, I.; Al Smail, N. H.; Easun, T. L.; Savage, M.; Godfrey, H. G. W.; Parker, S. F.; Manuel, P.; Yang, S.; Schröder, M., Unravelling exceptional acetylene and carbon dioxide adsorption within a tetra-amide functionalized metal-organic framework. *Nat. Commun.* **2017,** *8*, 14085.
54. Gao, J.; Qian, X.; Lin, R.-B.; Krishna, R.; Wu, H.; Zhou, W.; Chen, B., Mixed Metal–Organic Framework with Multiple Binding Sites for Efficient C2H2/CO2 Separation. *Angew. Chem., Int. Ed.* **2020,** *59*, 4396-4400.